Organic Solvent Nanofiltration (OSN) Modelling – From Pure Solvents to Highly Rejected Solutes

by

Pedro Silva

A thesis submitted for the degree of *Doctor of Philosophy of the University of London* and the *Diploma of Membership of Imperial College London*

May 2007

Department of Chemical Engineering and Chemical Technology
Imperial College London
London SW7 2AZ, United Kingdom

Abstract

The primary focus of this research is to extend the principles of nanofiltration (NF) to non-aqueous systems using organic solvent nanofiltration (OSN) membranes. Solvent transport in organic solvent nanofiltration membranes has been studied in a lab-scale cross-flow nanofiltration rig over extended periods using the common solvents methanol, toluene, ethyl acetate and their mixtures. The organic solvent nanofiltration membranes STARMEM^{TM} 122* (W.R Grace and Co.) and MPF-50 (Koch Membrane Systems) were investigated. Both solution-diffusion and pore-flow models can be used to predict permeation of solvent mixtures. For the solvents studied, it is possible for reasonable predictions of solvent mixture flux to be made over the whole concentration range, based on the data for pure solvents.

To understand solute transport, flux and rejection performances under cross-flow, for concentrated (5-30 wt. %) methanol-dimethyl methylsuccinate (DMMS) solutions, were examined. The experimental flux/rejection data for the flat-sheet membranes was fitted using pore-flow and solution-diffusion models, coupled with film theory for liquid mass transfer effects. It was found that solution-diffusion gives a better description of some of the experimental trends. In the practical range of concentrations studied, rejection should be seen as a variable, dependent on the mass transfer characteristics of the nanofiltration system in use.

Pilot plant OSN spiral-wound performance was investigated for highly concentrated solutions of a highly rejected solute. Flat-sheet determined model transport parameters were used, with success, for predictive modelling of pilot-plant spiral-wound experimental data.

Lastly, this work presents a new modelling approach for solvent transport though OSN membranes. In this study an adsorption-diffusion membrane transport model, able to describe the experimental flux of a reasonable number of solvents permeating through a polyimide polymeric membrane, was derived. The main contribution of this modelling approach is its ability to incorporate all OSN flux determining factors in a predictive mathematical model.

* STARMEM^{TM} is a trademark of W.R.Grace

Acknowledgements

I wish to express my appreciation and gratitude to my supervisor Professor Andrew Livingston through his guidance and invaluable advice.

I would like to give thanks to my colleagues particularly to Dr Han and Dr Peeva who assisted me with experimental work during my PhD. I would also like to thank my other labmates who help me in one way or another.

I would to thank Dr. Shengfu for his guidance in the pilot plant work and for the fruitful discussions that we had.

I would like to thank the Fundação para a Ciência e Tecnologia for their sponsorship.

Last but not least, I would like to thanks to my parents and my girlfriend for their support and encouragement.

Publications

Parts of this thesis have been published:

1. Silva, P. and A. G. Livingston, New Approach to Organic Solvent Nanofiltration (OSN) Modelling, submitted to *J. Membr. Sci.* (Chapter 6)

2. Silva, P. and A. G. Livingston, Organic Solvent Nanofiltration (OSN) with Spiral-Wound Membrane Modules – Highly Rejected Solute System, submitted to *J. Membr. Sci.* (Chapter 5)

3. Silva, P. and A. G. Livingston, Effect of solute concentration and mass transfer limitations on transport in organic solvent nanofiltration-partially rejected solute, *J. Membr. Sci.* (2006) 280, 889–898. (Chapter 4)

4. Silva, P. and A. G. Livingston, Solvent transport in solvent nanofiltration membranes, *J. Membr. Sci.* (2005) 262, 49–59. (Chapter 3)

Table of Contents

List of Figures and Tables

Nomenclature

a	Activity
A	Membrane area (m^2)
c	Molar concentration inside the membrane ($mol.m^{-3}$)
d_h	Hydraulic diameter (m)
D	Maxwell-Stefan diffusivity ($m^2.s^{-1}$)
D	Effective mass diffusivity ($m^2.s^{-1}$)
D^e	Effective molar diffusivity ($m^2.s^{-1}$)
D^T	Thermal Maxwell-Stefan diffusivity ($m^2.s^{-1}$)
F	External force ($N.mol^{-1}$)
k	Mass transfer coefficient ($m.s^{-1}$)
K^{mass}	Mass partition coefficient (-)
K^{molar}	Molar partition coefficient (-)
m	Mass (Kg)
M	Molecular weight ($Kg.mol^{-1}$)
n	Mass flux ($Kg.m^{-2}.s^{-1}$)
N	Molar flux ($mol.m^{-2}.s^{-1}$)
N_v	Total volume flux ($m.s^{-1}$)
p	Pressure (Pa)
P	Permeability ($mol.m^{-2}.s^{-1}$)
R	Ideal gas constant ($Pa.m^3.mol^{-1}.K^{-1}$)
r_p	Pore radius (m)
RR	Real rejection (-)
OR	Observed rejection (-)
Re	Reynolds number (-)
Sh	Sherwood number (-)
Sc	Schmidt number (-)
T	Temperature (K)
t	Time (s)
u	Velocity ($m.s^{-1}$)
$\overline{V}$	Partial molar volume ($m^3.mol^{-1}$)
V	Volume (m^3)
w	Mass fraction (-)
x	Molar fraction (-)
SW	Swelling (-)
K_c	Hindrance factor for convection (-)
K_d	Hindrance factor for diffusion (-)
Pe'	Modified Peclet number (-)

Greek letters

α'	Viscous flow characterization parameter (-)
β_0	Membrane viscous flow parameter (m^2)
χ	Flory-Huggins interaction parameter (-)
δ	Hildebrand solubility parameter ($MPa^{1/2}$)
ε	Porosity (-)
ϕ	Volume fraction (-)
Γ	Mass activity coefficient (-)
γ	Molar activity coefficient (-)
η	Viscosity (Pa.s)
μ	Chemical potential ($J.mol^{-1}$)
π	Osmotic pressure (Pa)
π^a	Osmotic pressure in terms of activity (Pa)
ρ	Density ($Kg.m^{-3}$)
ς	Film layer thickness (m)
τ	Tortuosity factor (-)
σ	Surface tension (-)

Subscripts

i, j,1,2	Species
$M, (m)$	Membrane
F,0	Feed side
P, l	Permeate side
p	Polymer
s	Solvent
sat	Saturation
sol	Solution
sw	Swollen
R	Retentate
t	Total
T	Constant temperature

Superscripts

m	Membrane
e	Equilibrium
F, f	Feed
p	Permeate
h	Hydrogen bonding
d	Dispersive forces
LV	Liquid-Vapour
SL	Solid-Liquid
SV	Solid-Vapour

1. Introduction

1.1 Overview

Liquid phase separations are common in the chemical, pharmaceutical and food industries. Unit-operations such as distillation and liquid-liquid extraction are some of the most popular traditional technologies employed in separating liquid mixtures. However, increased energy and downstream processing costs have driven research towards the development of more efficient and less energy-intensive processes. This has led to the development and use of separation processes involving membranes, which operate at much milder operating conditions when compared to traditional chemical engineering unit-operations. Such membrane-based processes can be classified into several categories depending on the type of driving force. The most common driving forces encountered are: pressure gradient (Reverse Osmosis (RO), Nanofiltration (NF), Ultrafiltration (UF) and Microfiltration (MF)), concentration gradient (Pervaporation, Vapour Permeation, Gas Permeation and Dialysis) and electrical gradient (Electrodialysis).

The industrial development of membranes dates back to the 60's with the implementation of the first water desalination plants based on reverse osmosis technology. Nowadays membranes play a key role in modern life and medicine. However their liquid phase applications are still mainly limited to separations in aqueous streams. The development of nanofiltration membranes for use in organic solvents has attracted much attention as they have potential applications in diverse areas, such as organometallic catalyst separation, solvent exchange, lube oil dewaxing etc. This creates a new opportunity for membrane technology, and a large expansion of membrane processes is expected in unexploited areas such as petroleum, electrochemical, pharmaceutical and fine chemical synthesis. Unfortunately, currently available OSN membranes have limited solvent compatibility and lifetime, and the central challenge for membrane technology is to produce membranes which are functionally stable in a broad range of organic solvents and at a variety of temperatures. Thus the search for efficient and cost-effective solvent and thermally resistant materials continues.

Several models have been formulated to describe the specie transport in aqueous NF/RO processes. These models can be classified into three main categories: solution-diffusion, pore-flow and irreversible thermodynamics based models. The solution-diffusion model approach (Londsdale et al., 1965) assumes a dense membrane, where the penetrating specie sorbs and diffuses through. The pore-flow approach (Sourirajan et al., 1965) assumes a membrane made of nanometer sized pores where the penetrating species flow through. Finally, the irreversible thermodynamic theory (Kedem and Katchalsky, 1958; Spiegler and Kedem, 1966) treats the membrane as a black box and uses phenomenological equations to describe specie transport. Although these models have been widely used in describing aqueous NF/RO systems, their applicability in organic solvent systems, where complex solvent-solute-membrane interactions take place, is still being explored.

1.2 Aim and Outline of this Thesis

This thesis is concerned with extending and testing the applicability of established aqueous nanofiltration principles to non-aqueous systems. The broad objectives can be summarized as follows:

(a) Understand the factors that determine solvent/solute transport through OSN membranes;

(b) Explore the applicability of literature aqueous transport models from the literature and develop a coherent OSN transport model, able to describe flux/rejection behaviour of flat-sheet/spiral-wound membrane systems;

(c) Develop a new approach to OSN modelling able to predict solvent fluxes by the use of model parameters determined from independent experiments.

Literature relevant to this study is reviewed in Chapter 2. This includes a description of OSN membrane types, OSN membrane characterization techniques and modelling of OSN based systems.

In Chapter 3, the performance of OSN membranes was evaluated for the permeation of binary solvent mixtures. Factors affecting OSN transport characteristics were assessed and

predictive solvent nanofiltration models based on the pore-flow and solution-diffusion approach were built.

In Chapter 4, the flux/rejection behaviour of OSN membranes was studied by using a solvent partially-rejected-solute model system. The effect of solute concentration in the flux/rejection profiles was assessed and the experimental results were fitted with solution-diffusion and pore-flow transport models coupled with film for liquid phase mass transfer. From the goodness of the fit insight was gained into the dominant transport phenomena present in these OSN systems.

In Chapter 5, a pilot plant apparatus was used to determine the flux/rejection behaviour of spiral-wound modules. An attempt to predict spiral-wound performance using membrane transport parameters derived from flat-sheet experiments was performed. The level of spiral-wound model complexity required to accurately describe OSN in spiral-wound elements was also assessed.

In Chapter 6, a new OSN transport model was developed. This model is able to predict solvent fluxes, by the use of model parameters determined from independent experiments and its predictive capability was tested against cross-flow solvent permeation data.

Finally, Chapter 7 provides a concluding discussion and highlights areas for further work.

2. Literature Review

2.1 Membrane Processes

Starting in the late sixties, membrane processes have gradually found their way into industrial applications and now serve as viable alternatives for more traditional processes such as distillation, evaporation or extraction. Many membrane processes can be distinguished based on the main driving force applied to accomplish the separation. An overview of the driving forces and the related membrane separation processes is given in Table 1.

Table 1: Driving forces and their related membrane separation processes.

Driving force	*Membrane process*
pressure difference	microfiltration, ultrafiltration, nanofiltration, reverse osmosis or hyperfiltration
chemical potential difference	pervaporation, pertraction, dialysis, gas separation, vapor permeation, liquid membranes
electrical potential difference	electrodialysis, membrane electrophoresis, membrane electrolysis
temperature difference	membrane distillation

Many textbooks have been written on the basic mechanisms and the various applications of these processes. Pressure driven membrane separation processes, electrodialysis, dialysis and gas separation are industrially implemented and are generally considered as proven technologies. Most of the other processes, however, are still in the development stage. This work will focus on pressure driven separation, more specifically nanofiltration (NF). The term nanofiltration was introduced at the end of the eighties to indicate an area of membrane technology, situated between ultrafiltration and reverse osmosis. In the literature nanofiltration is usually characterized by a membrane pore size between 0.5 and 2 nm, which corresponds to a molecular weight cut-off of approximately 300-500 $g.mole^{-1}$. The operating pressures used in this process are usually between 5 and 40 bar. NF is used to achieve a separation between sugars, other organic molecules and multivalent salts on one hand and monovalent salts and water on the other. In contradiction to the ideal situation where the ratio of pore size to particle size determines the selectivity of filtration, while the pore size and surface porosity of the membrane determines the hydrodynamic resistance and the permeability as a function of the pressure gradient NF is far from being completely

understood. Some authors (Bowen and Mukhtar, 1996) claim that the nano-pore scale induces interaction effects between solutes and the membrane material that will also influence the separation mechanism, but they also state that the calculation of these pore sizes does not necessarily mean that the pores really exist. Others (Wijmans and Baker, 1995) claim that the mechanism for NF transport is situated somewhere in a transient zone between the transport mechanisms of ultrafiltration and reverse osmosis.

2.2 Membranes

In order to fully understand a membrane separation process such as NF there is a need to understand the membrane itself. It is the membrane that has the ability to selectively transport one component of the feed phase over the other.

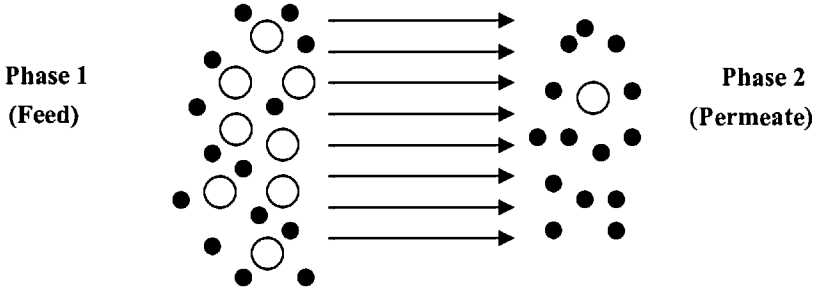

Figure 1: Schematic representation of a pressure driven membrane process.

The separation of the different species is based on physical/chemical interactions between the membrane and the components, resulting in a concentrated stream (retentate) and a diluted one (permeate).

2.2.1 Polymeric Membranes

Most polymeric OSN membranes have an asymmetric structure, and are porous with a dense top-layer. This asymmetry can be divided into two major types; the integral type, where the whole membrane is composed of the same material and the thin-film-composite (TFC) where the membrane separating layer is made of a different material.

Polymeric membranes generally fail to maintain their physical integrity in organic solvents because of their tendency to swell or dissolve. This is a major drawback since non-aqueous processes generally require polymers which are; rigid and crystalline, thermally stable, resistant to compaction, inert and non-swollen by solvents, and stable over long usage. Nevertheless, there are several polymeric materials that exhibit satisfactory solvent resistance. McCarthy (1985) states that "The chemical resistance of a polymeric material is its ability to withstand chemical attack with minimal change in appearance, dimensions, mechanical properties, and weight over a period of time" and is often interconnected with the thermal stability, i.e., factors that favour thermal stability often favour chemical stability as well. As a general rule the higher the glass transition temperature the more rigid the polymer, and the better its stability in solvents. Usually the factors that promote chemical stability are (Gebben, 1988):

- Aromatic or heterocyclic backbone structures, i.e., the presence of resonance structures.
- Absence of "reactive" groups such as unsaturated bonds, -OH groups, free -NH groups, aliphatic groups.
- Presence of high bond energies that cause strong chemical bonds, e.g., C-F, C-Si, C-P.
- Polybonding: atoms are linked to the polymer chain with two or more bonds, which implies that chains cannot be broken by the rupture of one single bond, e.g., in ladder polymers.

Some examples of classes of highly resistant polymers are presented in Table 2 (Critchley et al., 1983).

Table 2 : Classes of highly resistant polymers.

polymer class	stability promoted by	Examples
thermosetting	high cross linking density	phenol-formaldehyde resin
fluorinated	strong chemical bonds	polytetrafluorethylene
inorganic	strong chemical bonds	polyphosphazene, polysiloxane
aromatic	resonance stability	polyphenylene, aromatic polyamide
heterocyclic	resonance stability	polyimide, polybenzimidazole
ladder polymers	polybonding, resonance	polypyrrone

2.2.1.1 Integral Asymmetric Polymeric Membranes

Integral asymmetric polymeric membranes are prepared by the phase inversion immersion precipitation process. For this purpose, a solution of the polymer is cast as a thin film (usually on a nonwoven fabric), dried for a few seconds to create a dense top-layer, and immersed in a coagulation bath which contains a non-solvent for the polymer. The solvent starts to diffuse out of the homogeneous liquid polymer film, whereas the non-solvent diffuses into the film. Due to the presence of non-solvent, phase separation takes place in the polymer film and the polymer precipitates as a solid phase to form a porous asymmetric membrane structure. The thermodynamic properties of the casting system and the kinetics involved in the exchange of solvent and non-solvent affect the morphology of the membrane, and consequently its permeability and solvent rejection (Park et al., 2000). More detailed information about membrane preparation techniques can be found elsewhere (Mulder, 1997).

Few of the highly resistant polymers mentioned in 2.2.1 are suitable for producing integral asymmetric OSN membranes, mainly due to the fact that to perform the phase inversion the polymer needs to be soluble in at least one solvent. Some soluble commercially available polymers are polysulfone (PSF), polyethersulfone (PES), polyacrylonitrile (PAN), polyvinylidenefluoride (PVDF), polyetherimide (PEI) and BTDA-based polyimide (PI) (BTDA = benzophenone tetracarboxylic dianhydride). Several researchers have compared the chemical resistance of these polymers and the main conclusions are summarized in Table 3 (Beerlage et al., 1994).

Table 3 : Resistance of Soluble commercially available polymers.

Solvent class	PSF	PES	PAN[a]	PVDF	PEI	PI[b]
alcohols.	+	+	+/-	+	+	+
aliphatic h.c.	+	+	+	+	+	+
aromatic h.c.	-	+	+	+	-	+
ethers	-	+/-[c]	+	+	+/-[c]	+
esters.	-	-	+	-	+	+
ketones	-	-	+	-	+	+
aliphatic acids.	+	+	+	+	-	+/-[d]
amides	-	-	-	-	-	-
halogenated h.c.	-	-	+	+	-	+

a: pure polyacrylonitrile
b: soluble BTDA-copolyimide: P84 / PI 2080
c: not stable in tetrahydrofuran
d: stable in aqueous dilutions, not stable in concentrated acid
h.c: hydrocarbons
+: stable, no visible change
-: not stable, highly swollen or soluble

The information presented in Table 3 suggests PAN and PI as solvent resistant polymers. Both polymers can be processed by the phase inversion technique. PIs are commonly used for integral asymmetric NF membranes preparation, and will be addressed in this section. PAN is mainly associated with the preparation of integral asymmetric ultrafiltration (UF) membranes and consequently serves as a support for composite NF membranes to be discussed in the next chapter.

PIs are made by the reaction of diamines (DA) with dianhydrides, to form the soluble polymer precursor known as poly(amic acid). This can then be processed converting it into the final PI by cyclodehydration of the amide-acid (imidization). Figure 2 shows the mechanism for the pyromellitic dianhydride (PMDA) case.

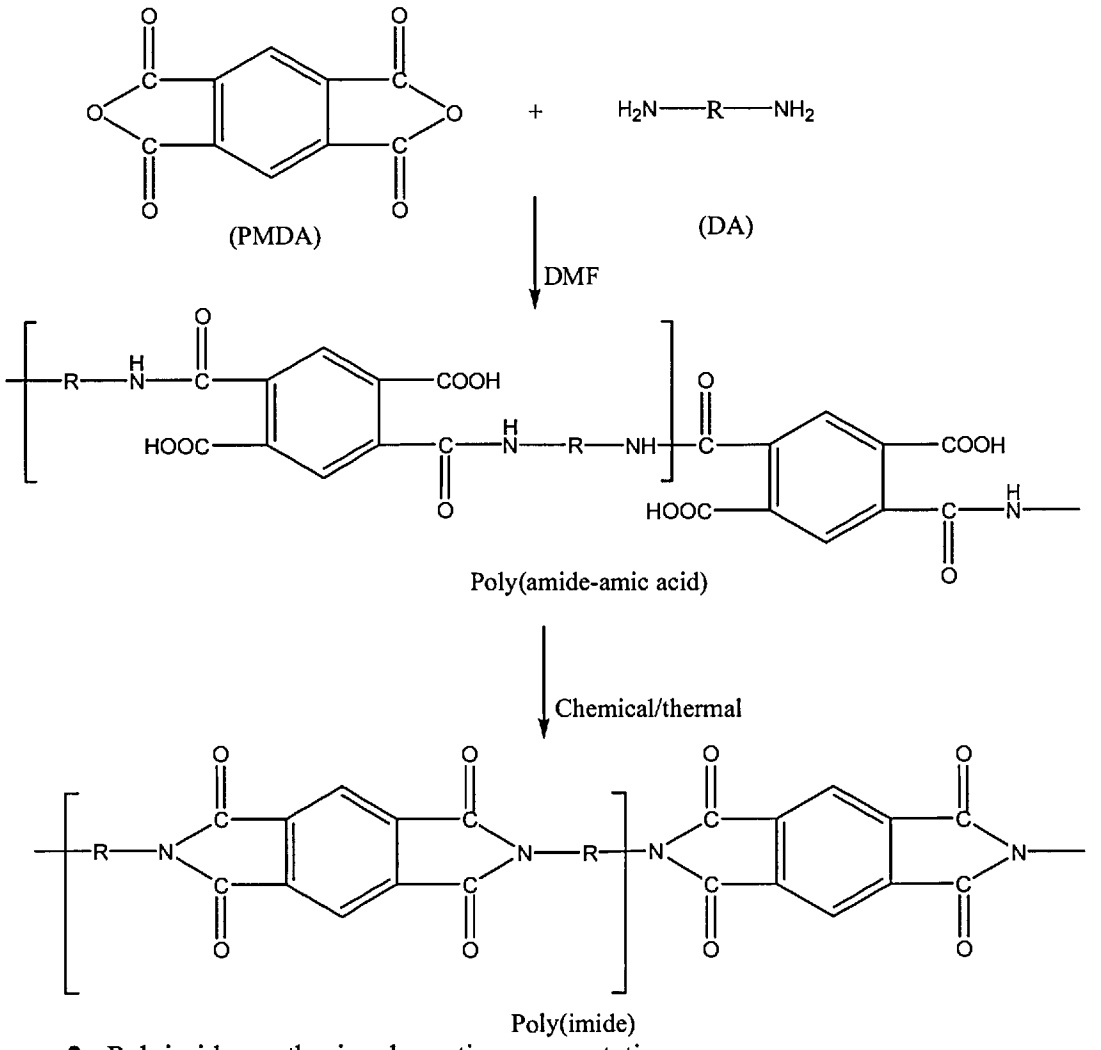

Figure 2 : Polyimide synthesis schematic representation.

Some of the most common commercially available PIs used for forming integral asymmetric polymeric OSN membranes are shown in Table 4.

Table 4 : Commercially available soluble polyimides.

Polymer	Chemical Structure
P 84 (Lenzing) BTDA-TDI/MDI soluble in amides	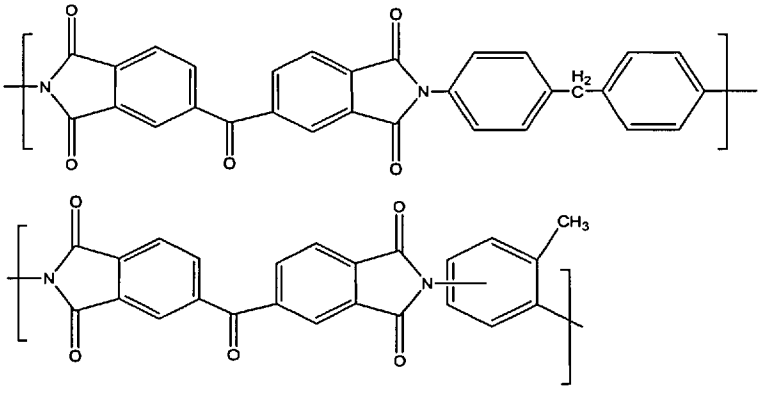
Matrimid 5218 (Ciba Geigy) BTDA-AAPTMI soluble in amides, chloroform and THF	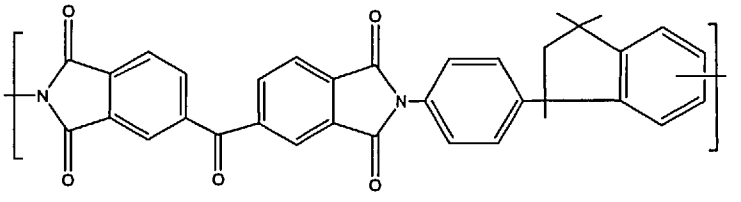
Sixef-44 (Hoechst Celanese) 6FDA-6FipDA soluble in amides, THF chloroform and acetone	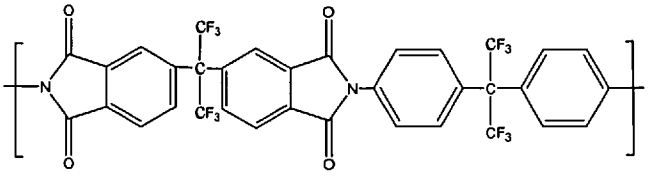
Kapton® HN (DuPont) PMDA-ODA soluble in amides and THF	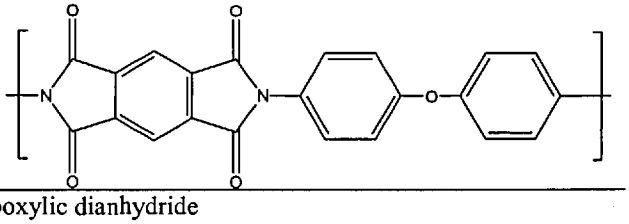

BTDA:	benzophenone-3,3',4,4'-tetracarboxylic dianhydride
TDI:	toluene diisocyanate
MDI:	4,4'-methylene bis(phenyl isocyanate)
AAPTMI:	5(6)-amino-1-(4'-aminophenyl)-1,3-trimethylindane
6FDA:	5,5-[2,2,2-trifluoro-1-(trifluoromethyl)-ethylidene]-bis-1,3-isobenzofuranedione
6FipDA:	hexafluoro-2,2-bis(4-aminophenyl)propane
PMDA:	pyromellitic dianhydride
ODA:	4,4'-oxydianiline

There are several published examples of OSN membranes based on PIs:
(Strathmann, 1978) developed solvent stable membranes based on PDMA-ODA (by reacting benzidine with pyromellitic anhydride). For increased solvent/thermal resistance these membranes were cyclized with N,N-dicyclohexylcarbodiimide. After all processing steps the membranes were able to withstand 50 days exposure to dichloromethane and cyclohexane without loss of mechanical stability. Alegranti (1978) developed OSN membranes by a similar procedure, differing only in the cyclization step. At 5.5 MPa these membranes could perform hexane/ethanol (50 %/50 %) mixture separation (75 % ethanol in the permeate).

Matrimid 5218 based OSN membranes were developed for lube oil separation (White et al, 1993), and were able to achieve 96 % lube oil rejection and 12.9 $L.m^{-2}.h^{-1}$ solvent flux for a blend of methyl ethyl ketone (MEK) and toluene at 4.1 MPa and 263 K. These are the first OSN membranes employed in a commercial plant installation at Mobil's Beaumont, Texas refinery.

2.2.1.2 Thin-Film-Composite (TFC) Membranes

Composite membranes consist of at least two different materials. Usually, a selective membrane material is deposited as a thin layer upon a porous sub-layer which serves as support. The advantage of this kind of membrane over the integrally skinned ones is that each layer can be optimised independently in order to achieve the desired membrane performance. There are several well established techniques to apply a thin top layer upon a support: dip-coating, spray coating, spin coating, interfacial polymerisation, in-situ polymerisation, plasma polymerisation and grafting. Details of these techniques can be found elsewhere (Mulder, 1997). Due to the large variety of preparation techniques almost all polymeric materials can be used to produce this kind of membrane. The top layer and the support both contribute to the overall performance. High solvent resistance makes PAN a good support material for TFC membranes as can be seen from the following examples.
Preparation of crosslinked PAN supports has been reported in the literature by Peinemann et al. (2001), when an epoxidized PAN copolymer was subjected to ammonolysis providing highly solvent stable (including stability in dimethylformamide (DMF)) supports. A highly solvent resistant UF membrane based on poly(acrylonitrile-co-glycidyl methacrylate)

(PANGMA) was reported (Hicke et al., 2002). This membrane was prepared by phase inversion followed by ammonolysis and was also stable in DMF, thus being a very attractive support for preparation of OSN-TFC membranes.

Composite membranes made of a support layer of PAN (10-80 μm thick), and a top, thermally cross-linked, elastomeric barrier layer of an adduct of maleic acid anhydride and a poly(aliphaticterpene) have also been reported for lube oil dewaxing (Pasternack, 1993). These membranes were able to achieve 87.2 % lube oil rejection and 58.3 $kg.m^{-2}.h^{-1}$ fluxes at 5.5 MPa and 298 K. PAN homopolymers or copolymers cross-linked with acids or bases, functionalized with amino, hydroxyl or carboxylic groups and coated with an additional hydrophilic or polyelectrolyte polymer layer have been synthesised (Linder et al., 1991).The resultant composite membrane was stable in solvents such as DMF, methylethyl ketone and dichloromethane and could achieve fluxes of 147.5 $L.m^{-2}.h^{-1}$ and 99 % congo-red dye rejections at 2.9 MPa and room temperature. Polydimethylsiloxane is extensively used in OSN applications as TFC membrane top layer, and dewaxing solvents were separated from dewaxed oils by non-porous silicone rubber membranes cross-linked with polyisocyanates, polyacidchlorides or silanes (Pasternack, 1992). At 5.5 MPa and 298 K these membranes were able to achieve 88.7 % rejections and 37.1 $kg.m^{-2}.h^{-1}$ fluxes.

2.2.2 Inorganic Membranes

Due to the upper temperature constraint for polymeric based membranes (Mulder, 1997), there is a growing market for membranes based on solvent resistant materials able to withstand high temperatures. Ceramic materials (silicium carbide, zirconium oxide, titanium oxide) endure harsh temperature conditions and show stable performance in solvent medium, and so are excellent materials for membrane preparation. On that basis a new generation of OSN membranes have been developed, the inorganic composite membranes.

Inorganic membranes with the stable, defect-free nano-pore structure required for OSN are prepared by the sol-gel process. Two different routes are widely used (Figure 3), the colloidal gel route and the polymeric gel route. Both of these routes start with an alkoxide

precursor that is hydrolysed and polymerized. The drying of the gel structures is regarded as the critical step and the calcination temperature determines the membrane pore size.

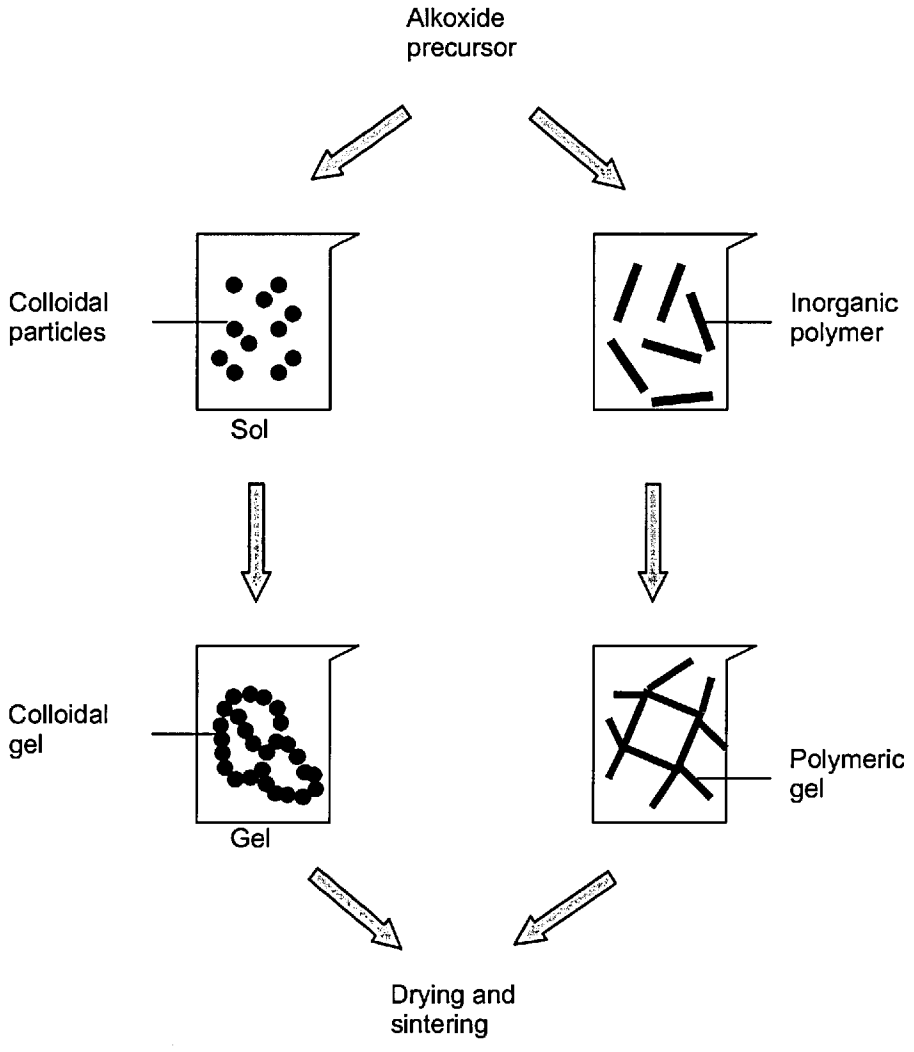

Figure 3 : Inorganic membrane preparation by the sol-gel process.

Porous OSN membranes (1-4 nm pore size) were prepared from silica-zirconia colloidal sols, by the sol-gel processes (Tsuru et al., 2001). Pore size control for these membranes was possible by appropriate choice of the colloidal particle size. These membranes were tested in non-aqueous solutions of ethanol and methanol. At 323 K and 1.5 MPa the pure methanol flux was 28.8 $L.m^{-2}.h^{-1}$ and a 200 Da polyethylene glycol rejection of 40 % was obtained.

One major drawback of the inorganic membranes has been their relatively high MWCO > 1000 Da, which makes them unsuitable for nanofiltration type separations. However,

recently inorganic membranes with a MWCO < 500 Da have been reported in the literature, although this rejection has been determined in aqueous solution for a mixture of PEGs (Puhlfurb et al., 2000; Weber et al., 2003). Table 5 summarises some of the reported performance data for the OSN membrane types mentioned above.

Table 5 : OSN performance data.

Membrane/material	Solute/solvent system	Permeability ($Lm^{-2}h^{-1}bar^{-1}$)	Separation factor*/rejection#	Reference
MPF-44 (KOCH)	Safranin(0.01%)/methanol	0.34	67.6%#	Whu et al., 2000
	Solvent blue (35mg/l)/methanol	0.19	85.0%#	Yang et al., 2001
MPF-60 (KOCH)	Safranin (0.01%)/methanol	0.50	86.9%#	Whu et al., 2000
	Solvent blue (35mg/l)/methanol	0.13	81%#	Yang et al., 2001
MPF-50 (KOCH)	Vitamin-B12 (0.01%)/methanol	0.98	89.0%#	Whu et al., 2000
	Methanol	1.24	-	"
	Octane	11.63	-	Machado et al., 1999
	Methanol	5.83	-	"
	Pentanol	1.03	-	"
	Acetone(40% molar)/propanol	6.67	1*	"
	Pentane (40% molar)/acetone	16.67	1*	"
	Ethanol	6.35	-	Van der Bruggen et al.,
	n-hexane	46.3	-	2002
Matrimid-5218(Ciba-Geigy)	Lube-oil (20%)/methyl ethyl ketone-toluene	0.11	99.0%#	White et al., 2000
Lenzing P84 (HP polymers)	*n*-decane (2%),	0.86	44.0%#	"
	1-methylnaphthalene (2%),		1.0%#	"
	n-hexadecane (2%),		79.0%#	"
	1-phenyl undecane (2%),		66.0%#	"
	pristine (2%),		95.0%#	"
	n-docosane (2%)/toluene (88%)		92.0%#	"
STARMEM™ 122	Jacobsen catalyst(1.2mM)/THF	2.73	96.0%#	Scarpello et al., 2002
	Jacbsen catalyst(1.2mM)/EA	4.24	99.0%#	"
PDMS-PAN	n-hexane	8.41	-	Robinson et al., 2004
	n-heptane	7.00	-	"
	i-hexane	7.80	-	"
	i-heptane	6.25	-	"
	i- octane	4.66	-	"
	Cyclohexane	3.66	-	"
	Xylene	4.90	-	"
	Sunflower oil(0%)/hexane	3.70	-	Stafie et al., 2004
	Sunflower oil(8%)/hexane	2.40	88%	"
	Sunflower oil(19%)/hexane	1.80	84%	"
	Sunflower oil(30%)/hexane	1.10	82%	"
Silica-zirconia	Methanol	1.92	-	Tsuru et al., 2001
	Polyethylene glycol(MW=200)		40%	"

2.3 OSN Membrane Characterization

For microfiltration and ultrafiltration membranes, where clearly defined pores are present in the membrane structure, characterization techniques focus on pore size determination and on assessing the characteristics of the pore network. In reverse osmosis, where membranes are usually dense films characterization techniques focus on membrane surface analysis, polymer nature and type of interactions between polymer and permeating species. In nanofiltration there is still some controversy on whether the membrane structure is dense or composed by nano-sized pores, therefore many pore membrane and dense membrane characterization techniques are applied to nanofiltration membrane characterization. Most

of these characterization techniques, for porous and dense membranes, are well established for aqueous processes and their main characteristics can be found in the literature (Mulder, 1997).

In this work there is an interest for characterization techniques that allow prediction/interpretation of membrane performance. Therefore this work will focus on techniques that can assess one of the most important factors determining permeation through OSN membranes: the membrane-solvent interaction.

2.3.1 Flory-Huggins Interaction Parameter

One of the foremost parameters to represent polymer-solvent interactions is the Flory-Huggins parameter or the χ (chi) parameter. Polymer solutions have unique thermodynamic properties and one of the first theories to account for such differences was the Flory-Huggins theory (Danner et al., 1993). The activity of the penetrant inside the polymer for a binary system according to the Flory-Huggins theory can be given as (Mulder, 1997):

$$\ln a_i = \ln \phi_i + \left(1 - \frac{V_m}{V_p}\right)\phi_p + \chi \phi_p^2 \qquad (1)$$

where, a_i is the activity of the penetrant molecule, ϕ_i is the volume fraction of the species, V_m is the molar volume of the solvent and V_p is the molar volume of the polymer. The χ parameter gives a qualitative estimate of the type of interactions possible between the polymer and the solvent. Some guidelines proposed for the χ values are as follows (Danner *et al.*, 1993; Mulder, 1997): A value of χ which is > 2 is considered large and in this case the magnitude of interactions are small between the chosen pair of polymer and the solvent. On the other hand for χ values between 0.5 and 2, the interactions are high between the polymer and the solvent and high permeabilities exist. However, for χ values < 0.5, the interactions are very large and the polymer and the solvent are compatible often leading to solvation between the two. Thus for the permeation of such solvents, a high degree of cross-linking would be required to cause maximum interaction without extensive swelling

of the polymeric membrane. Several methods have been used in literature to obtain the chi parameters between polymer-solvent systems. The direct method uses the Flory-Huggins equation and some indirect methods are based on: using the Hildebrand solubility parameter approach, inverse gas chromatography and precipitation values determined during membrane formation.

2.3.1.1 Determining (χ) using Flory-Huggins

Sorption capacity of the polymer for a solvent can be directly related to its interaction with the solvent. This is the approach of the Flory-Huggins theory to determine the χ parameter. The equation used for this approach can be derived simply from using the Flory-Huggins theory for binary systems, Eq. (1), setting the activity of the solvent equal to unity (pure solvent) and assuming that the molar volume of the penetrating specie is much smaller than the molar volume of the polymer. The resulting equation can be given by:

$$\chi = -\frac{\ln(1-\phi_p)+\phi_p}{\phi_p^2} \tag{2}$$

in the above formula the ϕ_p is the volume fraction of the polymer and can be obtained by using sorption experiments. Kim et al. (1997) have compared the values obtained by sorption studies to values obtained in literature. For example, the measured value for polysulfone-water system was 4.0 and that obtained using the Flory-Huggins approach was about 3.7. Thus, it can be seen that there is good agreement between the values thus validating the method.

2.3.1.2 Determining (χ) by the Hildebrand Solubility Parameter Approach

The chi parameter can be obtained from Hildebrand solubility parameters as follows (Danner et al., 1993; Van Kreleven, 1990):

$$\chi = \chi_S + \chi_H = \chi_S + \frac{V_1(\delta_1 - \delta_m)^2}{RT} \quad (3)$$

where χ_S and χ_H are the entropic and enthalpic contribution respectively. The entropic contribution, (χ_S), is generally the inverse of the coordination number for the lattice structure, which is found to be between 0.3 and 0.4 (Danner et al., 1993; Van Kreleven, 1990). The δ's are the Hildebrand Solubility parameters and these can be determined from group contribution methods (Sourirajan et al., 1985) for the solvent (1) and the polymer (m). Similar solubility parameters indicate a good compatibility of the polymer and the solvent.

The Hildebrand solubility parameter approach is a very simple one-parameter model for predicting the interaction parameter.

2.3.2 Membrane Surface Energy

Polymer-solvent interactions can be accounted for by using the chi parameters or the solvent-uptake values as has been shown above. However, an indirect measure of the level of interaction can also be obtained by using certain membrane properties. Surface energy, σ^{SV} for a membrane/polymer (analogous to the surface tension of a solvent), for example, can be used as an indirect measure of the hydrophilicity/hydrophobicity of the membrane material. Such values for a membrane or any solid surface can be measured using indirect techniques such as direct force measurements, contact angles and capillary penetration (Kwok and Neumann, 1999). Use of contact angles is a common method employed for measuring the membrane surface energy. Young's equation can be utilized to relate the contact angle to the three surface tension values of the system viz. the solid-liquid surface tension (σ^{SL}), the solid-vapour surface tension (σ^{SV}) and the liquid-vapour surface tension (σ^{LV}).

Figure 4 shows the definition of contact angle along with those for the individual surface tension.

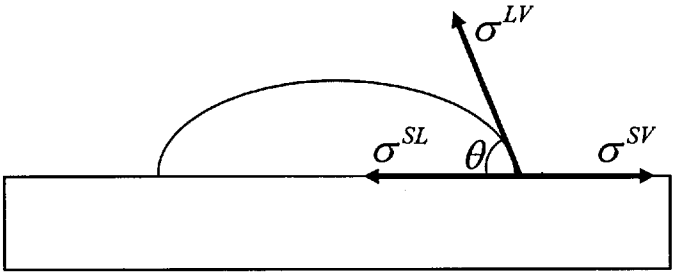

Figure 4 : Contact angle with surface tension components.

It is evident that the contact angle is definitely a function of the membrane and solvent type. Young's equation relates the three values as:

$$\sigma^{LV}\cos\theta = \sigma^{SV} - \sigma^{SL} \tag{4}$$

θ = Advancing contact angle between the solid and the liquid. Among these three values, the liquid-vapour surface tension values can be easily obtained through curvature analysis of pendant drops. The solid-liquid surface tension values σ^{SL} can be estimated through the use of several available theories, but the solid-vapour value, σ^{SV} which is essentially a constant, needs to be determined from a series of contact angle measurements for various liquids. Qualitatively, one can say that the lower the contact angles the higher the wetting ability of the solvent for the membrane.

The relevant equations based on the method proposed by Fowkes (1964), Owens and Wendt (1969) will be used to calculate the membrane surface energies:

$$\left(\sigma_d^{LV} + \sigma_p^{LV}\right)(1+\cos\theta) = 2\sqrt{\sigma_d^{LV}\sigma_d^{SV}} + 2\sqrt{\sigma_p^{LV}\sigma_p^{SV}} \tag{5}$$

by measuring the contact angles of two different liquids on the membrane surface the membrane's surface tension value can be derived. The two solvents commonly used for this method are water (polar solvent) and diiodomethane (apolar solvent). Table 6 presents the main characteristics of these solvents.

Table 6 : Properties of the solvents used in contact angle experiments.

Properties*	Water	Diiodomethane
Purity (%)	deionised	> 99
σ^{LV} (mJ.m^{-2})	72.8	50.8
σ_d^{LV} (mJ.m^{-2})	21.8	50.8
σ_p^{LV} (mJ.m^{-2})	51.0	0.0

* - Owens and Wendt (1969)

One could easily visualize the use of such interfacial tension values between the solvent and the polymeric material as a measure of the interaction; however, a finite contact angle needs to be obtained for the estimation. For systems where the solvent has a high level of interaction with the polymer and completely wets it the measurement of a contact angle is difficult, making this an inherent disadvantage of the technique.

2.3.3 Determination of Polymer Swelling

Swelling is a measure for the volume of liquid absorbed by the membrane and is defined as:

$$SW_i = \frac{1}{\rho_i} \frac{W_{eq} - W_{dry}}{W_{dry}} \tag{6}$$

with SW_i the degree of polymer swelling for a solvent i, ρ_i the solvent density, W_{eq} the weight of a wet polymer sample at equilibrium and W_{dry} the weight of the dry polymer sample. According to the procedure of Ho and Sirkar (1992), swelling is measured by immersion of the polymer sample in the organic solvent for 48 h. After wiping dry, the samples are weighed and then dried in a vacuum oven during 24 h, until a constant mass of the dry membrane is achieved. However, since most of the steps in the experimental procedure are not conducted under a controlled environment, this technique is subject to significant experimental errors. In an attempt to eliminate experimental errors, the dynamic vapour sorption technique (DVS) has been used in this work, to determine liquid polymer swelling, knowing that thermodynamics dictates that if a component in the vapour phase and liquid phase possess the same activity, the chemical potential of the two states is equal

and since the chemical potential is the driving force for sorption, the amount of penetrant sorbed into a polymer for a given activity will be the same whether it is being fed from the liquid or vapour state. This allows the use of vapour sorption to determine the sorption isotherms and apply them to a liquid separation (Rezac et al., 1997), which is quite useful due to the comparative ease of gathering accurate sorption data of vapours versus liquids. In this DVS method, a sample is exposed to the solvent vapour at a constant partial pressure and the kinetics of sorption and solubility of the solvent in the sample are determined by observing the rate of weight gain. The weight of the sample is measured by a computer-controlled microbalance that is connected to a vacuum system. The measurement of swelling for commercial membranes is complicated by the multilayer structure. In this work it is considered that the swelling of the porous backing and membrane's asymmetric structure have little influence on the membrane performance, therefore the swelling is measured for dense polymer films that simulate the characteristics of the membrane's top layer.

2.4 Modelling of Organic Solvent Nanofiltration - Solvents

Although aqueous nanofiltration systems have been studied for several years and much knowledge has been gained, OSN systems are not yet well understood. While some studies support the use of pore-flow models, others suggest using a solution diffusion approach. The derivation of these models is outlined below along with the major simplifying assumptions:

2.4.1 Pore-Flow Model

Stable pores are assumed to be present inside the membrane and the driving force for the transport is the pressure gradient across the membrane. Assuming a system at constant temperature where there are no external forces except pressure we can write from the Stefan-Maxwell equations (Thiel and Lloyd, 1988):

$$-x_{i(m)}\nabla_{T,p}\mu_i - x_{i(m)}\overline{V}_i\nabla p = \sum_k \zeta_{i,k}\frac{\left(x_{k(m)}N_i - x_{i(m)}N_k\right)}{c_{t(m)}\dfrac{\varepsilon}{\tau}} + \zeta_{i,m}\frac{N_i}{c_{t(m)}\dfrac{\varepsilon}{\tau}} + \alpha_i\frac{\zeta_{i,m}x_{i(m)}\beta_0}{\eta}\nabla p \qquad (7)$$

considering the pressure gradient contribution to the transport to be much more significant than the activity gradient Eq. (7) can be simplified to:

$$-x_{i(m)}\overline{V}_i\nabla p-\alpha_i'\frac{\zeta_{i,m}x_{i(m)}\beta_0}{\eta}\nabla p=\sum_k\zeta_{i,k}\frac{\left(x_{k(m)}N_i-x_{i(m)}N_k\right)}{c_{t(m)}\frac{\varepsilon}{\tau}}+\zeta_{i,m}\frac{N_i}{c_{t(m)}\frac{\varepsilon}{\tau}} \tag{8}$$

another reasonable assumption is to consider that the friction of a chemical specie (e.g. solvent) with the membrane is much higher than the friction between species, so we can write:

$$x_{i(m)}\overline{V}_i\nabla p+\alpha_i'\frac{\zeta_{i,m}x_{i(m)}\beta_0}{\eta}\nabla p=-\zeta_{i,m}\frac{N_i}{c_{t(m)}\frac{\varepsilon}{\tau}} \tag{9}$$

usually the first term in the left side of Eq. (9) is much lower than the second due to the small value of the species partial molar volume, so it is reasonable to write:

$$N_i=-\alpha_i'\frac{c_{i(m)}\beta_0}{\eta}\frac{\varepsilon}{\tau}\nabla p \tag{10}$$

for small permeating species in relation to the pore size the viscous selectivity is one and the total volume flux is given by (Thiel and Lloyd, 1988):

$$N_v=-\frac{\beta_0}{\eta}\frac{\varepsilon}{\tau}\nabla p \tag{11}$$

in Eq. (11) β_0 is the specific permeability and depends on membrane structure. If the membrane is composed of more or less cylindrical pores we get the Hagen-Poiseuille equation:

$$N_v = -\frac{d_{pore}^2}{32\eta}\frac{\varepsilon}{\tau}\nabla p \tag{12}$$

on the other hand if the membrane consists of a packed bed of particles we get the Carman-Kozeny equation (Thiel and Lloyd, 1988):

$$N_v = -\frac{d_{particle}^2}{180(1-\varepsilon)^2\eta}\frac{\varepsilon^3}{\tau}\nabla p \tag{13}$$

2.4.2 Solution-Diffusion Model

In the solution-diffusion model, it is assumed that each permeating molecule dissolves in the membrane phase and diffuses through the membrane in response to the concentration gradient. There is no pressure gradient inside the membrane and the Stefan-Maxwell equivalent of Eq. (7) for this kind of system is:

$$-x_{i(m)}\nabla_{T,p}\mu_i = \sum_k \zeta_{i,k}\frac{\left(x_{k(m)}N_i - x_{i(m)}N_k\right)}{c_{t(m)}} + \zeta_{i,m}\frac{x_m N_i}{c_{t(m)}} \tag{14}$$

assuming again that the friction between species has a much smaller magnitude than the friction of species with the membrane itself Eq. (14) becomes:

$$-x_{t(m)}\nabla_{T,p}\mu_i = \zeta_{i,m}\frac{x_m N_i}{c_{t(m)}} \tag{15}$$

neglecting kinetic coupling and approximating the gradient of chemical potential with a molar fraction gradient, Eq. (15) is simplified to:

$$N_i = -\frac{c_{i(m)}}{x_m \zeta_{i,m}} \nabla x_{i(m)} \tag{16}$$

integrating the one dimensional version of Eq. (16) over membrane thickness with the proper boundary conditions for chemical potential, constant x_m and assuming the activity coefficient for each penetrant inside the membrane remains constant (Peeva et al., 2004), the following equation is obtained (the detailed derivation of this model can be found in Appendix I):

$$N_i = P_{im}^{molar}\left(x_{if} - \frac{\gamma_{ip}}{\gamma_{if}} x_{ip} \exp\left(-\frac{\overline{V}_1 \Delta p}{RT}\right)\right) \tag{17}$$

the above equation assumes that the swelling of the membrane separating layer is negligible, and is similar to the well known equation presented by Wijmans and Baker (1995), differing only by the ratio of $\frac{\gamma_{ip}}{\gamma_{if}}$ which has been shown to be important when there are significantly different concentrations on each side of the membrane. For cases where the membrane layer is a rubbery layer, the assumption of low swelling is unlikely to be true and in fact the membrane will often be highly swollen - in that case the analysis developed by Paul through a series of papers in the 1970s and recently reformulated (Paul, 2004) is more appropriate.

Both pore-flow and solution-diffusion models have been used in previous work. Robinson et al. (2004) reported that their experimental data for the permeation of *n*-alkanes, *i*-alkanes and cyclic compounds in a polydimethylsiloxane (PDMS) composite OSN membrane was well consistent with the Hagen-Poiseuille pore-flow model Eq. (12). Whu et al. (2000) also suggest this pore-flow model for fluxes through the commercial OSN membrane MPF-60 (Koch Membrane Systems). The membranes employed in both papers comprised rubbery materials attached to a support, and at least in the case of Robinson et al. (2004) were highly swollen under operation. Application of the Hagen-Poiseuille model implies that a pressure gradient exists across the thin PDMS layer. The careful argument presented by Paul (1970) based on mechanics, suggests that such a pressure gradient is not possible in a

swollen rubber phase, and so the exact physical picture in the pore-flow interpretation of the data of (Whu et al., 2000; Robinson et al., 2004) is not clear.

Bhanushali et al. (2001) suggested that solvent viscosity and surface tension are dominant factors controlling solvent transport through NF membranes, and a solution-diffusion approach was proposed to predict pure solvent permeation. Stafie et al. (2004) employed the solution-diffusion model to describe sunflower oil/hexane and polyisobutylene/hexane permeation through a composite PDMS membrane with poly(acrylonitrile) (PAN). Some of the work reported by Bhanushali et al. (2001) and all of the data presented by Stafie et al. (2004) employs rubber based membrane separation layers, for which the swollen rubber models of Paul are probably more appropriate than the simple solution-diffusion model actually employed based on Wijmans and Baker (1995).

White (2002) investigated the transport across a series of asymmetric polyimide OSN membranes with normal and branched alkanes, and aromatic compounds. His experimental results were consistent with the solution-diffusion model presented by Wijmans and Baker (1995). Since polyimides are reported to swell by less than 15 %, and usually considerably less, in common solvents (Beerlage, 1994) the simple solution-diffusion model (Wijmans and Baker, 1995) can be used. However, the solution-diffusion model assumes a discontinuity in pressure profile at the downstream side of the separating layer. When the separating layer is not a rubbery polymer coated on to a support material, but is a dense top layer formed by phase inversion, as in the polyimide membranes reported by White (2002), it is not clear where this discontinuity is located, or whether it will actually exist.

Finally, some authors have attempted to find simple membrane/solvent property based models able to describe OSN performance. Machado et al. (2000) were the first to develop a membrane/solvent property based model for the permeation of pure solvents and solvent mixtures through OSN membranes. These authors developed a resistances-in-series model and proposed that solvent transport through the MPF-50 (Koch Membrane Systems) membrane consists of three main steps: (1) transfer of the solvent into the top active layer which is characterised by surface resistance; (2) viscous flow through NF pores and (3) viscous flow through support layer pores, all expressed by viscous resistances, i.e.:

$$N_v = \frac{\Delta p}{R_s^0 + R_\mu^1 + R_\mu^2} \tag{18}$$

where R_s^0, R_μ^1 and R_μ^2 are the surface resistance (proportional to the membrane-solvent surface tension difference) and viscous resistances (proportional to the solvent viscosity) through the NF active layer and the support layers, respectively. The surface resistance is proportional to the surface tension difference between the solvent and the OSN membrane top layer, and viscous resistances are proportional to solvent viscosity.

Bhanushali et al. (2001) derived the following relation for solvent flux through OSN membranes, starting from a solution-diffusion basis:

$$N_i \approx \left(\frac{\overline{V_i}}{\eta_i}\right)\frac{1}{\phi_i^n \sigma_m} \tag{19}$$

where $\overline{V_i}$ is the solvent molar volume, η_i its viscosity, ϕ_i the solvent sorption value, σ_m the membrane surface tension value, and n an empirical constant.

Recently Geens et al. (2006) questioned the inverse correlation of flux with sorption proposed by Bhanushali et al. (2001), and replaced the product of sorption and membrane surface tension in Eq. (26) by a single parameter describing solvent-membrane affinity, the difference in surface tension between the liquid solvent and the solid membrane surface:

$$N_i \approx \left(\frac{\overline{V_i}}{\eta_i}\right)\frac{1}{\sigma_m - \sigma_i} \tag{20}$$

besides showing a good fitting capability for hydrophilic solvent permeation through hydrophilic membranes, significant improvement was found in fitting hydrophilic solvent permeability through hydrophobic membranes. The broad applicability of this semi-empirical model for solvent permeability through OSN membranes seems to indicate that

solvent flux depends on viscosity, molecular size and the difference in surface tension between the membrane and the solvent.

These models can be used to gain insight into the transport processes, and also for design calculations. While most of the above mentioned references have focussed on the former use, in this work the main concern is the latter, i.e. the design problem of how to best predict fluxes from over a wide range of solvent mixtures from a limited data set of the pure solvent fluxes. Therefore, it is desirable to have confidence in the predictive power of the models. However, in the last chapter a physically meaningful model, able to describe solvent fluxes and able to justify the applicability of Eq. (18) to (20), will be derived.

2.5 Modelling Organic Solvent Nanofiltration - Solutes

2.5.1 Irreversible Thermodynamics Based Models

The key assumption in models based on the concept of irreversible thermodynamics (IT) is that the membrane is not far from equilibrium. The basic premise of this model is that the flux of the components is affected by the other permeating components. As stated in Appendix I we can write:

$$N_i = -\sum_j L_{ij}^c \frac{d\mu_j}{dz} \tag{21}$$

Kedem and Katchalsky (1958) proposed one of the early models based on this approach. They assumed that solvent and the solute fluxes were linked by a coupling coefficient called the Staverman reflection coefficient.

$$N_v = \frac{L_p}{\Delta z}\left(|\Delta p| - \sigma|\Delta \pi^a|\right) \tag{22}$$

$$N_{solute} = \frac{w}{\Delta z}|\Delta \pi^a| + \langle c_{solute(m)}\rangle(1-\sigma)N_v \tag{23}$$

where, L_p and w are phenomenological coefficients, $\langle c_{solute(m)} \rangle$ is the average solute concentration in the membrane and σ is the Staverman reflection coefficient. The inherent disadvantage of this model is that the phenomenological coefficients were concentration dependent. To avoid this dependence, the Spiegler-Kedem model (Jagur-Grodzinski and Kedem, 1966) was developed which also considered the convective coupling aspects of the solute transport. The Spiegler-Kedem model assumes that the solute flux is a combination of diffusion and convection (Gilron *et al.*, 2001; Burghoff *et al.*, 1980; Jagur-Grodzinski and Kedem, 1966).The relevant Spiegler-Kedem model equations are present in Table 29 Appendix I, if we simplify the osmotic pressure gradient by using the dilute solution approach, we can write:

$$N_{solute} = \overline{P}\frac{dc}{dz} + \langle c_{solute(m)} \rangle (1-\sigma) N_v \tag{24}$$

where $\overline{P}$, is the local solute permeability. For the observed rejection we can write:

$$OR = \frac{(1-F)\sigma}{1-\sigma F} \tag{25}$$

where:

$$F = \exp\left[-\frac{N_v(1-\sigma)}{P_s}\right] \text{ and } P_s = \frac{\overline{P}}{\Delta z} \tag{26),(27}$$

this type of model can be easily used after determining the two model parameters, using permeation and rejection data for the specific solvent-solute system. It is a black box approach to transport, being incapable of giving us deep insight into the mechanism determining membrane permeation; therefore, we will not use this kind of approach in this work.

2.5.2 Solution-Diffusion Model

In the previous section it was outlined the general membrane transport models and derived the solution-diffusion model, showing the major simplifying assumptions. In solvent-solute systems, the solution-diffusion expression used for the solute remains the same:

$$N_i = P_{im}\left(x_{if} - \frac{\gamma_{ip}}{\gamma_{if}} x_{ip} \exp\left(-\frac{\overline{V}_i \Delta p}{RT}\right)\right) \tag{28}$$

here the solute and solvent fluxes are dependent on their specific permeability values.

2.5.3 Pore-Flow Model

The pore-flow expression for solvent-solute systems cannot remain the same as the one used for solvent permeation, as we are now working with rejected species for which viscous selectivity becomes important. In recent pore-flow models (Nakao, 1994) it is assumed that the thermodynamic forces driving the solute and solvent, which are gradients of their chemical potential, are counterbalanced by mechanical frictional forces. Expressions for these frictional forces are derived from the sphere in a tube analogy (Deen, 1987). The first generation of these pore-flow models (Nakao, 1994; Bowen et al., 1997) relied on two parameters to describe uncharged solute rejection: r_p and $\Delta x / A_k$, with r_p as the membrane pore radius and $\Delta x / A_k$ as the effective ratio of membrane thickness to porosity. However, by including the effects of pressure on chemical potential, and hence on solute transport, Bowen and Welfoot (2002) were able to describe the variation of uncharged solute rejection with effective pressure driving force, using r_p as the single model parameter. Due to its simplicity and successful history of use in aqueous systems, Bowen's model was adopted in this work (the detailed derivation of this model can be found in Appendix I).

The real rejection, for a solute i, is given by:

$$RR = 1 - \frac{C_{if(m)}}{C_{ip}} = 1 - \frac{\left\{K_{ic} - \frac{D_{ip}\overline{V}_i 8\eta}{RTr_p^2}\right\}\Phi}{1 - \left[1 - \left\{K_{ic} - \frac{D_{ip}\overline{V}_i 8\eta}{RTr_p^2}\right\}\Phi\right]\exp\left[Pe'\right]} \tag{29}$$

where $\overline{V}_i$ is the solute molar volume, D_{ip} the solute diffusion coefficient in the membrane pores, r_p the membrane pore radius, K_{ic} an hydrodynamic drag coefficient, Φ the solute partition coefficient and η the solution viscosity.

The modified Peclet number Pe' is given by:

$$Pe' = \frac{\left(K_{ic} - \frac{D_{ip}\overline{V}_i 8\eta}{RTr_p^2}\right) r_p^2 N_v}{8\eta D_{ip} P_{jm}} \tag{30}$$

and the total flux by:

$$N_v = P_{jm}\left(\Delta p - \Delta\Pi\right) \tag{31}$$

where P_{jm} is the permeability of the solvent j in the membrane and Π the osmotic pressure.

In order to apply this pore-flow membrane transport model for the prediction of nanofiltration data two input parameters need to be determined; the solvent permeability and the membrane pore radius.

The use of these membrane transport models in OSN is not novel. The solution-diffusion model was used for the first time to describe solute transport in OSN by Paul and co-workers (Paul et al., 1976) who analysed solute transport through solvent-swollen rubbery membranes, arriving at the conclusion that solute transport was reasonably described by the model, and mainly determined by solvent viscosity and polymer swelling. Stafie et al. (2004) also arrived at the same conclusion using a solution-diffusion approach to describe sunflower oil/hexane and PIB/hexane permeation through a polydimethylsiloxane active

layer coated on a polyacrylonitrile (PAN) support, for several pressures and solute concentrations. However, they noticed signs of solvent-solute coupling (solute flux increased with increasing solvent flux). White (2002) and Scarpello et al. (2002) also analysed solute permeation though OSN membranes using a solution-diffusion approach.

The pore-flow view of OSN membrane transport has also been used to interpret solute permeation; Van der Bruggen et al. (2002) related OSN rejection curves to log-normal pore size distributions in the commercially available membranes tested. Whu et al. (2000) suggested that for Koch MPF series commercial OSN membranes compaction can be explained by pore shrinkage through time and rejection by size exclusion mechanisms. Bhanushali et al. (2002) suggested that a pore-flow model including an interaction parameter between the membrane and the permeating species could qualitatively describe OSN solute rejection data.

Although this exploratory work is of interest, these membrane transport models have all been tested with dilute (< 1wt. %) solute concentrations. Moreover, most of this work neglects the influence of the liquid phase mass transfer limitations on the flux/rejection profiles. In this thesis the membrane transport models will be tested for concentrated solutions which more closely resemble those found in real industrial applications, and an adequate solution mass transfer film theory model will be coupled with the membrane transport models in order to assess the liquid phase mass transfer importance in solute transport. The detailed derivation of this film theory mass transfer model is present in the next subchapter of this literature review.

2.6 Liquid Mass Transfer Modelling

The use of film theory to describe solution mass transfer phenomena in pressure driven membrane processes has a proven track record for aqueous systems. In fact, under flow conditions such as those encountered in nanofiltration, the simplified film theory description of mass transfer has an accuracy close to that obtained by CFD modelling (Zydney, 1997).

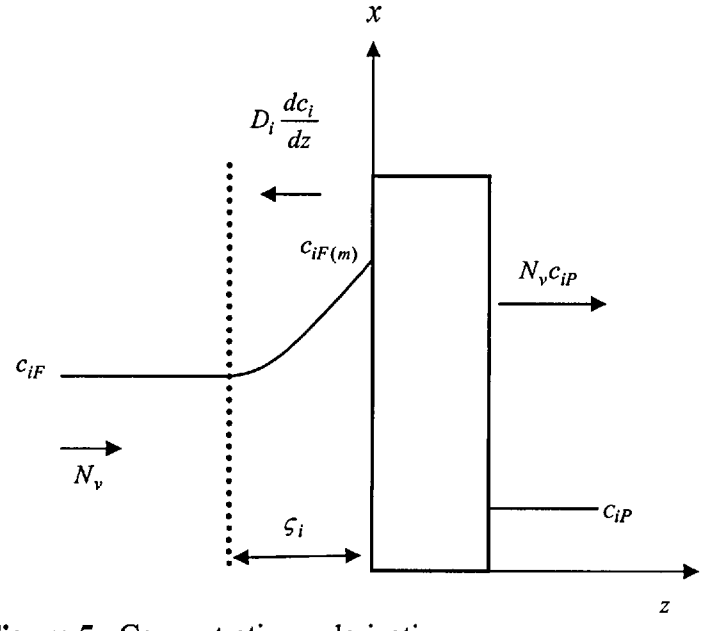

Figure 5 : Concentration polarization.

The general steady state mass balance equation within the mass transfer boundary layer ($-\varsigma_i$ [z[0) can be expressed as:

$$u\frac{\partial c_i}{\partial x} + v\frac{\partial c_i}{\partial z} = \frac{\partial}{\partial z}\left(D_i^e \frac{\partial c_i}{\partial z}\right) \tag{32}$$

for relatively small values of flux and transverse Reynolds number ($J \vee u_0$; Re_z'0.5) like the ones encountered in nanofiltration, concentration polarization can be described by the stagnant film model (Michaels, 1968; Zydney, 1997). Mass transfer is assumed to occur across a stagnant film of thickness ς, where the one dimensional steady state mass balance for rejected specie i is given by:

$$N_v c_i - D_i^e \frac{dc_i}{dz} - N_v c_{iP} = 0 \tag{33}$$

this equation can be integrated over the boundary layer thickness in order to give:

$$N_v = \frac{D_i^e}{\varsigma_i} \ln\left(\frac{c_{iF(m)} - c_{iP}}{c_{iF} - c_{iP}}\right) = k_i \ln\left(\frac{c_{iF(m)} - c_{iP}}{c_{iF} - c_{iP}}\right) \tag{34}$$

the problem is that the value of $c_{iF(m)}$ is not obtainable by direct measurements so, in order to get its real value there is the need to estimate the mass transfer coefficient (k_i). There are two general methods to perform this task (Table 7):

Table 7 : Mass transfer coefficient determination.

Method	Equations	Assumptions	Reference
Experimental velocity variation	$OR = \frac{(c_{iF} - c_{iP})}{c_{iF}}$ $RR = \frac{(c_{iF(m)} - c_{iP})}{c_{iF(m)}}$ $\ln\left(\frac{1-OR}{OR}\right) = \ln\left(\frac{1-RR}{RR}\right) + b\left(\frac{N_v}{u^a}\right)$	$k_i \propto u^a$	Nakao et al, 1981 Herath et al, 2000
Theoretical mass transfer correlation	$Sh = 1.62\left(\mathrm{Re}\, Sc \frac{d}{L}\right)^{\frac{1}{3}}$	Analogy between heat and mass transfer is valid and: Laminar flow regime -Developing concentration boundary layer	Gekas and Hallstrom, 1987
	$Sh = \left(3.66^3 + 1.6119^3\, \mathrm{Re}\, Sc \frac{d}{L}\right)^{\frac{1}{3}}$	-Fully developed concentration and hydrodynamic boundary layer	Rautenbach and Helmus, 1994
	$Sh = 0.026\, \mathrm{Re}^{0.8}\, Sc^{0.33}$ with: $Sh = \frac{k_i d}{D_i^e}\ \mathrm{Re} = \frac{u\rho d}{\mu}\ Sc = \frac{\mu}{\rho D_i^e}$	Turbulent flow regime	Peeva et al, 2004

In the experimental velocity variation method (Jonsson and Boesen, 1977) the plot of $\ln\left(\frac{1-OR}{OR}\right)$ vs. $\frac{N_v}{u^a}$ is assumed to be a straight line, and the intercept on the y-axis, corresponding to infinite circulation, will yield the value of the true rejection. The weakness of this method is the fact that true rejection, RR depends on N_v, which in turn depends on the circulation velocity, u. Therefore the previously mentioned plot is in fact a curve that needs to be extrapolated to regions of infinite circulation velocity. Furthermore, this RR then corresponds to rejection values where the circulation velocity is infinite and, therefore, it can not be used for mass transfer coefficient calculation for finite circulation velocities except when the true rejection is independent of the total flux.

According to the analysis presented in the last paragraph the theoretical mass transfer correlation method seems to be the most reliable choice to obtain the mass transfer coefficients, but, the fact that mass transfer coefficients are a function of feed flow rate, cell geometry and solute, makes the task of obtaining the correct correlation parameters that are able to describe a particular system relatively complicated.

Concentration polarisation for liquid film mass transfer can be coupled with the model for membrane transport, for example the solution-diffusion model Eq. (17) (Nakao et al., 1986; Van der Berg and Smolders, 1989), to describe membrane transport in a mass transfer limited system. Combined solution-diffusion/pore-flow - film theory models have been presented previously in several publications on aqueous systems, where detailed experimental flux and rejection results are obtained and used to determine parameters through nonlinear parameter estimation (Murthy and Gupta, 1997). The first work to consider the effect of concentration polarization in OSN was presented by Peeva et al. (2004). The solution-diffusion membrane transport model, Eq. (17), was coupled with film theory Eq. (34), to describe flux and rejection of toluene/docosane and tolune/TOABr binary mixtures. This approach was able to predict fluxes for a wide range of solvent/solute mixtures from a limited data set of the pure solvent/solute fluxes.

Until now it was only considered the transport mechanism related to membrane permeation, but when dealing with concentrated solutions highly rejected by the membrane, the boundary layer concentration polarization will also be a determining factor for the flux/rejection profiles.

2.7 Modelling Performance of Spiral-Wound Modules

Spiral-wound modules are essentially flat membrane sheets separated by highly porous spacer material. The modules are relatively simple to build and have a high packing density ($> 900\ m^2.m^{-3}$), but are difficult to clean.

Spiral-wound modules are constructed from a number of membrane envelopes. Two membrane sheets are glued together on three sides to form an envelope. The fourth edge is attached to a central collection tube, around which one or more envelopes are wound, and

the feed flows parallel to the central tube outside the membrane envelope. Material permeates into the interior of the membrane envelopes and flows along the spiral, towards the central tube. The classic approach to model these systems is to neglect the curvature of the channels and to consider flow through two flat spacer-filled channels either side of the membrane. Rautenbach and Albrecht (1989) states that this assumption can be justified, because the ratio of channel height to the mean module diameter is small. There are essentially two types of models developed to describe spiral wound modules: one dimensional plug-flow models that assume constant values on either the feed or the permeate side of the membrane; and two dimensional models that describe the true cross-flow nature of the flow. The former category includes the Ohya and Taniguchi (1975) model which assumes a constant concentration in the permeate channel. The membrane model is then described by an axial mass balance for the feed channel assuming plug-flow.

More recent two-dimensional models disregard this assumption. Important examples of this include the works of Pan (1983), Evangelista and Jonsson (1988), and Ben-Boudinar et al. (1992). These models allow concentration and permeation variation in both the axial and radial directions, but neglect the component of feed flow in the spiral direction and permeate flow in the axial direction. Flow trough the module is then described by the solution of two perpendicular one-dimensional balances on either side of the membrane. This approach was also implemented in models developed by Rautenbach and Dahm (1987) and Rautenbach and Albrecht (1989). Therefore, there are two model complexity levels to describe spiral-wound nanofiltration:

Simple Models

The simplest way of modelling spiral-wound elements is to consider the element as a flat-sheet membrane and ignore pressure, velocity and concentration gradients throughout the radial and axial dimensions of the element. Therefore, this simple spiral-wound model will merely consist in a membrane transport model coupled with the film theory model for solution mass transfer. The momentum, velocity and pressure gradients will be zero.

Complex Models

When a more detailed description of the transport in spiral-wound elements systems is required, the variation of process variables with the axial and radial dimensions of the element should be taken into account.

A considerable number of two-dimensional mathematical models for aqueous nanofiltration using spiral-wound elements have been published (Rautenbach and Dahm, 1987;

Evangelista and Jonsson, 1988; Chiolle et al. 1978; Boudinar et al. 1992). By analysing the details behind published models it is clear that most systems can be accurately described with a model obeying the following assumptions:

1. Negligible diffusive mass transport in comparison to the convective mass transport along the main flow direction of the spiral-wound channels.
2. Plug flow in both permeate and feed channels.
3. The spiral-wound module is considered to comprise a stack of two flat, spacer-filled channels (curvature of the channels is neglected).

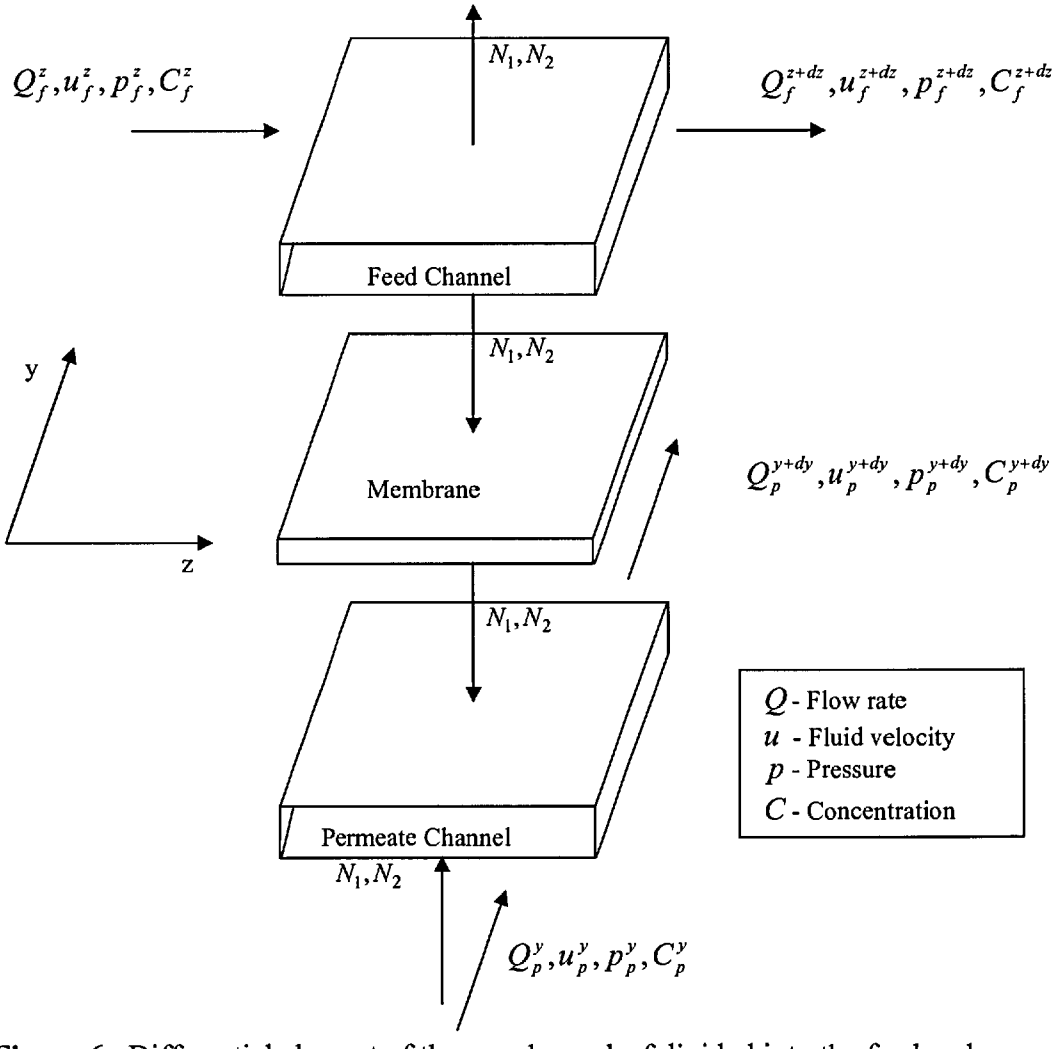

Figure 6 : Differential element of the membrane leaf divided into the feed and permeate channel showing the input and output flow conditions.

From the above assumptions and considering the geometry of the system (Figure 6) the differential solute and solvent material and momentum balances can be derived. For the feed channel we can write:

$$\frac{\partial u_f(z,y)}{\partial z} = -\frac{2N_v(z,y)}{h_f \varepsilon_f} \text{ and } \frac{\partial (u_f(z,y).c_{1f}(z,y))}{\partial z} = -2\frac{N_1(z,y)}{h_f \varepsilon_f} \quad (35),(36)$$

for the permeate channel we can write

$$\frac{\partial u_p(z,y)}{\partial y} = \frac{2N_v(z,y)}{h_p \varepsilon_p} \text{ and } \frac{\partial (u_p(z,y).c_{1p}(z,y))}{\partial y} = 2\frac{N_1(z,y)}{h_p \varepsilon_p} \quad (37),(38)$$

where h and ε represent the height and the porosity of the channel respectively. Moreover, to correctly describe the performance of a spiral-wound element, knowledge concerning the pressure drop in the feed and permeate channels is essential. Schock and Miquel (1987) showed that independently of the type of spacers used in a flat channel, for $100 < \text{Re} < 1000$ the pressure drop could be given by:

$$\frac{\partial p_f(z,y)}{\partial z} = \frac{6.23}{2d_{h_f}} \text{Re}(z,y)^{-0.3} \rho u_f(z,y)^2 \quad (39)$$

and for $\text{Re} < 100$ by:

$$\frac{\partial p_p(z,y)}{\partial y} = \frac{105}{2d_{h_p}} \text{Re}(z,y)^{-0.8} \rho u_p(z,y)^2 \quad (40)$$

since this work will be dealing with high concentration solutions of highly rejected specie, solution mass transfer will play an important role in the transport. Previously, it was shown (Peeva et al., 2004; Silva and Livingston, 2006) that the film theory model could accurately predict concentration polarization phenomena for concentrated solutions, once an accurate mass transfer coefficient value is determined. Once again the work of Schock and Miquel

(1987) provides us with a correlation able to predict the mass transfer coefficient, for any type of spacer-filled flat channel under common cross-flow conditions.

$$\frac{k(z,y)d_{h_f}}{D_{12}} = 0.065\,\mathrm{Re}(z,y)^{0.875}\,Sc(z,y)^{0.25} \tag{41}$$

Although the use of these spiral-wound model equations is widespread for aqueous nanofiltration systems, there is no literature data on OSN modelling in spiral-wound elements. In this thesis the set of equations derived above, will be used to predict flux/rejection trends in spiral-wound based OSN. Moreover, the ability to predict spiral-wound performance using membrane parameters determined in cross-flow flat-sheet experiments will be assessed. Finally, the level of spiral-wound model complexity required to accurately describe spiral-wound performance will be assessed and the factors determining this level will be identified.

From all the equations present in this literature review there are some fundamental ones that will be crucial for the following chapters: For instance, Eq. (11) in section 2.4.1 and Eq. (17) in section 2.4.2 will be used in chapter 3, for the study of solvent mixture permeation through OSN membranes. In chapter 4 the use of Bowen's pore-flow model (Eq. (29) section 2.5.3) and the solution-diffusion model (Eq. (28) section 2.5.2) together with the film theory for liquid phase mass transfer (Eq. (34) section 2.6), will be crucial in determining the transport mechanism behind the permeation of a partially rejected solute through OSN membranes. In chapter 5 Eq. (35) to Eq. (41) were used together with the film theory (Eq. (34) section 2.6), to describe the performance of spiral-wound elements. Finally, Eq. (5) and Eq. (6) were used in chapter 6, in the development of a new model describing solvent permeation through OSN membranes.

3. Solvent Transport in Organic Solvent Nanofiltration

3.1 Aim and Scope

In recent years, solvent stable nanofiltration membranes with molecular weight cut offs (MWCOs) ranging from 200 – 1000 g mol^{-1} have emerged (White et al., 1993; Linder et al., 1993; White, 2001). This new generation of organic solvent nanofiltration (OSN) membranes have been employed in a wide range of applications to full process (White and Nitsch, 2000) and lab scale (Raman et al., 1996; Zwijenburg et al., 1999; Luthra et al., 2000 Luthra et al., 2002; Gosser et al., 1997; De Smet et al., 2001; Nair et al., 2001; Livingston et al., 2003; Datta et al., 2003; Krockel and Kragl, 2003; Sheth et al., 2003; Dijkstra et al. 2002) . Concomitantly, a growing number of publications concerning the transport of organic solvents in OSN membranes have appeared (Whu et al., 2000; Bhanushali et al., 2001; Bhanushali et al., 2002; Yang et al., 2001; Van der Bruggen et al., 2002; White et al., 2002; Gibbins et al., 2002; Machado et al., 1999; Machado et al., 2000; Peeva et al., 2004; Robinson et al., 2004; Stafie et al., 2004; Wijmans and Baker, 1995). This work is dynamic and interesting. However, it can be observed that:

- Much of the data published for OSN membranes has been obtained using dead end tests for a short period of time (typically a few hours). There are a few studies over longer time periods using cross-flow equipment, which is more representative of larger scale processes. White and Nitsch (2000) reported continuous two-month tests of a polyimide membrane to separate light hydrocarbon solvent from lube oil filtrates at 41 atm and at -10 °C, demonstrating a purity of over 99 % with a steady permeate rate. They also reported data for solvent fluxes from a commercial plant for 400 days. Although De Smet (2001) and Dijkstra et al. (2002) report OSN membranes in continuous cross-flow membrane reactors, they do not report any in depth data concerning the transport characteristics of OSN membranes;
- In the comparison of models with data, it is often not clear how one can use the data presented to make predictions, or what methodology should be employed. Mostly data is treated by considering trends, for example the relationship between viscosity

and flux, and then using this to infer whether one or other transport model is better applied to describe membrane transport;

- There is as yet little available data for mixtures of solvents. These can be interesting as solvent mixtures can assist in separating the effects of solvent viscosity and membrane-solvent interaction, on the solvent flux.

In this chapter, continuous cross-flow nanofiltration cells have been used to study the performance of STARMEM^{TM} 122 (W.R.Gace and Co) and MPF-50 (Koch Membrane Systems) OSN membranes over periods of weeks. The binary systems toluene/methanol and toluene/ethyl acetate have been used to investigate transport characteristics of OSN membranes and to elucidate the effect of the factors such as solvent viscosity on the solvent transport. The effects of membrane history and membrane uniformity on membrane performance are reported. Finally, simple versions of the solution-diffusion and pore-flow models were applied to predict data (in this work there is a clear distinction between "prediction" and "fitting" of data) for solvent mixture fluxes based on the data for pure solvents, and propose a methodology for estimating the solvent flux for mixtures.

3.3 Materials and Methods

3.3.1 Chemicals

Three organic solvents, ethyl acetate (EA, HPLC grade), toluene and methanol (analytical grade) were used in this study as these solvents are commonly used in the pharmaceutical and chemical industries. Tetraoctylammonium bromide (TOABr) with a molecular weight of 547 g mol^{-1} was selected as a marker in this study to check rejection of the membranes. Aldrich, UK, supplied all chemicals.

3.3.2 Membranes

STARMEM^{TM} 122, an asymmetric OSN membrane with an active layer of polyimide, in a "dry" form but with a lube oil soaked into the membrane as a preserving agent, with a nominal MWCO of 220 g.mol^{-1} (manufacturer's data) was supplied by Membrane Extraction Technology Ltd (UK). MPF-50, a composite membrane comprising an active

layer of crosslinked polydimethylsiloxane (PDMS) mounted on a polyacrylonitrile (PAN) support (Linder et al., 1993; Vankelecom et al., 2004), was purchased from Koch Membrane Systems. MPF-50 has a MWCO of 700 Dalton (manufacturer's data). MPF-50 was supplied soaked in 50 % ethanol/water.

3.3.3 Filtration Equipment and Experimental Measurements

Figure 7 shows the diagram of the cross-flow nanofiltration rig. It consists of four cross-flow nanofiltration cells connected in series, a solution reservoir, a backpressure regulator, and a piston pump. Each cell had a membrane area of 1.4×10^{-3} m^2 and the height of the chamber from the surface of the membrane was 50 mm, giving a fluid volume of 7 ml. The solution enters the cross flow cell tangentially from the cell wall and exits the cell from the top centre, providing turbulent hydrodynamic conditions to minimise the effect of concentration polarisation during filtration. The applied pressure was controlled at 30 bar using the backpressure regulator and the temperature at 30 ± 0.5 °C using a water bath and heat exchanger. When the solution in the rig was swapped, the second solution was used to wash the rig at least 4 times to ensure that there were no significant traces of the previous solution present in the rig.

During filtration the solvent flux was obtained by:

$$N_v = \frac{V}{A.t} \tag{42}$$

Where V is the sampling volume in the permeate, A the effective membrane area and t the sampling time. The rejection was defined as

$$OR_i = \left(1 - \frac{C_{ip}}{C_{ir}}\right) \times 100\% \tag{43}$$

Where C_p and C_r are the final concentrations in the permeate and retentate respectively.

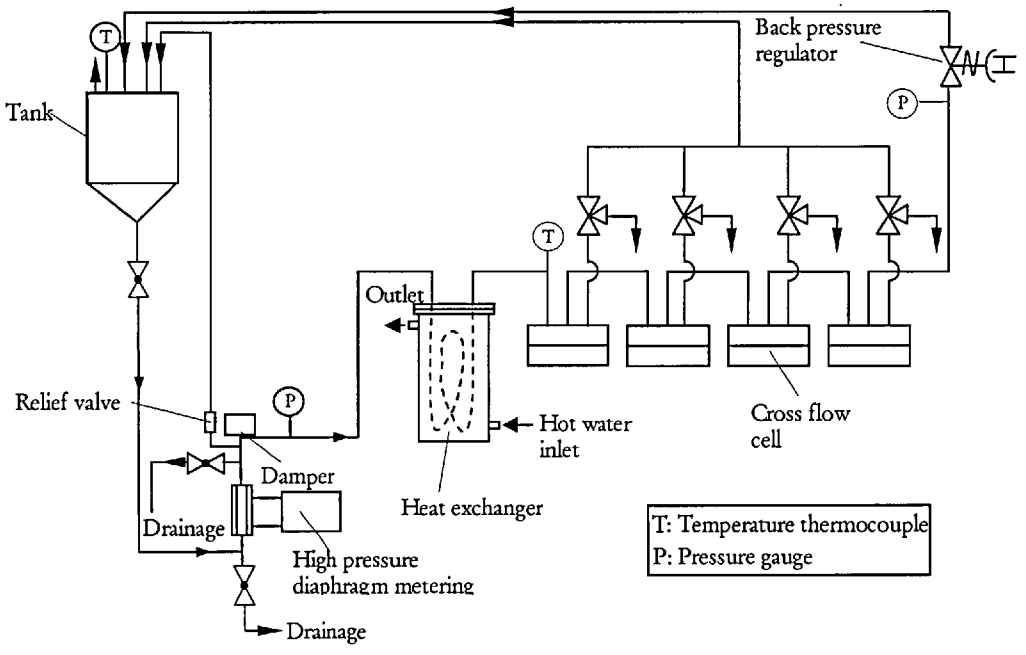

Figure 7 : Cross-flow nanofiltration rig.

3.3.4 Analytical Methods

Concentrations of TOABr, methanol and toluene were determined using a Perkin-Elmer Gas Chromatograph with a flame ionisation detector and a Megabore column 25 m long and with 0.23 mm i.d. with BP1 (SGE, Australia) as the stationary phase. The temperature programme ran from 80 °C to 300 °C at a rate of 25 °C.min^{-1}, and the column temperature was held at 80 and 300 °C for 3 minutes respectively. The coefficient of variation was 5 % for 3 independent measurements. Due to losses from evaporation of solvents during sampling, the accuracy of the measurement of the fraction of toluene had an error of up to 5 % of the concentration of toluene present.

Viscosities of methanol/toluene and ethyl acetate/toluene mixtures were measured by U-Tube Viscometer (PSL Scientific, UK), respectively. The data is shown in Figures 9 and 10. All the measurements were conducted at 30 °C.

3.4 Results and Discussion

3.4.1 Membrane Compaction

It is important to establish that the order in which the solvent mixture composition is altered does not have any lasting effect on the subsequent performance of the membrane, i.e. that the membrane flux measured for any solvent mixture is a property only of the membrane sample and the solvent mixture, and not of the system history. Figure 8 shows the solvent flux profiles when toluene and methanol are swapped for the same membrane discs. It can be seen that following initial compaction, toluene and methanol fluxes are stable after a few swaps, i.e. 25-30 $L.m^{-2}.h^{-1}$ for toluene and 60-70 $L.m^{-2}.h^{-1}$ for methanol. It can be concluded that solvent transport in STARMEM^{TM} 122 is not affected by "membrane history" and that this membrane has a good uniformity between sample discs. Clearly these are key factors for obtaining reliable and repeatable data for the system.

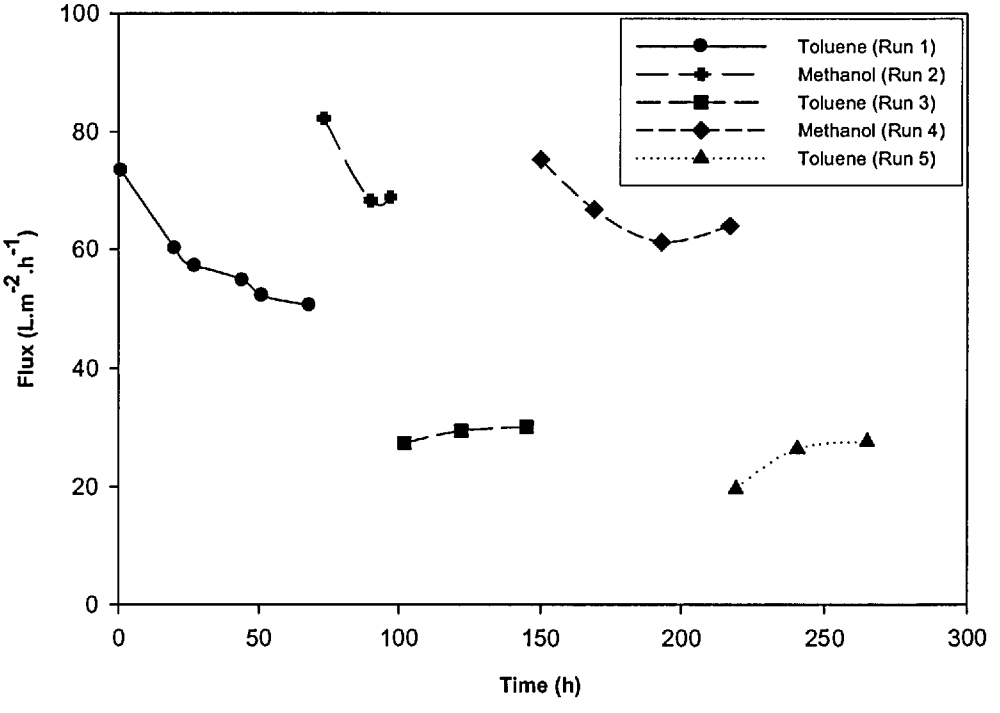

Figure 8 : Membrane compaction.

When starting with new membrane discs in the first test with pure toluene, it usually took about 3 days to get a stable solvent flux, and 1-2 days were always needed for stable

solvent fluxes in subsequent tests. This means that membrane compaction is a slow process and the flux data collected in dead-end cell testing with a limited collection period (typically 1-3 hours) may not be reliable for predicting long term performance. It is interesting to note that in Runs 3 and 5 toluene fluxes increased rather than typically decreased with time until becoming stable. One explanation may be that methanol has a stronger interaction with STARMEM^{TM} 122 than toluene. Once the membranes are wetted by methanol, the active layer would be saturated with methanol molecules bound to the polymer chains. A swap of methanol to toluene requires toluene molecules to wash methanol molecules out from the active layer so that toluene can permeate through the membrane. Therefore toluene flux may initially increase due to the slow washing away of methanol molecules from the active layer.

3.4.2 Solvent Fluxes

Tables 8 and 9 show solvent fluxes and TOABr rejections with different solvent compositions for methanol/toluene and toluene/ethyl acetate mixtures.

Table 8 : Solvent fluxes of methanol/toluene mixtures and TOABr rejections at 30 bar and 30 °C

	Run 1				**Run 2**			
MPF-50	*Flux, $Lm^{-2}hr^{-1}$*		*Rejection*		*Flux, $Lm^{-2}hr^{-1}$*		*Rejection*	
Solution	*Disc 1*	*Disc 2*	*Disc 1*	*Disc 2*	*Disc 3*	*Disc4*	*Disc3*	*Disc 4*
Pure methanol	67.3	51.7	92%	94%	53.7	61.8	>99%	>99%
80 wt % methanol	68.0	46.5	92%	90%				
50 wt % methanol	90.7	68.0	87%	92%	38.2	37.4	>99%	>99%
20 wt % methanol	89.0	74.0	89%	86%				
Pure toluene	132.5	113.0	79%	83%	47.4	50.9	>99%	99%
STARMEM^{TM} 122								
Solution	*Disc 1*	*Disc 2*	*Disc 1*	*Disc 2*	*Disc 3*	*Disc4*	*Disc3*	*Disc 4*
Pure methanol	84.7	85.7	98%	97%	121.0	110.7	>99%	>99%
80 wt % methanol	50.3	52.3	99%	>99%				
50 wt % methanol	44.5	45.0	>99%	>99%	44.8	42.5	>99%	>99%
20 wt % methanol	38.5	37.5	>99%	>99%				
Pure toluene	29.5	28.0	>99%	>99%	28.9	27.1	>99%	>99%

Table 9 : Solvent fluxes of ethyl acetate/toluene mixtures and TOABr rejections at 30 bar and 30 °C

MPF-50	**Run 3**				**Run 4**			
	Flux, $Lm^{-2}hr^{-1}$		*Rejection*		*Flux, $Lm^{-2}hr^{-1}$*		*Rejection*	
Solution	*Disc 5*	*Disc6*	*Disc 5*	*Disc6*	*Disc 7*	*Disc8*	*Disc 7*	*Disc8*
Pure ethyl acetate	33.5	40.7	>99%	>99%	43.4	32.6	97%	97%
80 wt % ethyl acetate	32.5	46.4	>99%	>99%				
50 wt % ethyl acetate	31.0	41.2	98%	96%	49.8	36.6	95%	96%
20 wt % ethyl acetate	31.3	36.4	90%	90%				
Pure toluene	30.5	32.0	91%	93%	56.3	43.3	77%	77%
STARMEM™ 122								
Solution	*Disc 5*	*Disc6*	*Disc 5*	*Disc6*	*Disc 7*	*Disc8*	*Disc 7*	*Disc8*
Pure ethyl acetate	100.5	92.5	>99%	>99%	102.4	101.7	>99%	>99%
80 wt % ethyl acetate	95.9	73.4	>99%	>99%				
50 wt % ethyl acetate	65.7	49.6	>99%	>99%	54.9	56.4	>99%	>99%
20 wt % ethyl acetate	45.9	33.8	>99%	>99%				
Pure toluene	31.0	22.7	>99%	>99%	21.9	22.6	>99%	>99%

The arrows in the tables show that for each run the tests started with pure methanol or ethyl acetate and went to pure toluene with a gradually increase in toluene concentration. Since STARMEM™ 122 has a preserving agent within the membrane in its dry form and MPF-50 is supplied in ethanol-water solution, pure methanol was used to pre-condition the membrane discs before starting any data collection. The resulting permeate solution was thrown away for the first 15-20 minutes then subsequently fed back to the tank.

For methanol/toluene mixtures, it can be seen that in Run 1 solvent flux increased as concentration varied from pure methanol to pure toluene for MPF-50, but decreased for STARMEM™ 122. To confirm these results, Run 2 with two pure solvents and a 50/50 (wt.) mixture was conducted in new membrane discs with the same testing order as Run 1. It was found that the solvent profile in Run 2 was very different from that in Run 1 for MPF-50. However, the solvent fluxes are comparable between Run 1 and Run 2 for STARMEM™ 122, i.e. the solvent flux decreases with increasing toluene concentration. As shown in Table 9, MPF-50 did not give repeatable measurements in Runs 3 and 4 for toluene/ethyl acetate mixtures either. Van der Bruggen et al (2002) reported that after 10 days exposure to different organic solvents MPF-50 characteristics significantly changed in terms of solvent flux and solute rejections. Scanning electron microscopy images of MPF-50 membranes were quite different before and after exposure to ethyl acetate. This suggests

that membrane history affects solvent transport in this membrane. Even with the same membrane history, the solvent fluxes measured for two different discs of MPF-50 could not be repeated in this study.

Solvent flux data in STARMEM^{TM} 122 is also comparable between Runs 3 and 4 for toluene/ethyl acetate mixtures, as shown in Table 9. It can be concluded that STARMEM^{TM} 122 gave stable solvent flux measurements. As the data for MPF-50 was not repeatable, the modelling interpretation below will be limited to STARMEM^{TM} 122.

In order to gain insight into the flux profiles for STARMEM^{TM} 122 membrane solvent-polymer interaction parameters can be considered. The solvent-polymer interaction χ was described in section 3.3.1 where it is stated that when χ is large (>2) the solvent-polymer interaction is small, but strong solvent – polymer interactions exist for small values ($0.5<\chi<2.0$) (Mulder, 1997). The solubility parameters for the solvents and polyimide are shown in Table 10.

Table 10 : Solubility parameters, molar volumes and molecular diameters for the species.

Item	*Solubility parameter*** $(MPa)^{1/2}$	*Molar volume* $(cm^3\ mol^{-1})$	Molecular diameter *(nm)**
Matrimid 5218	23.2	-	-
Lenzing P84	26.8	-	-
Methanol	29.7	41	0.41
Toluene	18.2	106	0.69
Ethyl acetate	18.6	98	0.62

* - Van der Bruggen et al. (1999)
** - Barton (1983)

For determining the solubility parameter for the STARMEM^{TM} 122 membrane, solubility parameter values for typical polyimides used for forming OSN membranes such as Lenzing P84 and Matrimid 5218 (White, 2001;White 2002), were calculated, using a group contribution method (Barton, 1983). The solubility parameter does not vary significantly between these two polyimides.

Beerlage et al. (1994) reported the swelling ratio for methanol (12.2 wt %), toluene (2.7 wt %) and ethyl acetate (2.8 wt %) in Lenzing P84 polyimide. This can be explained by solubility parameter difference between the solvent and the polymer. The solubility parameter difference of 2.9 $(MPa)^{1/2}$ between methanol and STARMEM^{TM} 122 is much

smaller than 8.6 $(MPa)^{1/2}$ for toluene and 8.2 $(MPa)^{1/2}$ ethyl acetate, i.e. a stronger methanol-polymer interaction takes place, according to Eq. (3).

The solvent flux trends in STARMEM^{TM} 122 can be explained by both solution-diffusion and pore-flow models. If it is assumed that the transport mechanism is solution-diffusion, the key factors are partition and diffusion coefficients. Therefore in the methanol-toluene system methanol flux should be much higher than that of toluene due to methanol's higher partition (low interaction parameter) and diffusivity (membrane more swollen in methanol) in the polymer matrix. For the ethyl acetate-toluene system the solvents have almost identical interaction parameters, therefore the controlling factor can only be diffusivity. Considering Table 10 it is clear that the molecular diameters of toluene and ethyl acetate are similar, and other data suggests that the diffusion coefficients of both solvent molecules in organic liquids are similar (Perry and Green, 1998). The shape of the diffusing molecule is important and it has been shown (White, 2002) that branched and bulky molecules are retarded compared to more linear molecules of equivalent molecular weight – perhaps this explains the difference of the permeabilities of these two solvents.

The pore-flow perspective of membrane transport suggests viscosity as a flux controlling factor. However looking at Figures 9 and 10 it is clear that the viscosity changes in both systems are too small to justify the big changes in fluxes between solvents. The fact that viscosity alone can not correlate the solvent mixture flux for the systems studied in this chapter, is in agreement with the observations of Machado et al. (1999), for the permeation of acetone-water mixtures through the MPF-50 OSN membrane.

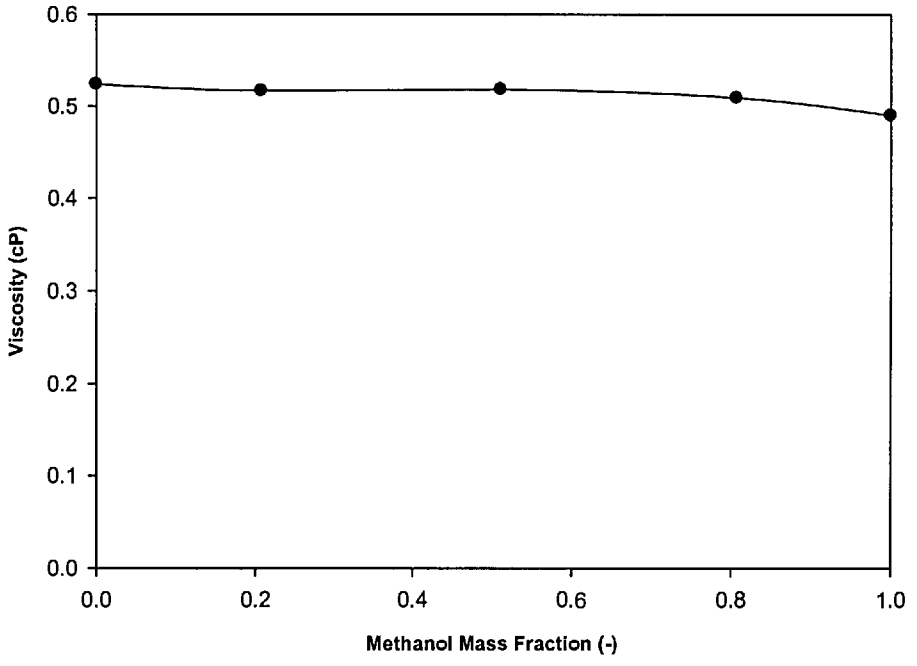

Figure 9 : Methanol-toluene mixture viscosity.

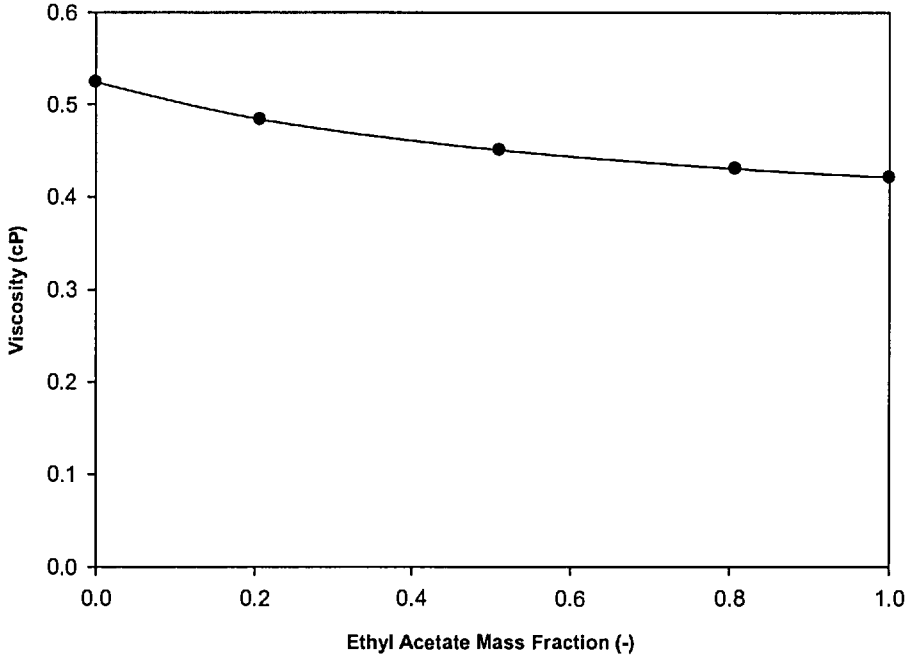

Figure 10 : Ethyl acetate-toluene mixture viscosity

Therefore, some other flux determining factor must be controlling the permeation through the membrane. This could be the specific permeability, related to the effective pore structure changing from solvent to solvent due to different polymer-solvent interactions and swelling of the polymer matrix. From this perspective also, since there is little difference in swelling between toluene and ethyl acetate, it is difficult to explain the much higher flux of ethyl acetate compared to toluene, since both swell the membrane in approximately the same amount.

TOABr was selected as a marker compound to check for any leaks and/or break up of the membrane discs. Its concentration was 1 $g.L^{-1}$ for all the tests. TOABr rejection is > 97 % in STARMEM^{TM} 122 and in the range of 77 % to >99 % in MPF-50 for all the tests conducted in this study. This can be attributed to the fact that STARMEM^{TM} 122 has a MWCO of 220 $g.mol^{-1}$ compared to 700 $g.mol^{-1}$ for MPF-50, while TOABr has a molecular weight of 547 Dalton. The rejection values lead us to conclude that there were no major leaks or membrane failures during the experiments.

3.4.3 Predictions of Solution-Diffusion and Pore-Flow Models

Both solution-diffusion and pore-flow models will be used to analyse the experimental solvent flux data shown in Tables 8 and 9.

For the solution-diffusion model it can be assumed that concentration polarization does not exist and the activity coefficients in the permeate and in the retentate are equal for each species. Therefore, Eq. (17) for a binary mixture can be simplified as:

$$n_1 = P_{1m}^{mass}\left(w_{1f} - \frac{n_1}{n_1+n_2}\exp\left(-\frac{V_1\Delta p}{RT}\right)\right) \tag{44}$$

$$n_2 = P_{2m}^{mass}\left(w_{2f} - \frac{n_2}{n_1+n_2}\exp\left(-\frac{V_2\Delta p}{RT}\right)\right) \tag{45}$$

Where n_i is the mass flux and w_i the mass fraction of species i. Mass fraction units are used above in Eqs. (44) and (45) instead of the commonly used mole fraction. A molar basis for the generalized Stefan-Maxwell equations is not recommended, since mole fraction is not a good measure of composition for mixtures of molecules of greatly different sizes. It should also be noted that the solvent mixtures are not assumed to be ideal solutions; rather it is assumed that the activity coefficients are equal in the permeate and in the retentate for each solvent.

It can be seen that the permeability for each solvent has to be determined if Eqs. (44) and (45) are used to predict solvent fluxes. In this study, it is assumed that the permeability for each solvent is independent of solvent compositions in the solution. The permeabilities for each solvent were determined by using pure solvent flux data, and are shown in Table 11.

Table 11 : Model parameters.

	Permeabilities		
Item	*Solution-Diffusion (kg. $m^{-2}.s^{-1}$)*	*Solution-Diffusion (mol. $m^{-2}.h^{-1}$)*	*Pore-Flow (x 10^{-15} m)*
Methanol	0.481	54056	3.91
Toluene	0.054	2107	1.32
Ethyl acetate	0.226	9251	1.62

The toluene permeability is similar to that reported previously by White (2002) - 2803 $mol.m^{-2}.h^{-1}$ for toluene in a polyimide (Lenzig P84) nanofiltration membrane, corresponding to a mass permeability of 0.072 $kg.m^{-2}.s^{-1}$.

Eqs. (44) and (45) were then used to calculate mass flux for each solvent mixture. The predicted mass flux for each solvent was converted to give a total volumetric flux by using

$$J = \frac{n_1}{\rho_1} + \frac{n_2}{\rho_2} \tag{46}$$

The comparison of predicted and experimental solvent flux data are shown in Figures 11 and 12.

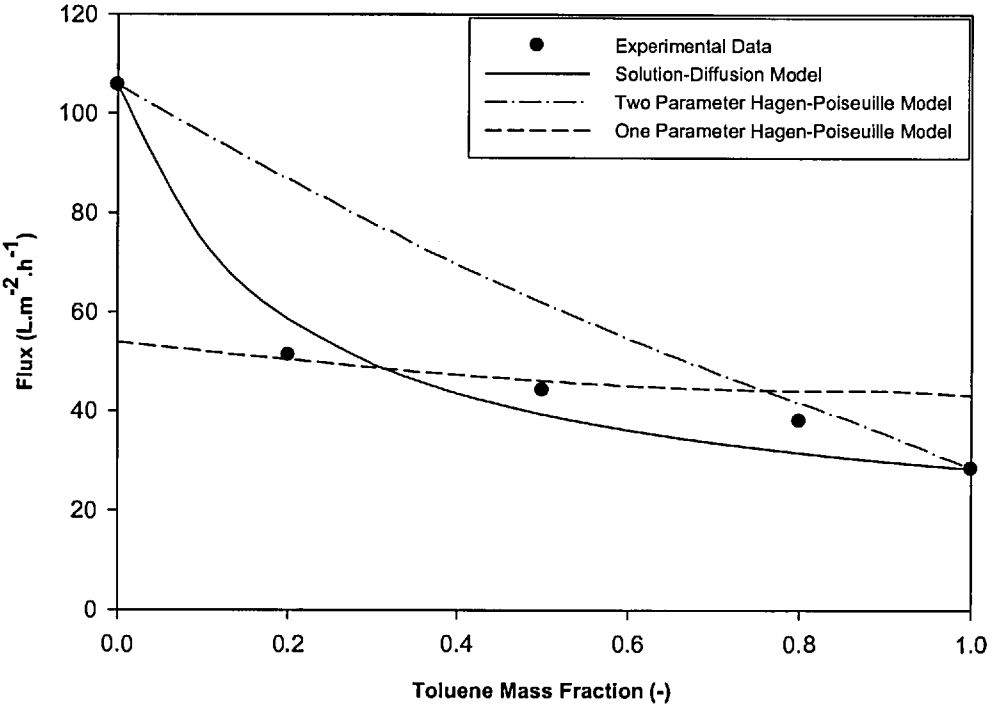

Figure 11 : Flux of methanol-toluene mixtures at 30 °C and 30 bar.

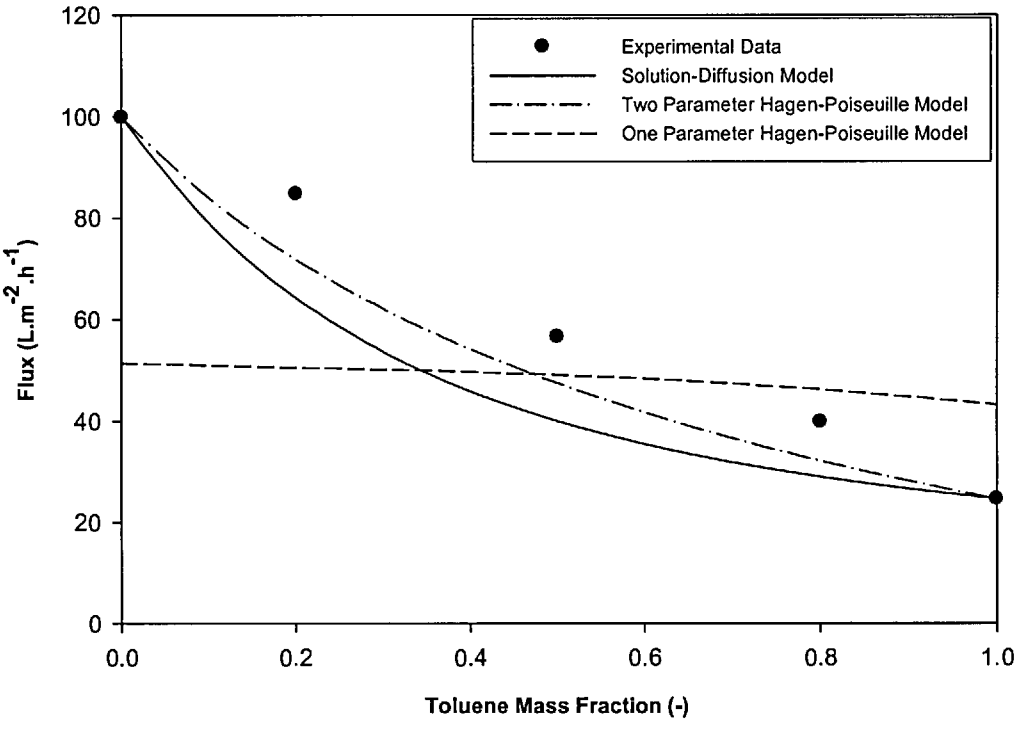

Figure 12 : Flux of ethyl acetate-toluene mixtures at 30 °C and 30 bar.

It is clear that the model provides a reasonable fit to the experimental data for both systems. Two Hagen-Poiseuille models (a one parameter model and a two parameter model) were also used to describe the experimental solvent flux data shown in Figures 11 and 12. The permeability term $\left(\varepsilon d_{pore}^{2}/32l\tau\right)$ in Eq. (12) is determined by the physical properties of the membrane. When membrane geometry remains constant, i.e. there is no membrane compaction or membrane swelling, this term should be independent of the solvent mixtures investigated, and one parameter value should describe fluxes of all solvents. In fact, the derived values for this term are very different (Table 11) for pure methanol (3.91×10^{-15} m), toluene (1.32×10^{-15} m) and ethyl acetate (1.62×10^{-15} m). Nevertheless for the one parameter Hagen-Poiseuille model an arithmetic average of these specific pemeabilities was taken (2.28×10^{-15} m) and have the viscosity as the only composition dependent parameter. For the two parameter Hagen-Poiseuille model, the idea that the physical properties of the membrane change with the solvent due to different solvent-polymer interactions, i.e. different degrees of swelling, was incorporated. For this two parameter

Hagen-Poiseuille model, an approximate approach was used to describe the term $\left(\varepsilon d_{pore}^{2}/32l\tau\right)_{mix}$ for the solvent mixtures by considering a concentration average of the pure solvent values, i.e. going back to Eq. (10) assuming no viscous selectivity and a linear pressure profile inside the membrane the following relation using these two pure solvent parameters is obtained to describe the total flux of a binary mixture:

$$N_v = \frac{\Delta p}{\eta}\left(\bar{V}_1 c_{1(m)}\left(\varepsilon d_{pore}^{2}/32l\tau\right)_1 + \bar{V}_2 c_{2(m)}\left(\varepsilon d_{pore}^{2}/32l\tau\right)_2\right) \tag{47}$$

Together with the viscosities for solvent mixtures shown in Figures 9 and 10, Eq. (47) was used to predict solvent flux data. The predicted values using both one parameter and two parameter Hagen-Poiseuille models are also shown in Figures 11 and 12. It is clear that the one parameter model fits the data poorly, while the two parameter model provides much better predictions. The reason for the one parameter Hagen-Poiseuille model predictive failure is that the permeability change due to swelling of the polymer matrix is ignored by the use of a constant average permeability. Therefore viscosity is clearly not the determining factor in the transport. The most appropriate comparison is between the two parameter Hagen-Poiseuille model and the solution-diffusion model, since the solution diffusion is also effectively a two parameter model (i.e. it uses two permeabilites). It can be seen from Figure 11 that solution-diffusion model better predicts solvent fluxes of methanol/toluene mixtures than the two parameter Hagen-Poiseuille models, while the two parameter Hagen-Poiseuille model gives a slightly better description for solvent fluxes of toluene/ethyl acetate mixtures in Figure 12, although there is not much in it. These results indicate that the solution-diffusion model gives moderately better results for predicting mixtures of solvent fluxes from pure solvent permeability data in STARMEM^{TM} 122 than the two parameter Hagen-Poiseuille model. A key factor which might distinguish between pore-flow and solution-diffusion transport mechanisms is the degree of solvent separation. In the Hagen-Poiseuille approach, no solvent separation is expected, while the solution-diffusion model predicts, as presented in Figures 13 and 14, a small solvent separation through methanol enrichment in the permeate.

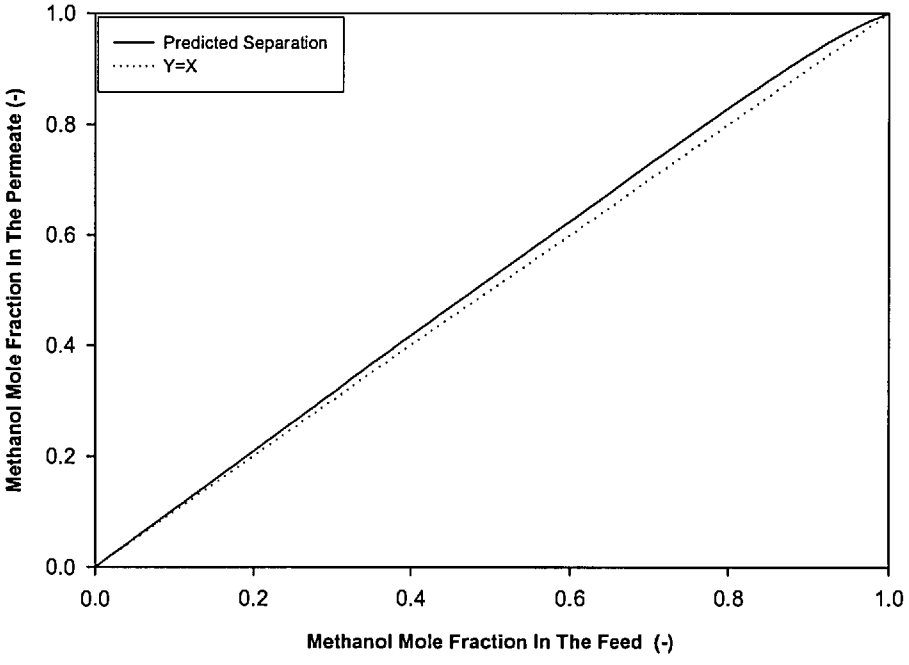

Figure 13 : Methanol-toluene mixture separation.

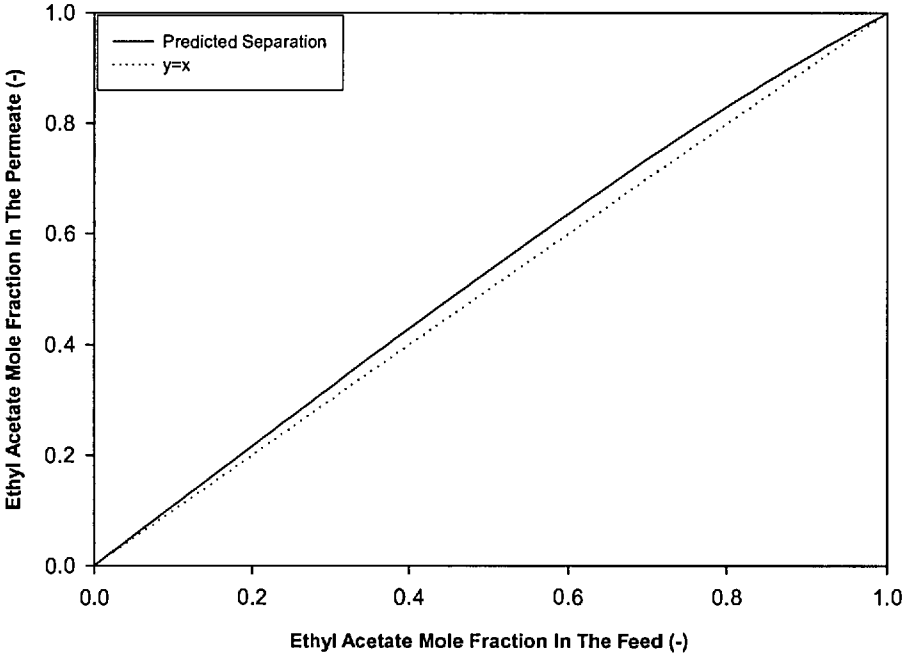

Figure 14 : Ethyl acetate-toluene mixture separation.

Solvent separation has been reported for other solvent mixtures in the literature (White, 2002; Adam et al., 1983). In this thesis, for methanol/toluene and toluene/ethyl acetate mixtures, the measurements showed that the compositions in the permeate are the same, within experimental error, as those in the retentate. However, the possibility of solvent separation cannot be ignored since the predicted separation is within the experimental error of the analytical method used for the measurement. The absence of solvent separation for solvent mixtures, where pure solvent components have large permeation differences, was also observed by Machado et al. (1999) for the MPF OSN membrane series.

3.5 Conclusion

Solvent fluxes for methanol/toluene and ethyl acetate/ toluene mixtures in STARMEM^{TM} 122 can be well described by the solution-diffusion model. The two parameter Hagen-Poiseuille model predicts solvent fluxes for toluene/ethyl acetate mixtures in STARMEM^{TM} 122, but is not very successful for predictions in methanol/toluene. The membrane-solvent interaction is important in the mechanism that governs solvent transport in a particular system, although there is no clear explanation for the difference in flux between toluene and ethyl acetate. Experimental data shows that the compaction of polyimide OSN membranes is a slow process, i.e. occurs over a few days not a few hours, and solvent fluxes in STARMEM^{TM} 122 are independent of "membrane-using history". The central conclusion is that it is possible to predict solvent fluxes for solvent mixtures using pure solvent data. To do this for polyimide membranes, this work recommendation is to measure steady fluxes of pure solvents, and use these to determine membrane permeabilities. These permeabilities, together with the simple solution-diffusion model presented in this work, should be used to make design calculations for solvent mixtures. The modelling approach developed in this chapter works relatively well, when describing linear (methanol-toluene) and exponential (methanol-ethyl acetate) solvent mixture flux trends. Therefore, it should be easily applicable to other membrane-solvent mixture that exhibit similar flux behaviour, for instance the acetone-water and acetone-alcohol mixture permeation through MPF-50, presented by Machado et al. (1999) or the methanol-ethanol mixture permeation through hydrophobic and hydrophilic membranes presented by Geens et al. (2005). However, there is some literature data where the solvent mixture flux trend

has a parabolic behaviour, passing by a minimum value. Machado et al. (1999) reported this type of behaviour for the permeation of acetone-paraffin mixtures through MPF-50, and Geens et al. (2005) reported this flux behaviour for the permeation of water-alcohol mixtures through a series of hydrophilic membranes. For these systems that present a minimum in solvent mixture flux, the models developed in this chapter will not be able to give accurate predictions, since the mathematical expressions that form them demand a monotonically increases in flux. However, this predictive capability could be extended to solvent minima flux systems by introducing concentration dependent permeabilities.

A general methodology to describe solvent mixture permeation through OSN membranes can be defined by two simple steps:

- Step 1: Obtain experimental pure solvent permeabilities from the slope of the plot containing solvent flux vs applied pressure.
- Step 2: Use the obtained permeabilities in the solution-diffusion model (Eq. (44) and Eq. (45)) and predict fluxes for the different concentrations.

4. Effect of Solute Concentration and Mass Transfer Limitations on Transport in Organic Solvent Nanofiltration – Partially Rejected Solute

4.1 Aim and Scope

In recent years the possibility of using polymeric organic solvent nanofiltration (OSN) membranes for non-aqueous separations has been explored for a wide range of applications, as the ones described in chapter 3. In the existing publications concerning the fundamental mechanisms involved in solute transport through OSN membranes it was observed that:

- Controversy still exists in relation to whether pore-flow or solution-diffusion models should be employed to describe OSN transport. Some authors (White, 2002; Peeva et al., 2004; Stafie et al., 2004; Wijmans and Baker, 1995; Paul, 2004; Paul, 1970) suggest that species dissolve in the membrane and subsequently diffuse through it, driven by an activity gradient. Others (Bhanushali et al., 2002; Machado et al., 2000; Robinson et al., 2004) suggest the specie transport is caused by pressure driven viscous flow through nano-pores.
- Much of the data published for OSN transport studies has been obtained for short duration experiments using dead-end cells, operating in the low specie concentration range (< 1wt.% solute in solvent). In actual applications, solutes will usually be more concentrated (> 5wt. %). For instance, in solute lube oil dewaxing (White and Nitsch, 2000) the nominal feed composition is around 20 wt. % of solute. Ideally, a robust OSN transport model should cover all practical concentration ranges of species.

In this study, continuous cross-flow nanofiltration cells have been used to study the flux and rejection behaviour of STARMEM^{TM}122 (S-122) and MPF-50 (Koch Membrane Systems Ltd.) OSN membranes over periods of several weeks. The binary system methanol/dimethyl-methylsuccinate has been used as a model system since it has been reported by others as a hydrogenation system (Tang et al., 2003), for which OSN can be used for catalyst recycle. This system was used to investigate the transport mechanism in

OSN membranes, and to clarify the effect of solute concentration on the flux/rejection profiles, for a partially rejected specie (DMMS). The experimental flux and rejection results are fitted with solution-diffusion and pore-flow membrane transport models each with a single adjustable parameter, coupled with a single adjustable parameter film theory model describing concentration polarization phenomena. From the goodness-of-fit and analysis of the results, insight will be gained into which idealized model comes closest to describing the actual transport phenomena in OSN. The detailed transport models used in this work, incorporating a membrane transport model and the film theory model, and using two adjustable parameters for each model, are described in Table 12. The main equations in the solution-diffusion, film theory and Bowen's pore-flow models are described in chapters 2.4 to 2.7, and their detailed deduction can be found in Appendix I.

Table 12 : Pore-flow and solution-diffusion model mathematical description.

Solution-Diffusion plus mass transfer	**Pore-Flow plus mass transfer**
$N_1 = P_{1m}\left(\frac{c_{1F(m)}}{c_{1F(m)}+c_{2F(m)}} - \frac{c_{1P}}{c_{1P}+c_{2P}}\exp\left(-\frac{\overline{V}_1\Delta p}{RT}\right)\right)$ $N_2 = P_{2m}\left(\frac{c_{2F(m)}}{c_{1F(m)}+c_{2F(m)}} - \frac{c_{2P}}{c_{1P}+c_{2P}}\exp\left(-\frac{\overline{V}_2\Delta p}{RT}\right)\right)$ $\eta_F = 6E\text{-}11w_{1F}^4 - 8E\text{-}09w_{1F}^3 + 4E\text{-}07w_{1F}^2 - 9E\text{-}07w_{1F} + 0.0005$ $D_{12}^0 = \frac{RT}{6\pi N_a \eta r_1}$ $k_0 = k_b\left(\frac{\rho_{methanol}}{\rho_{water}}\right)^{-0.47}(1000\eta)^{-0.47}\left(\frac{D_{12}^0}{8E-10}\right)^{0.67}$ $x_{1F} = \frac{\frac{w_{1F}}{MW_1}}{w_{1F}\left(\frac{1}{MW_1}-\frac{1}{MW_2}\right)+\frac{1}{MW_2}}$ $c_{1F} = \frac{x_{1F}}{x_{1F}\left(\overline{V}_1-\overline{V}_2\right)+\overline{V}_2}$ $c_{1F(m)} = \left(c_{1F}-c_{1p}\right)\exp\left(\frac{N_v}{k_0}\right)+c_{1p}$ $c_{1F(m)}\overline{V}_1 + c_{2F(m)}\overline{V}_2 = 1$ $N_v = N_1\overline{V}_1 + N_2\overline{V}_2$ $c_{1p} = \frac{N_1}{N_V}$ $c_{1P}\overline{V}_1 + c_{2P}\overline{V}_2 = 1$ $OR = 1-\frac{c_{1P}}{c_{1F}}$	$N_v = P_{2m}\left(\Delta p - 8.32T\left(c_{1P} - c_{1F}\left(\frac{1-OR}{1-RR}\right)\right)\right)$ $\lambda_1 = \frac{r_1}{r_p}$ $\Phi_1 = (1-\lambda_1)^2$ $K_c = \left(2-\Phi_1\right)\left(1+0.0054\lambda_1 - 0.988\lambda_1^2 + 0.441\lambda_1^3\right)$ $K_d = -2.30\lambda_1 + 1.154\lambda_1^2 + 0.224\lambda_1^3$ $\eta_F = 6E\text{-}11w_{1F}^4 - 8E\text{-}09w_{1F}^3 + 4E\text{-}07w_{1F}^2 - 9E\text{-}07w_{1F} + 0.0005$ $D_{12}^0 = \frac{RT}{6\pi N_a \eta r_1}$ $D_{12} = D_{12}^0 K_d$ $Pe` = \frac{(K_c - Y)r_p^2}{8\eta D_{12}}\frac{N_v}{P_{2m}}$ $Y = \frac{D_{12}}{RT}\overline{V}_1\frac{8\eta}{r_p^2}$ $RR = 1 - \frac{(K_c-Y)\Phi_1}{1-[1-(K_c-Y)\Phi_1]\exp(-Pe`)}$ $k_0 = k_b\left(\frac{\rho_{methanol}}{\rho_{water}}\right)^{-0.47}(1000\eta)^{-0.47}\left(\frac{D_{12}^0}{8E-10}\right)^{0.67}$ $x_{1F} = \frac{\frac{w_{1F}}{MW_1}}{w_{1F}\left(\frac{1}{MW_1}-\frac{1}{MW_2}\right)+\frac{1}{MW_2}}$ $c_{1F} = \frac{x_{1F}}{x_{1F}\left(\overline{V}_1-\overline{V}_2\right)+\overline{V}_2}$ $\frac{OR}{1-OR} = \frac{RR}{1-RR}\exp\left(\frac{N_V}{k_0}\right)$ $OR = 1-\frac{c_{1P}}{c_{1F}}$
Parameters: $R, T, N_a, \eta_1, MW_1, MW_2, \overline{V}_1, \overline{V}_2, \Delta p, P_{2m}$	**Parameters:** $R, T, N_a, \eta_1, MW_1, MW_2, \overline{V}_1, \overline{V}_2, \Delta p, P_{2m}$
Variables: $\eta, D_{12}^0, k_0, x_{1F}, c_{1F}, N_1, N_2, c_{1F(m)}, c_{2F(m)}$ c_{1P}, c_{2P}, N_v, OR	**Variables:** $\eta, D_{12}^0, \lambda_1, k_0, x_{1F}, c_{1F}, \Phi_1, K_c, K_d, D_{12}, Pe`, c_{1P},$ N_v, OR, Y, RR
Fitting parameter: P_{1m}, k_b	**Fitting parameter:** r_p, k_b

4.2 Materials and Methods

4.2.1 Chemicals

Two organic solvents methanol (analytical grade) and dimethyl methylsuccinate (DMMS, analytical grade) were used in this study. Tetraoctylammonium bromide (TOABr), (MW= 547 $g.mol^{-1}$) was selected as a marker to check for membrane leakage paths (no leakage eas observed). All chemicals were obtained from Aldrich, UK.

4.2.2 Membranes

S-122, an asymmetric OSN membrane with an active layer of polyimide, in a "dry" form but with a lube oil soaked into the membrane as a preserving agent, and with a nominal MWCO of 220 $g.mol^{-1}$ (manufacturer's data) was supplied by Membrane Extraction Technology Ltd (UK). MPF-50, a composite membrane comprising an active layer of crosslinked polydimethylsiloxane (PDMS) mounted on a polyacrylonitrile (PAN) support (Linder et al., 1993), was purchased from Koch Membrane Systems. MPF-50 has a MWCO of 700 Dalton (manufacturer's data). MPF-50 was supplied soaked in 50% ethanol/water.

4.2.3 Filtration Equipment and Experimental Measurements

Cross-flow permeations were performed for several concentrated solutions of DMMS in methanol (5-35 wt. %) in order to test the effect of concentration on OSN fluxes and rejections. The experiments were conducted at 30 °C and three different pressures were tested (20, 25 and 30 bar).

Figure 7 shows the diagram of the cross-flow nanofiltration rig. It consists of four cross-flow nanofiltration cells connected in series, a solution reservoir, a backpressure regulator, and a piston pump. Each cell had a membrane area of $1.4x10^{-3}$ m^2 and the height of the chamber from the surface of the membrane was 50 mm, giving a fluid volume of 7 ml. At a flow rate of 60 $L.h^{-1}$ the solution enters the cross flow cell tangentially from the cell wall and exits the cell from the top centre, providing turbulent hydrodynamic conditions. The

applied pressure was controlled using a backpressure regulator and the temperature at 30 ± 0.5 °C using a water bath and heat exchanger.

During filtration the solvent flux was obtained by:

$$N_v = \frac{V}{A.t} \tag{48}$$

Where V is the sampling volume in the permeate, A the effective membrane area and t the sampling time. The observed rejection was defined as

$$OR_i = \left(1 - \frac{C_{ip}}{C_{ir}}\right) \times 100\% \tag{49}$$

Where C_{ip} and C_{ir} are the concentrations of specie i in the permeate and retentate respectively.

4.2.4 Determination of Cross-Flow Cell Mass Transfer Coefficient

The cross-flow cell mass transfer coefficient for DMMS was estimated by dissolution of a plate of benzoic acid into water at a cross flow rate of 60 $L.h^{-1}$ and 30 °C. The benzoic acid plate preparation procedure and mass transfer coefficient calculation technique are the same as the ones presented by Peeva et al. (2004).

4.2.5 Analytical Methods

Concentrations of DMMS were determined using a Perkin-Elmer Gas Chromatograph with a flame ionisation detector and an HP1 methyl siloxane column 30 m long 0.35 mm i.d. The temperature programme ran from 80 °C to 300 °C at a rate of 25 $°C.min^{-1}$, and the column temperature was held at 80 and 300 °C for 3 minutes at the start and finish of the temperature programme respectively. The standard error of three independent measurements was 2 %.

Viscosities of methanol/DMMS mixtures were measured by U-Tube Viscometer (PSL Scientific, UK), respectively. The data is shown in Figure 15, all the measurements were conducted at 30 °C.

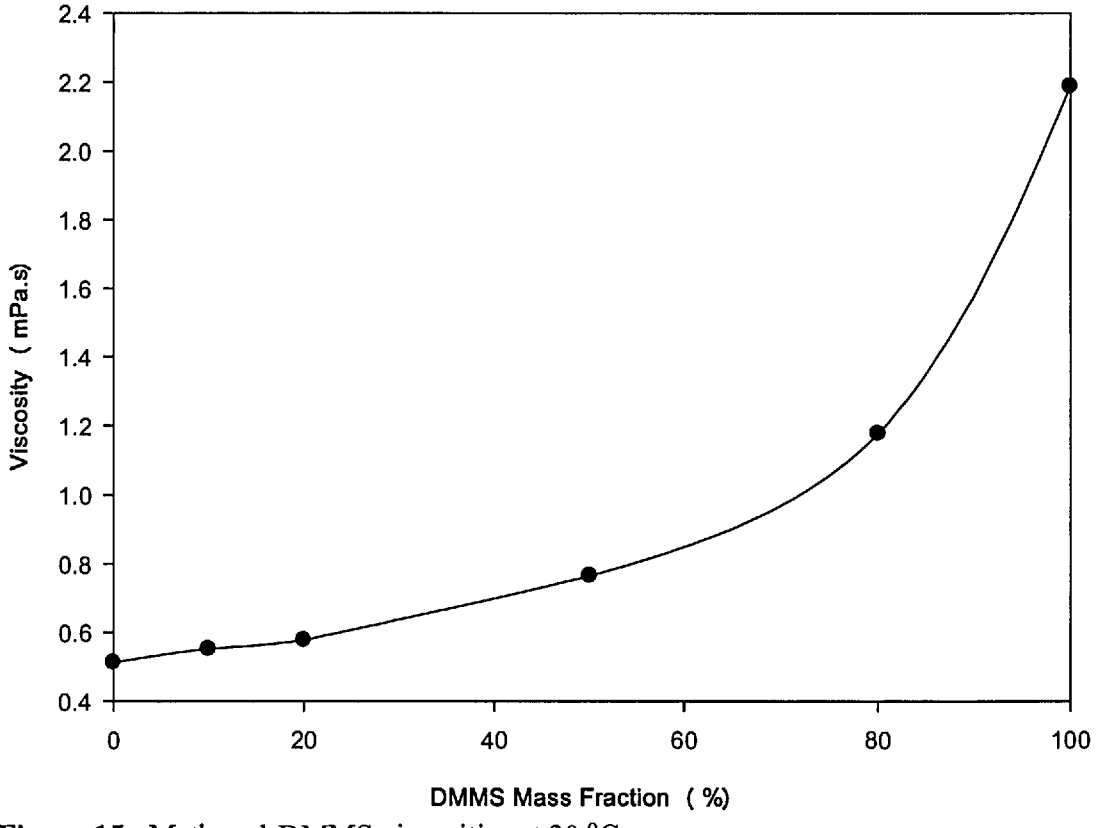

Figure 15 : Methanol-DMMS viscosities at 30 °C.

4.3 Results and Discussion

4.3.1 Membrane Compaction

As can be seen in Figure 16 concentration changes in the methanol-DMMS solutions were performed randomly, in order to minimize any systematic error.

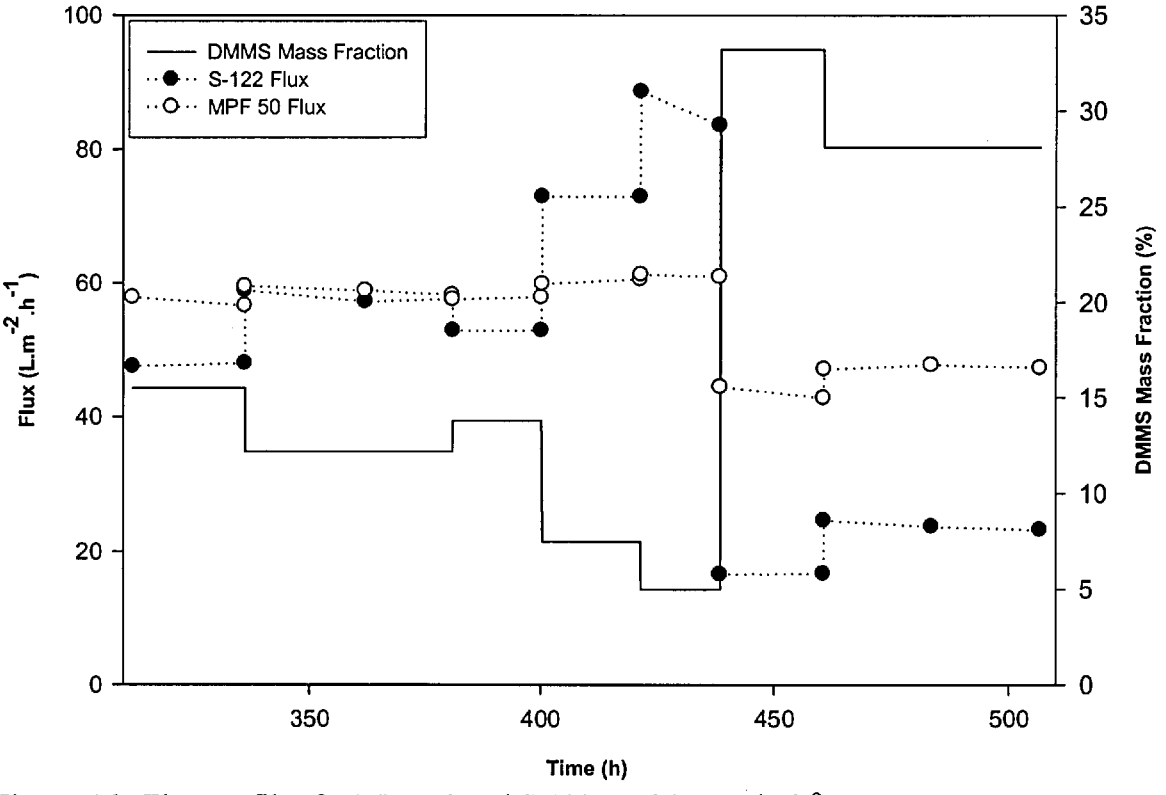

Figure 16 : Flux profiles for MPF-50 and S-122 at 30 bar and 30 °C.

During the experiment the procedure used to exchange from one solution to another was performed without stopping the pump. Solutions were diluted or concentrated into the next solution, maintaining system pressurization. When permeating solvent mixtures through a cross-flow system, significant flux decline over time was observed during several hours for the start and restart of experiments (Silva et al., 2005). However, for long operating times (greater than a few days), steady state fluxes were achieved. It is interesting to note that for extended times of continuous permeation, as presented in this work, the compaction effects are negligible and steady fluxes are obtained (Figure 16). Therefore, long term continuous pressurization seems to be a requirement for obtaining reliable, time invariant flux and rejection data.

The effect of solute concentration on the flux is quite clear in Figure 16, and is as expected from the osmotic pressure dependence on concentration; as solute concentration increases the flux decreases. For S-122 even slight changes of concentration are able to produce quite significant changes in flux. MPF-50 is not that sensitive to concentration changes. This

difference in behaviour can be easily related to the different rejection characteristics of the membranes (DMMS rejections by S-122 are approximately three times those for MPF-50).

4.3.2 Effect of Concentration on Flux

As expected, the flux decreases with increasing concentration (Figure 17), for both S-122 and MPF-50.

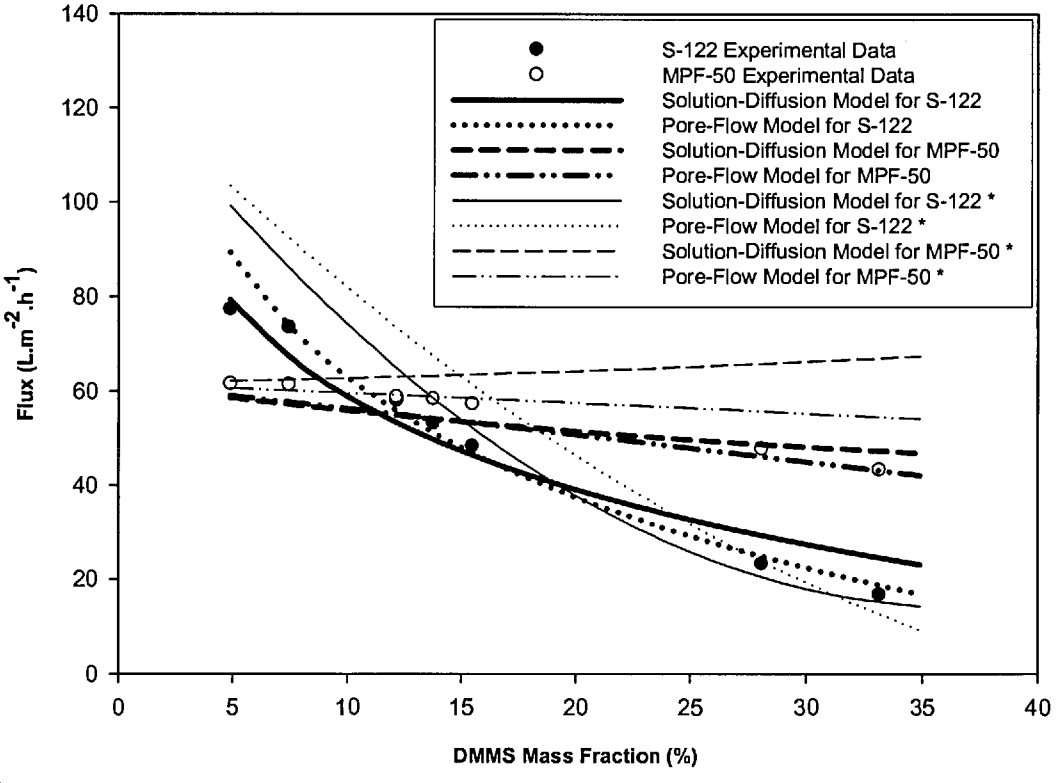

*- For Infinite mass transfer coefficient.

Figure 17 : Experimental and simulated Methanol-DMMS flux profiles for MPF-50 and S-122 at 30 bar and 30 °C.

This behaviour is common throughout the OSN literature and it is easily explained by the osmotic pressure increase (Stafie et al., 2004) combined with the concentration polarization phenomena (Peeva et al., 2004). The higher values of flux for S-122 are due to the greater methanol affinity of this membrane when compared with MPF-50. The reported solubility parameters for this membranes (≈26.8 $MPa^{1/2}$ for S-122 (Silva et al., 2005) and 14.9-15.6

$MPa^{1/2}$ for PDMS MPF-50 active layer (Stafie et al., 2004)) support this claim since the solubility parameter for methanol is 29.7 $MPa^{1/2}$.

Before discussing the fitting results obtained for the two OSN transport models, the following should be pointed out:

- Both solution-diffusion and pore-flow models were used to analyse the experimental data. For the solution-diffusion model it was assumed that the solution has an ideal behaviour (activity coefficients of unity) and for the pore-flow approach the van't Hoff description of osmotic pressure was used (Stafie et al. (2004) showed that it could provide reliable results for highly concentrated organic solutions).
- DMMS diffusivities in methanol are based on the Stokes-Einstein relation, for which the effective DMMS molecular diameter was determined using Gaussian 3.0 molecular modelling software. Within Gaussian, the highly accurate ground state DFT, B3LY method with a 6-31G+(d,p) basis set was used. The IEFPCM solvation method (Frisch et al., 2004) was included in order to account for the solvent (methanol) influence on the molecular geometry optimization of the solute. After achieving optimized geometry, the effective molecular diameter was calculated according to (Van der Bruggen et al., 2000):

$$d_1 = \frac{\pi}{4} H + \frac{D}{2} \tag{50}$$

  Where H is the height and D the base diameter, for the smallest cylinder containing the molecule (Figure 18). In addition to the precise molecular dimensions used the DMMS diffusivity accuracy was increased by incorporating a concentration dependent viscosity term.
- Solvent permeabilies for both membranes were obtained from pure solvent experiments, following the same approach as Silva et al. (2005). It was assumed that this permeability is independent of solution composition. The permeability values are presented in Table 13.
- The optimal value for the fitting parameters was obtained using the gEXT tool of the simulation software gPROMS 2.2.4 (Process Systems Enterprise Ltd., 2002). This tool uses a HQP sequential quadratic code to optimize the objective function.

The minimized objective function (f) included both flux and rejection variables, i.e. the obtained fits are overall performance type fits.

$$f = \sum_{i=1}^{n} (OR^{i}_{experimental} - OR^{i}_{simulated})^2 + (Nv^{i}_{experimental} - Nv^{i}_{simulated})^2 \quad (51)$$

The correct functioning of the optimization algorithm is monitored by output condition numbers. If the value of the condition number on gEXT output is bigger than 10^{10}, variable scaling is introduced in order to achieve proper function minimization, the characteristics of this variable scaling are described elsewhere (Process Systems Enterprise, 2002). In practice since both OR and N_v ranged from 0-100 units, no scaling was applied to Eq. (51). It was noticed however that when scaling is used it does not significantly alter the fit.

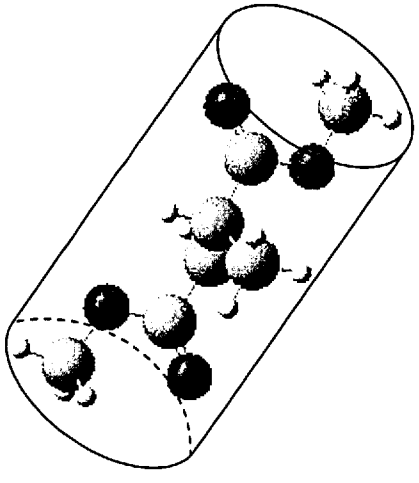

Figure 18 : Optimized molecular structure for DMMS.

Table 13 : Pore-flow and solution-diffusion model parameters for S-122.

Parameters	Transport model								Determination Method
	Solution-Diffusion				Pore-Flow				
	S-122		MPF-50		S-122		MPF-50		
r_1 (m)	0.44×10^{-9}								Molecular Modelling
k_0 (m.s^{-1})	8.19×10^{-6}	∞^b	7.57×10^{-6}	∞^b	8.33×10^{-6}	∞^b	8.89×10^{-6}	∞^b	Nonlinear Fitting
r_p (m)	n/a	n/a	n/a	n/a	9.10×10^{-10}	7.74×10^{-10}	2.19×10^{-9}	3.58×10^{-9}	Nonlinear Fitting
P_{1m} (mol.m^{-2}.s^{-1})	0.21	0.10	0.74	1.70	n/a	n/a	n/a	n/a	Nonlinear Fitting
P_{2m} ([a])	17.5	17.5	8.9	8.9	1.06×10^{-11}	1.06×10^{-11}	5.71×10^{-12}	5.71×10^{-12}	Pure Solvent Permeation

a - mol.m^{-2}.s^{-1} for Solution-Diffusion model and m.s^{-1}.Pa^{-1} for Pore-Flow model.
n/a - not applicable.
b - fixed value set by modeller.

It is interesting to note that both solution-diffusion and pore-flow models can explain the solvent flux dependence on concentration for S-122 and MPF-50, even in the absence of solution mass transfer limitations ($k_0 = \infty$). Analysing the fitting results in detail (Table 13), it is clear that both solute permeabilities for the solution-diffusion model, and pore radius for the pore-flow model, are estimated as physically feasible values in agreement with reported literature data (Table 14).

Table 14 : Literature data on membrane parameters.

Author	Membrane	Solvent	Solute	Cross-flow rate(L.h^{-1})	r_p (m)	P_{1m} (mol.m^{-2}.s^{1})	k x10^5 (m.s^{-1})
Peeva et al. (2004)	S-122	Toluene	0.33 M Docosane	40-80	-	0.0007	1.9
Tarleton et al. (2004)	PDMS based	Xylene	9,10-diphenylanthracene	42	2-2.5x10^{-9}	-	-
Gibbins et al. (2002)	S-122	Methanol	octylammoniumbromide	-	0.6-0.7x10^{-9}	-	-

In addition, the estimated mass transfer coefficients are quite close to those determined experimentally (Table 15), and to those reported in the literature for a similar setup (Peeva et al., 2004).

Table 15 : Experimentally determined benzoic acid mass transfer coefficient.

Compound	Concentration ($mol.dm^{-3}$)	Mass transfer coefficient at 60 $L.h^{-1}$ flow rate $x10^{5}$ ($m.s^{-1}$)
Benzoic acid	1.00E-03	1.15

The mass transfer coefficient similarity between different transport models and membranes indicates once again transport model feasibility. It appears that the total volumetric flux is mainly determined by the solvent permeability, independent of the porous or dense characteristics of the membrane barrier. For the systems studied, the solvent permeability is much higher than the solute permeability. This high solvent permeability maintains the high total volumetric flux, disregarding mass transfer limitations or small solute permeability changes.

4.3.3 Effect of Concentration on Rejection

In examining the rejection fitting results in Figure 19, the focus will be on the S-122 results, since MPF-50's rejection data is almost constant, and almost zero, with concentration, making it difficult to distinguish between the concentration effect and the experimental error associated with the measurements. This is not surprising, given the quoted MWCO of 700 $g.mol^{-1}$ for this membrane.

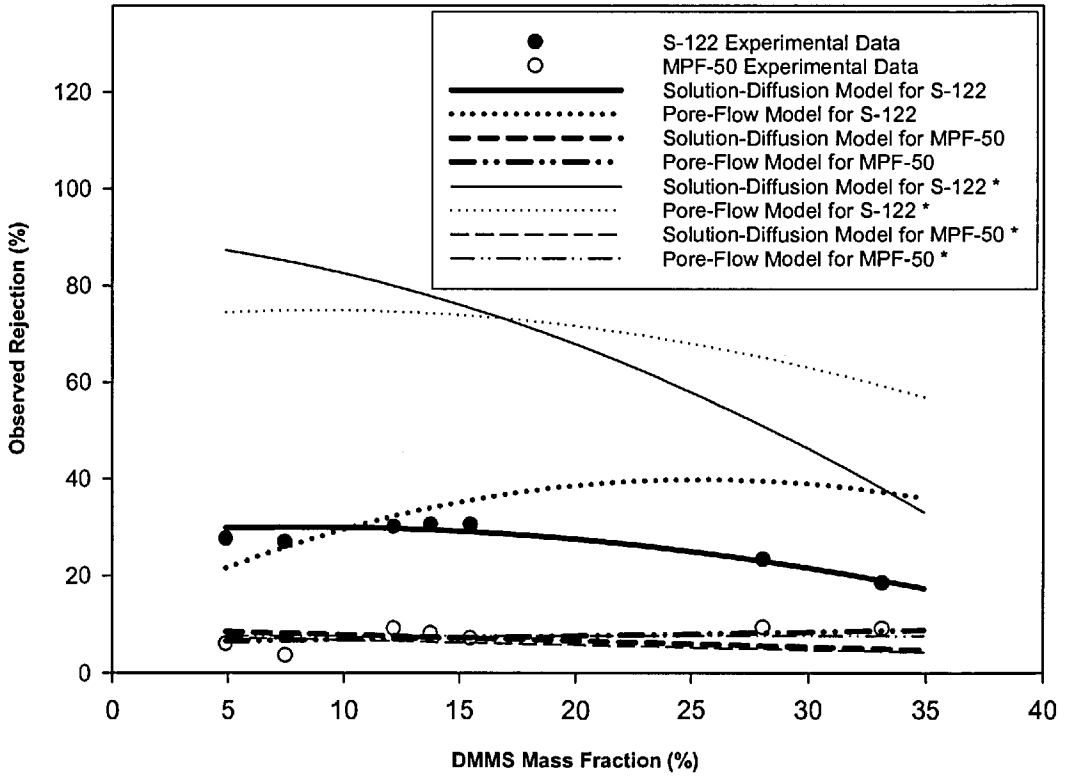

*- For Infinite mass transfer coefficient.

Figure 19 : Experimental and simulated Methanol-DMMS rejection profiles for MPF-50 and S-122 at 30 bar and 30 °C.

The S-122 experimental rejection versus concentration profile remains constant in the range 8-15 wt. % DMMS at around 30 % and then decreases to around 18 % at 33.2 wt. % DMMS. This is consistent with the OSN literature data which shows a rejection decrease with increasing concentration (Peeva et al., 2004). However, the opposite behaviour was also reported for stirred batch dead-end nanofiltration (Whu et al., 2000). It seems that the solution mass transfer characteristics of the nanofiltration setup in use are a crucial factor determining how rejection profile changes with concentration. To test this statement Figure 19 shows model predictions in the absence of mass transfer limitations ($k_0 = \infty$), the model predictions of rejection for infinite mass transfer coefficient are significantly different from the experimental values.

Although important, concentration polarization cannot be the only factor determining rejection behaviour, since mass transfer coefficients obtained by fitting are similar for both pore-flow and solution-diffusion models (Table 13), leading to similar membrane wall solute concentrations (Table 16).

Table 16 : Predicted concentration polarization effect.

	Membranes	Transport Model	Solvent bulk mass fraction						
			0.050	0.075	0.122	0.138	0.155	0.281	0.332
Solute Mass Fraction at the Membrane Surface	S-122	Pore-Flow	0.102	0.143	0.204	0.221	0.238	0.345	0.386
		Solution-Diffusion	0.110	0.143	0.193	0.208	0.223	0.329	0.372
	MPF-50	Pore-Flow	0.056	0.085	0.138	0.155	0.174	0.312	0.365
		Solution-Diffusion	0.061	0.091	0.144	0.161	0.180	0.310	0.360

In contrast, the model predicted rejections are quite different, the results suggest that for S-122 solute rejection, the solution-diffusion membrane transport model provides the best fit to the data. In addition, it is important to point out that the pore-flow model demands a distinction between solvent and solute, and that when this model is applied to the high concentration region of a partially rejected solute, where this distinction starts to break down, the model fails to predict the experimental results. On the other hand, the solution-diffusion does not distinguish solute from solvent, and is able to give reasonable predictions over the whole concentration range.

4.3.4 Effect of Pressure on Flux and Rejection

In the previous section, it was shown that a simple solution-diffusion model, coupled with film theory, was capable of describing S-122 flux and rejection data over a broad concentration range at 30 °C and 30 bar. To further assess the generality of the models, flux/rejection data for different pressures (20 and 25 bar) was collected, and the ability of the models to predict the experimental trends was tested using the model parameters determined from fitting at 30 °C and 30 bar.

As expected, the experimental flux decreases with decreasing pressure (Figure 20).

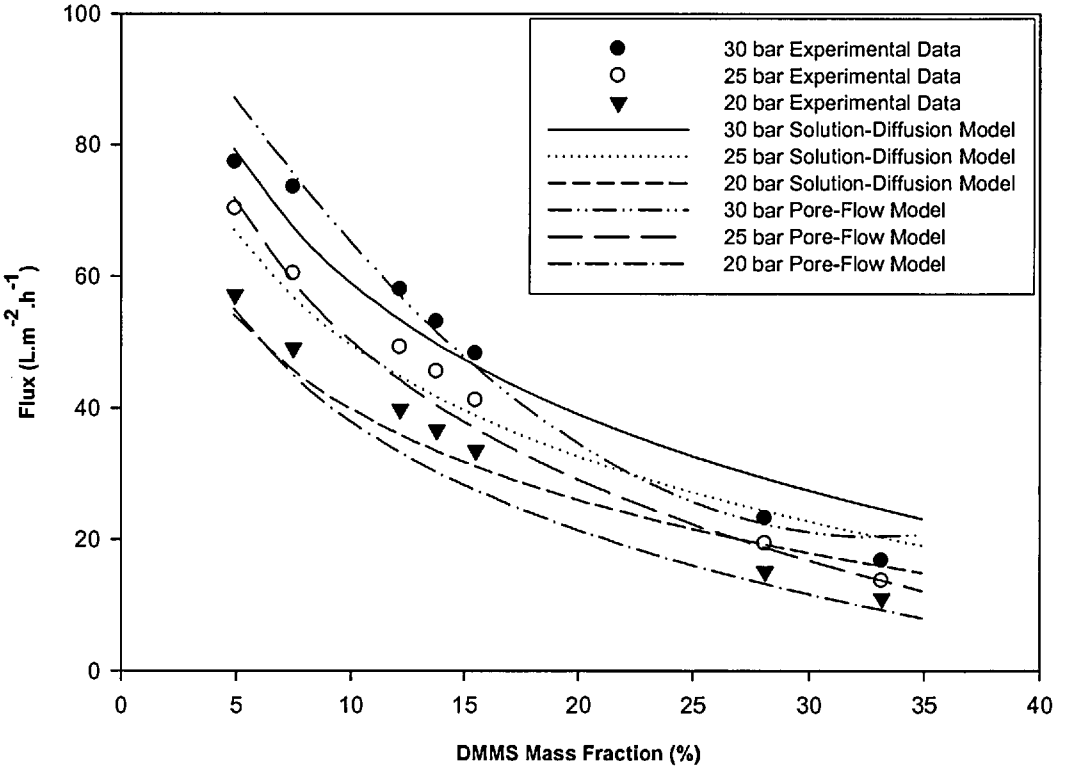

Figure 20 : Experimental and simulated S-122 Methanol-DMMS flux profiles at several pressures and 30 °C.

For S-122 both solution-diffusion and pore-flow models predicted this behaviour; actually the model predicted trends are very close to the experimental ones for all pressures. This is not only an indication of the predictive capabilities of the model, under pressure changes, but also indicates that after the effects of compaction are eliminated, the transport model parameters (solute permeability for the solution-diffusion model and pore radius for the pore-flow model) and the mass transfer coefficient are pressure independent. This is a very important point, proving model applicability throughout all pressures.

Following the previously reported work (Peeva et al., 2004), the experimental rejection values decreased with decreasing pressure (Figure 21).

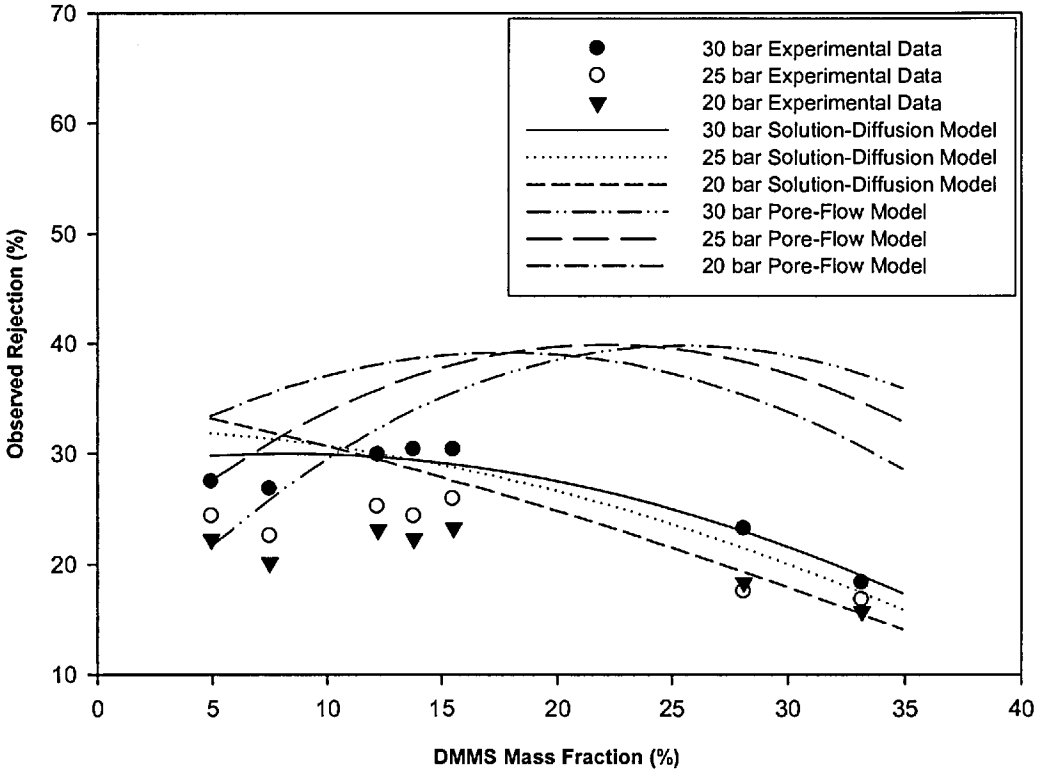

Figure 21 : Experimental and simulated S-122 Methanol-DMMS rejection profiles at several pressures and 30 °C.

From the model predicted trends, once again it is clear that the pore-flow model overestimates the high concentration rejection values, while for S-122 on the other hand the solution-diffusion predictions are quite close to the experimental trends.

These multi-pressure experiments produced marked changes in the MPF-50 flux, allowing transport model testing for this membrane. Figure 22 shows the model predicted results.

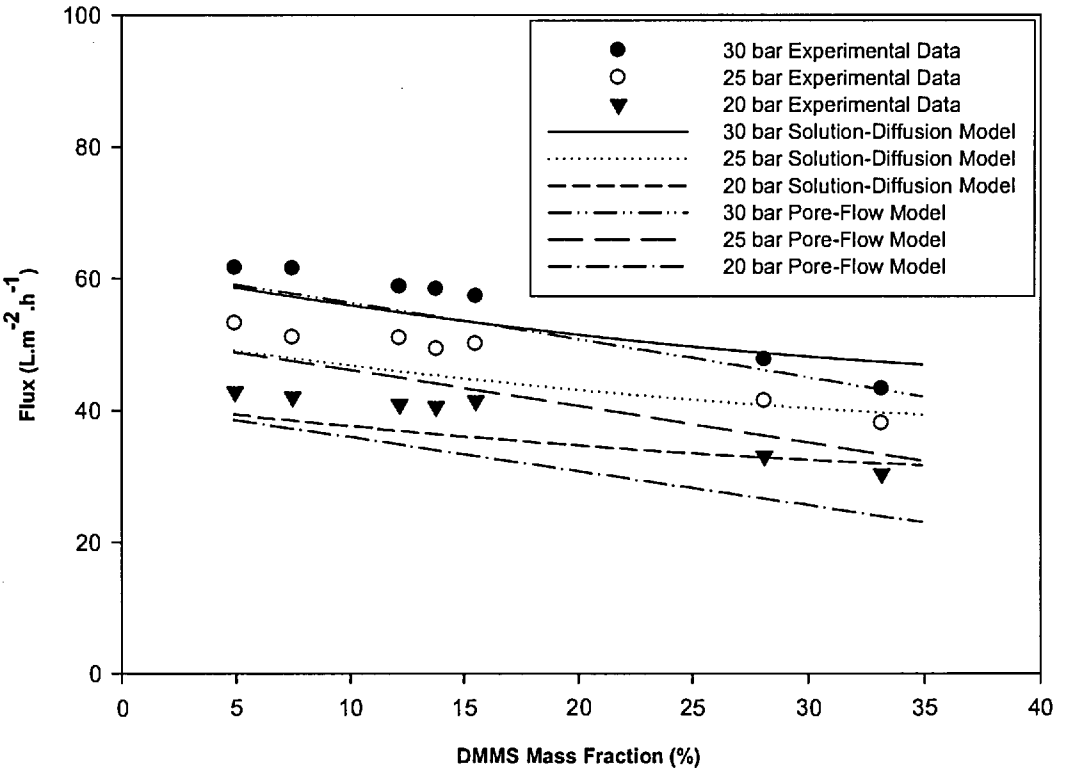

Figure 22 : Experimental and simulated MPF-50 Methanol-DMMS flux profiles at several pressures and 30 °C.

Both solution-diffusion and pore-flow models gave reasonable predictions for the several pressures; however, the solution-diffusion model was more accurate in the low pressure high concentration range. Therefore, solution-diffusion seems to be the most plausible transport mechanism for MPF-50. This result is in agreement with recent work on the physiochemical interpretation of solute transport trough PDMS based membranes (Gevers et al., 2006). Yet, the experimental rejection (Figure 23) is again too scattered to derive any solid conclusions.

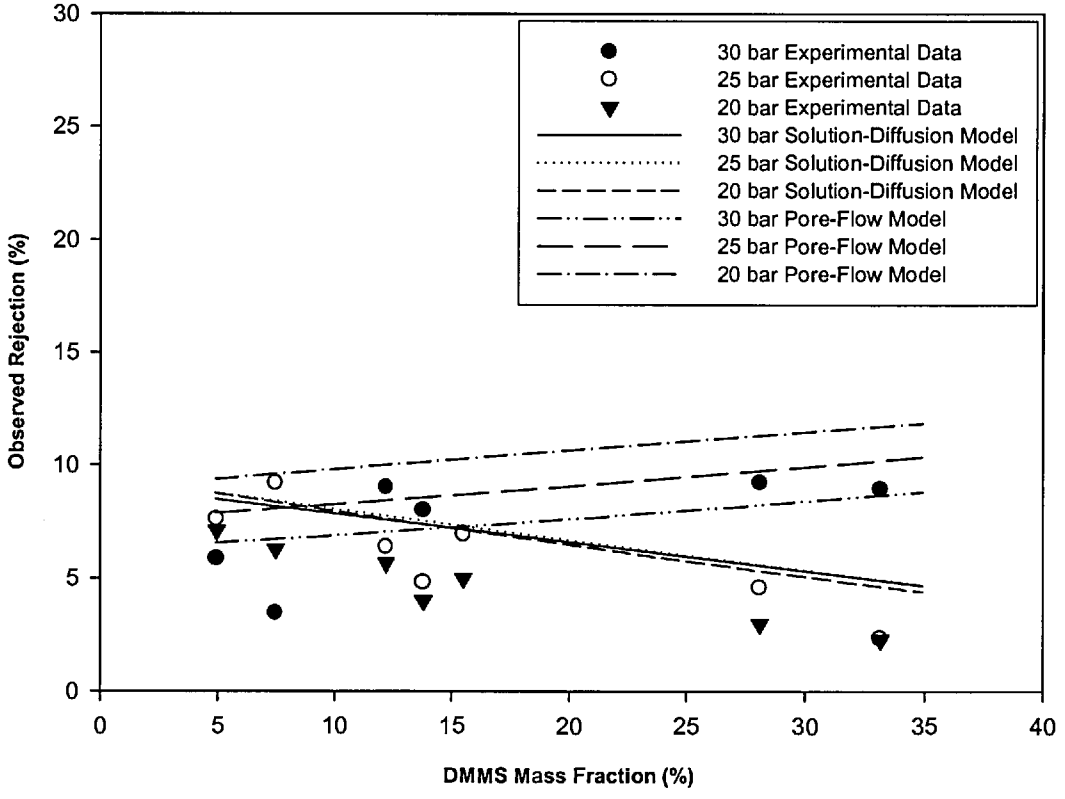

Figure 23 : Experimental and simulated MPF-50 Methanol-DMMS rejection profiles at several pressures and 30 °C.

Nevertheless, the solution-diffusion decreasing trends seem to be the best description for the experimental MPF-50 rejection profiles.

4.4 Conclusion

The rejection profiles for the permeation of concentrated methanol-DMMS solutions in S-122 and MPF-50 were reasonably described by a mathematical model combining the solution-diffusion membrane transport model with the film theory for mass transfer. The superior description of rejection by the solution-diffusion approach is probably related to the fact that solution-diffusion is indeed a more general model, where a solute-solvent distinction is not required.

S-122 rejection profiles are mainly determined by the mass transfer coefficient value, while rejection should not be seen as a constant value, but instead as a variable capable of

assuming a broad range of values, depending on the mass transfer characteristics of the nanofiltration system in use.

The flux trends are reasonably predicted by both transport models tested. It seems that the flux is mainly determined by the solvent permeability combined with osmotic pressure.

Previously, solvent mixtures were investigated and the solution-diffusion model was found to describe their permeation behaviour (Silva et al., 2005). Highly rejected species, where the distinction between solvent and solute is clear, were also investigated and once again the solution-diffusion approach gave a good description of the experimental data (Peeva et al., 2004). The remaining binary system requiring clarification is that of partially rejected species, such as methanol-DMMS mixtures. This has been addressed in the present study, and it was concluded that the solution-diffusion model coupled with the film theory for solution mass transfer is able to describe quite well the flux and rejection trends for a broad range of concentration and pressure, across several OSN systems (solvent mixtures, highly rejected solutes, partially rejected solutes). This general predictive capability is achieved by the means of three experimentally determined parameters (solvent permeability, solute permeability and solute mass transfer coefficient). It is interesting to notice that, contrarily to Bhanushali et al. (2002) and Geens et al. (2006) that stress the importance of convective flow in the description solute rejection in OSN, for the systems studied in this chapter, a purely diffusive solution-diffusion model can accurately describe the results. Moreover, contrarily to Gevers et al. (2006), that points out the importance of diffusive coupling, and the use of general solution-diffusion models (4 parameter based) involving solute-solvent diffusion coefficients to accurately describe solute rejection in OSN. In this work rejection was accurately described by the use of a simple solution-diffusion model (2 parameter based). This discrepancy between literature findings and the results obtained in this work, it is probably explained by the fact that none of the above mentioned authors has accounted for liquid phase mass transfer in their studies, this absence of solution mass transfer effects when analysing solute transport has probably masked the true nature of solute transport in these systems. However, more experimental work should be performed in order to test the validity of the previous statements.

5. Organic Solvent Nanofiltration (OSN) with Spiral-Wound Membrane Modules – Highly Rejected Solute System

5.1 Aim and Scope

With the increasing success of OSN membranes in non-aqueous separations at the laboratory scale, it is clear that, in order to establish effective commercial applications, OSN membrane modules must be used. Among modules, the spiral-wound element is usually preferred for nanofiltration, since it offers a favourable balance between ease of operation, fouling control, permeation rate and packing density. However, there is a lack of published research on spiral-wound elements used for OSN:

- Most published work describing spiral-wound nanofiltration refers to aqueous systems (Rautenbach and Dahm, 1987; Evangelista and Jonsson, 1988; Chiolle et al., 1978; Boudinar et al., 1992; Schock and Miquel, 1987). There is no literature data, or reports on modelling OSN using spiral-wound elements.
- The data covering OSN membrane transport models for highly rejected solutes is scarce. Peeva et al. (2004) showed that a modified solution-diffusion model for membrane transport coupled to a film theory approach to describe liquid phase mass transfer was successful for describing highly rejected solute systems under flat-sheet cross-flow conditions. However, no attempt to test model predictions at pilot-plant scale has yet been reported.
- In order to efficiently implement OSN separation processes based on spiral-wound elements, an engineering design model would be useful. It is not clear which level of model complexity is required to perform accurate modelling when using spiral-wound element nanofiltration systems. Most of the models presented in the literature for aqueous systems have discrepancies between 5 % and 35 % when compared with experimental data (Schwinge et al., 2004). However, given the lack of a substantial body of accurate experimental data for OSN, and the early stage of modelling transport processes in these systems, it seems sensible to start with simple models and to advance these, as understanding is improved.

In this study, a pilot plant apparatus was used to determine the flux and rejection behaviour of a spiral-wound STARMEM^{TM} 122 module. The binary system toluene/TOABr was used to investigate the mechanisms that determine solvent flux and solute rejection, by establishing comparisons with flat-sheet cross-flow nanofiltration results. The experimental flux and rejection for the spiral-wound element was predicted using membrane transport parameters obtained from flat-sheet experiments (Peeva et al., 2004).

Spiral-wound elements were described using two models. A simple model which considers uniform pressure and concentration on each side of the membrane (Table 17), and a complex model that takes into account radial and axial variation of: pressure, cross-flow velocity, and concentration (Table 18). The model equations were derived in the chapter 2.7. For the membrane transport model, the modified solution-diffusion model proposed by Peeva et al. (2004) (Eq. (17) chapter 2.4) was used and to describe solution mass transfer phenomena the film theory model (Eq. (34) chapter 2.6) was included.

Through considering the predictions and the experimental results, insight will be gained into the usefulness of flat-sheet data for predictions of spiral-wound element performance, and also into what level of model complexity is required to accurately describe OSN using spiral-wound elements.

Table 17 : Simple spiral-wound model mathematical description.

Membrane Transport Model

$$N_1 = P_{1m}\left(\frac{c_{1F(m)}}{c_{1F(m)}+c_{2F(m)}} - \frac{c_{1P(m)}}{c_{1P(m)}+c_{2P(m)}}\frac{\gamma_{1p(m)}}{\gamma_{1F(m)}}\exp\left(-\frac{\overline{V}_1\Delta p}{RT}\right)\right)$$

$$N_2 = P_{2m}\left(\frac{c_{2F(m)}}{c_{1F(m)}+c_{2F(m)}} - \frac{c_{2P(m)}}{c_{1P(m)}+c_{2P(m)}}\frac{\gamma_{2p(m)}}{\gamma_{2F(m)}}\exp\left(-\frac{\overline{V}_2\Delta p}{RT}\right)\right)$$

$$c_{1F(m)} = \left(c_{1F} - c_{1p(m)}\right)\exp\left(\frac{N_v}{k}\right) + c_{1p}$$

$$c_{1F(m)}\overline{V}_1 + c_{2F(m)}\overline{V}_2 = 1$$

$$N_v = N_1\overline{V}_1 + N_2\overline{V}_2$$

$$c_{1p(m)} = \frac{N_1}{N_V}$$

$$c_{1P(m)}\overline{V}_1 + c_{2P(m)}\overline{V}_2 = 1$$

$$OR = 1 - \frac{c_{1P}}{c_{1F}}$$

Differential Mass/Momentum Balances

Feed Side	**Permeate Side**
$\frac{\partial u_f}{\partial z} = 0$	$\frac{\partial u_p}{dy} = 0$
$\frac{\partial (u_f c_{1f})}{\partial z} = 0$	$\frac{\partial (u_p c_{1p})}{\partial y} = 0$
$\frac{\partial p_f}{\partial z} = 0$	$\frac{\partial p_p}{\partial y} = 0$
$u_f(0,y) = u_{f0}$	$u_p(z,0) = 0$
$c_{1f}(0,y) = c_{1f0}$	$\frac{\partial c_{1p}(z,0)}{\partial y} = 0$
$p_f(0,y) = p_{f0}$	$\frac{\partial p_p(z,0)}{\partial y} = 0$
	$p_p(z,W) = 0$

Mass Transfer Coefficient Model

$$\frac{kd_{h_f}}{D_{12}} = 0.065\,\mathrm{Re}^{0.875}\,Sc^{0.25}$$

Table 18 : Complex spiral-wound model mathematical description.

Membrane Transport Model

$$\ddot{N}_1 = P_{1m}\left(\frac{\ddot{c}_{1F(m)}}{\ddot{c}_{1F(m)}+\ddot{c}_{2F(m)}} - \frac{\ddot{c}_{1P(m)}}{\ddot{c}_{1P(m)}+\ddot{c}_{2P(m)}}\frac{\gamma_{1p(m)}}{\gamma_{1F(m)}}\exp\left(-\frac{\overline{V}_1\Delta\ddot{p}}{RT}\right)\right)$$

$$\ddot{N}_2 = P_{2m}\left(\frac{\ddot{c}_{2F(m)}}{\ddot{c}_{1F(m)}+\ddot{c}_{2F(m)}} - \frac{\ddot{c}_{2P(m)}}{\ddot{c}_{1P(m)}+\ddot{c}_{2P(m)}}\frac{\gamma_{2p(m)}}{\gamma_{2F(m)}}\exp\left(-\frac{\overline{V}_2\Delta\ddot{p}}{RT}\right)\right)$$

$$\ddot{c}_{1F(m)} = \left(\ddot{c}_{1F} - \ddot{c}_{1p(m)}\right)\exp\left(\frac{\ddot{N}_v}{\ddot{k}}\right) + \ddot{c}_{1p}$$

$$\ddot{c}_{1F(m)}\overline{V}_1 + \ddot{c}_{2F(m)}\overline{V}_2 = 1$$

$$\ddot{N}_v = \ddot{N}_1\overline{V}_1 + \ddot{N}_2\overline{V}_2$$

$$\ddot{c}_{1p(m)} = \frac{\ddot{N}_1}{\ddot{N}_V}$$

$$\ddot{c}_{1P(m)}\overline{V}_1 + \ddot{c}_{2P(m)}\overline{V}_2 = 1$$

$$\ddot{O}R = 1 - \frac{\ddot{c}_{1P}}{\ddot{c}_{1F}}$$

Differential Mass/Momentum Balances

Feed Side	**Permeate Side**
$\frac{\partial\ddot{u}_f}{\partial z} = \frac{-2\ddot{N}_v}{h_f\varepsilon_f}$	$\frac{\partial\ddot{u}_p}{dy} = \frac{2\ddot{N}_v}{h_p\varepsilon_p}$
$\frac{\partial(\ddot{u}_f\ddot{c}_{1f})}{\partial z} = -2\frac{\ddot{N}_1}{h_f\varepsilon_f}$	$\frac{\partial(\ddot{u}_p\ddot{c}_{1p})}{\partial y} = 2\frac{\ddot{N}_1}{h_p\varepsilon_p}$
$\frac{\partial\ddot{p}_f}{\partial z} = \frac{6.23}{2d_{h_f}}\ddot{\mathrm{Re}}^{-0.3}\rho\ddot{u}_f^{\,2}$	$\frac{\partial\ddot{p}_p}{\partial y} = \frac{105}{2d_{h_p}}\ddot{\mathrm{Re}}^{-0.8}\rho\ddot{u}_p^{\,2}$
$u_f(0,y) = u_{f0}$	$u_p(z,0) = 0$
$c_{1f}(0,y) = c_{1f0}$	$\frac{\partial c_{1p}(z,0)}{\partial y} = 0$
$p_f(0,y) = p_{f0}$	$\frac{\partial p_p(z,0)}{\partial y} = 0$
	$p_p(z,W) = 0$

Mass Transfer Coefficient Model

$$\frac{\ddot{k}d_{h_f}}{D_{12}} = 0.065\,\ddot{\mathrm{Re}}^{0.875}\,\ddot{S}c^{0.25}$$

Ïariable - Indicates that the model variables are functions of axial (z) and radial (y) coordinates.

5.2 Materials and methods

5.2.1 Chemicals

Toluene (Tennants Distribution Ltd, UK) was used as the solvent. The quaternary ammonium salt, tetraoctylammonium bromide (98% purity) was purchased from Dishman pharmaceuticals and chemicals limited, UK.

5.2.2 Membrane Module

The 2.5"x40" STARMEM^{TM} 122 spiral-wound element was supplied by Membrane Extraction Technology Ltd (UK).

5.2.3 Experimental Procedure

Pilot plant experiments using spiral-wound elements were performed for several concentrated solutions of TOABr in toluene (0-22 wt. %) in order to test the effect of concentration on OSN fluxes and rejections. The experiments were conducted at 30 °C and three different pressures were tested (10, 20, and 30 bar). The influence of feed flow rate on flux and rejection was also tested for the several pressures.

Figure 24 shows the diagram of the pilot plant nanofiltration rig. It consists of a spiral-wound nanofiltration element, a solution reservoir (20 L), a diaphragm pump, permeate and retentate flow meters, and permeate and retentate pressure transducers. The solution enters the spiral wound module at a controlled flow rate and both permeate and retentate are re-circulated to the feed tank. The applied pressure, the temperature and the feed flow rate were controlled by a programmable logic controller.

During filtration the solvent flux was obtained by:

$$N_v = \frac{F}{A} \tag{52}$$

Where F is the permeate flow rate red on the digital flowmeter and A the effective membrane area. The observed rejection was defined as

$$OR_i = \left(1 - \frac{C_{ip}}{C_{if}}\right) \times 100\% \tag{53}$$

Where C_{ip} and C_{ir} are the concentrations of specie i in the permeate and in the feed respectively.

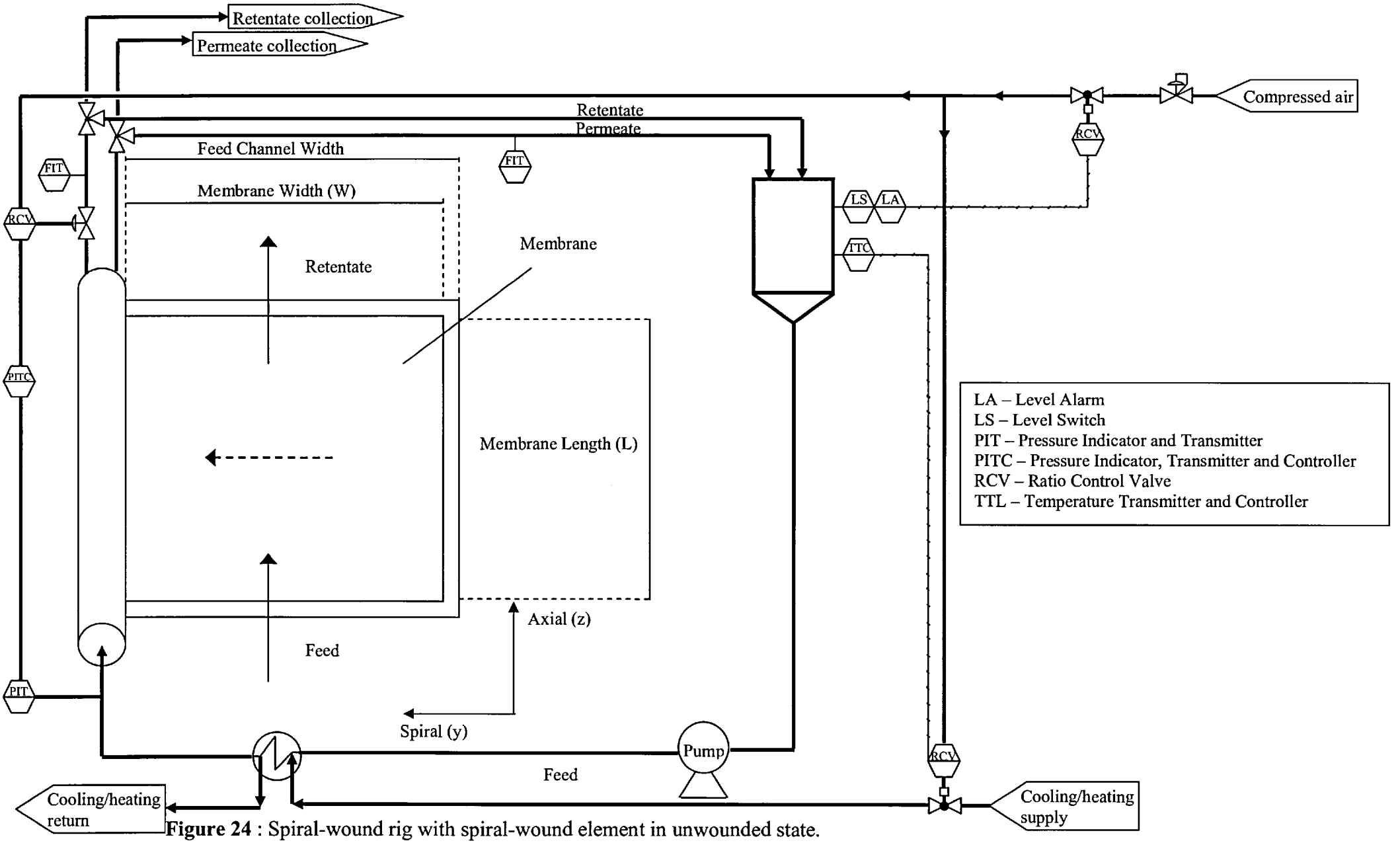

Figure 24 : Spiral-wound rig with spiral-wound element in unwounded state.

5.2.4 Analytical Methods

Concentrations of TOABr were determined using a Perkin-Elmer Gas Chromatograph with a flame ionisation detector and an HP1 methyl siloxane column 30 m long 0.35 mm i.d. The temperature programme ran from 80 °C to 300 °C at a rate of 25 °C.min^{-1}, and the column temperature was held at 80 °C and 300 °C for 3 minutes at the start and finish of the temperature programme respectively. The coefficient of variation was 2 % for three independent measurements.

5.3 Results and Discussion

Analysing the predicted results, it is clear that the membrane transport parameters, obtained from flat-sheet experiments, accurately predict the flux trends for OSN using spiral-wound elements. Moreover, the correlation used for the mass transfer coefficient determination seems to be applicable to the system studied, since the model predictions for different solute concentrations fit the experimental values well. Before detailed discussion of the modelling results, it is important to notice that:

- Both levels of modelling complexity were used in order to predict the experimental results and access the complexity level required for accurate predictions: A simple lumped model, considering uniform conditions throughout the membrane (simple spiral-wound model) area and a complex 2D model (complex spiral-wound model), accounting for changes throughout the axial and radial dimensions of the spiral-wound element.
- All membrane/solution mass transfer model input parameters were obtained from Peeva et al. (2004). These include solvent/solute permeabilities, solute diffusion coefficient, solution viscosity/density and solution activity coefficients (Table 19). The spiral-wound element specifications were supplied by the manufacturer and are present in Table 20.
- The complex spiral-wound model full mathematical description forms a system of partial differential algebraic equations (PDAEs) that was solved in gPROMS using a centred finite difference scheme (Process Systems Enterprise Ltd., 2002). The simple spiral-wound model mathematical

description consists in a nonlinear system of equations; this was solved using a Newton-Raphson routine implemented by gPROMS.

Table 19 : Flat-sheet membrane model parameter values.

Compound	Toluene	TOABr
Diffusion Coefficient ($m^2.s^{-1}$)*	-	0.88×10^{-9}
Molar Volume ($m^3.mol^{-1}$)*	106×10^{-6}	766×10^{-6}
Membrane Permeability ($mol.m^{-2}.s^{-1}$)*	1.1	3×10^{-5}
Activity coefficient (-)*	$\gamma_{Toluene} = -4.16x_{Toluene}^2 + 7.29x_{Toluene}$	$\gamma_{TOABr} = 1$

* - Peeva et al. (2004)

Table 20 : Spiral-wound element specifications.

W (mm)	L (mm)	h_p (mm)	ε_p (-)	d_{h_p} (mm)	h_f (mm)	ε_f (-)	d_{h_f} (mm)
350	861	0.80	0.40	0.63	0.70	0.73	1.02

5.3.1 Flux/Rejection Predictions

Simple spiral-wound model flux predictions (Figure 25) are higher than those for the complex spiral-wound model and closer to the experimental values.

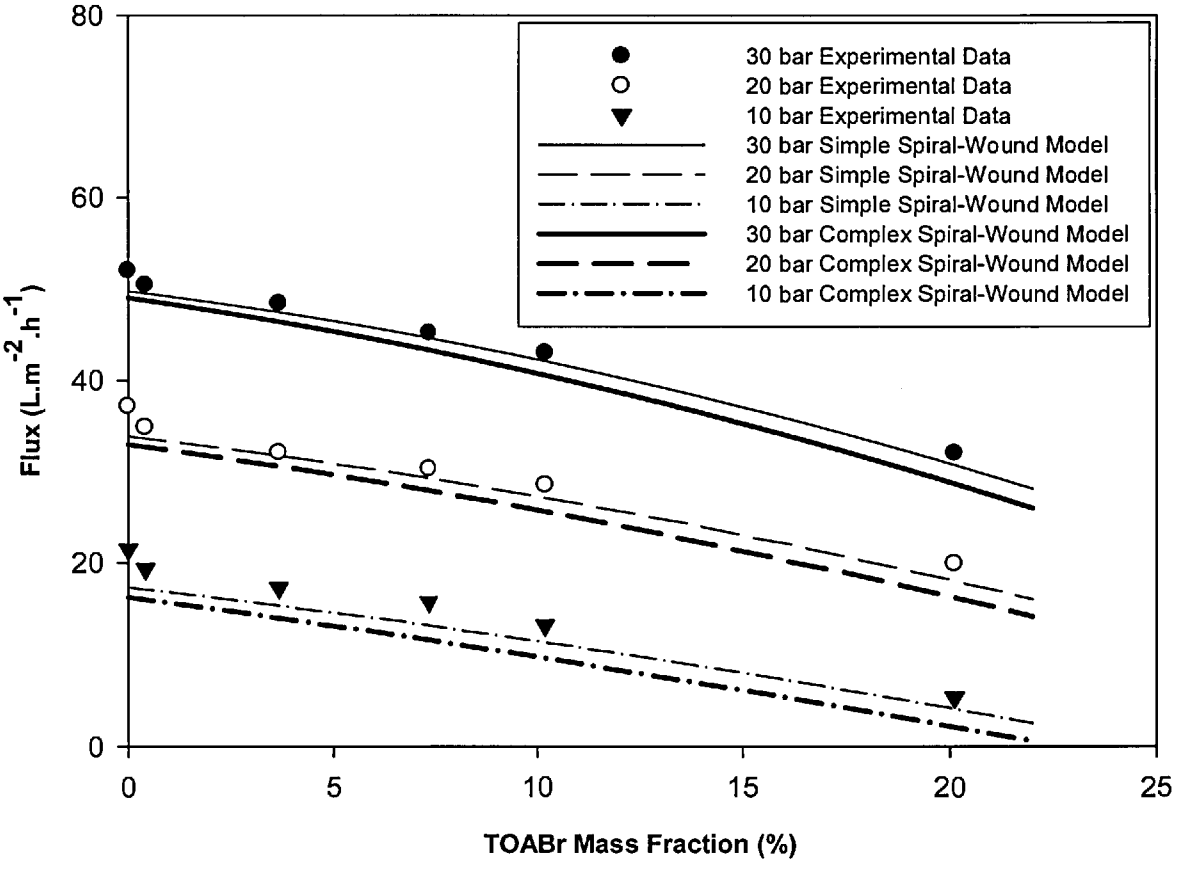

Figure 25: Simple and complex model predictions for spiral-wound flux of toluene/TOABr mixtures at several pressures and 30 °C.

They are better in this case because the experimental pure solvent permeability for the spiral-wound element is higher than the flat-sheet value used for modelling. Simple spiral-wound model flux predictions are higher than those of the complex spiral-wound model, due to the fact that the simple spiral-wound model does not account for pressure losses along the module and therefore constant (maximum) pressure is present along the whole length, leading to higher flux predictions than in the complex model, in which pressure experiences a decrease in the axial direction. For rejection, both models predict exactly the same trend, Figure 26. This was expected, since TOABr permeability is very low and rejection is throughout close to 100% value.

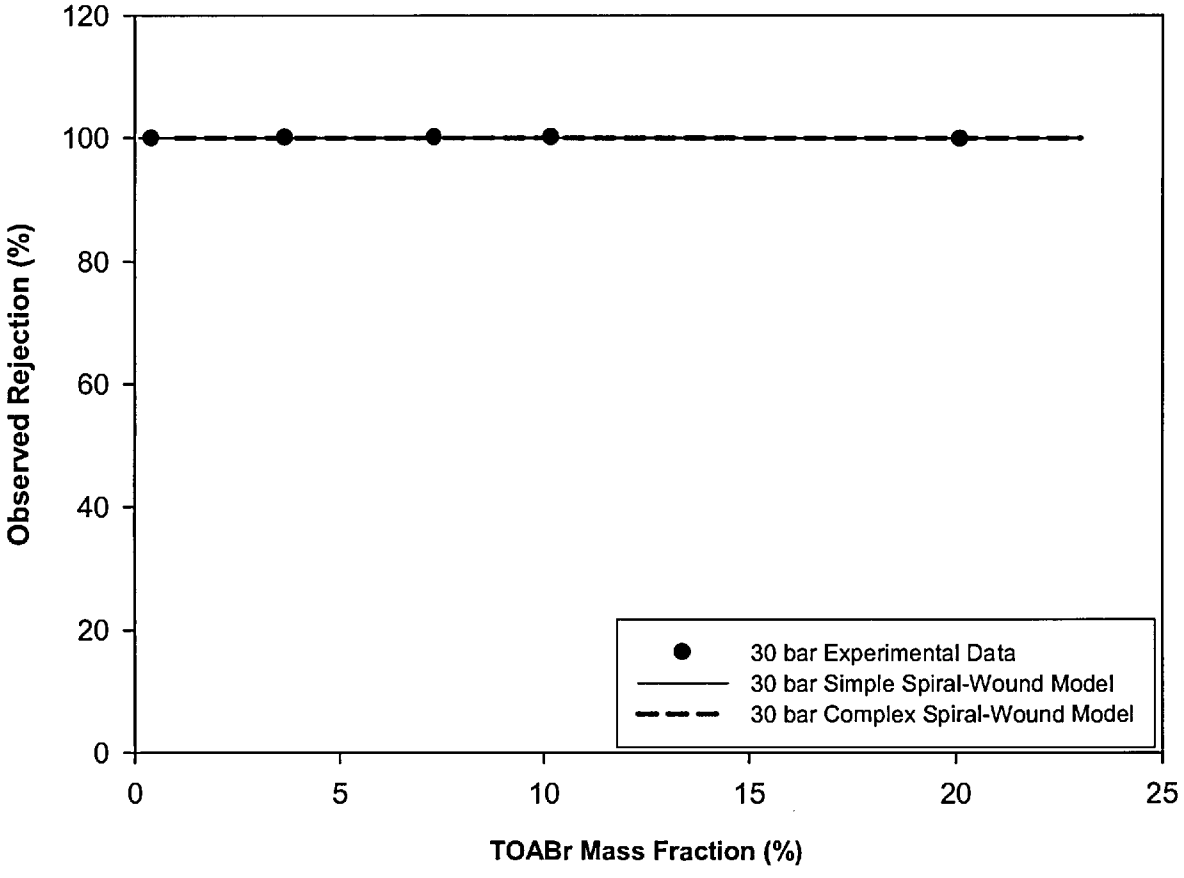

Figure 26 : Simple and complex model predictions for spiral-wound rejection for toluene/TOABr mixtures at 30 bar and 30 °C.

5.3.2 Stage Cut and Solution Concentration

The stage cut is defined as:

$$\frac{Permeate\ Flow\ Rate}{Feed\ Flow\ Rate} \times 100 \qquad (53)$$

Stage cuts in the experiments conducted ranged from1.7 % to 20 %. Importantly, the concentration of TOABr increases throughout the length of the element, leading to a more viscous solution (see insert plot in Figure 28) and to a decreasing mass transfer coefficient in the axial flow direction.

5.3.3 Mass Transfer

As expected, a flux decrease with increasing concentration was observed (Figure 25). This is a common behaviour encountered in the OSN literature and is explained by the increase in osmotic pressure (Peeva et al., 2004; Stafie et al., 2004), maximized by the rejected species' induced concentration polarization phenomena (Silva and Livingston, 2006).Mass transfer limitation on the flux is significant in this system at concentrations above 10 wt % TOABr (Figure 27).

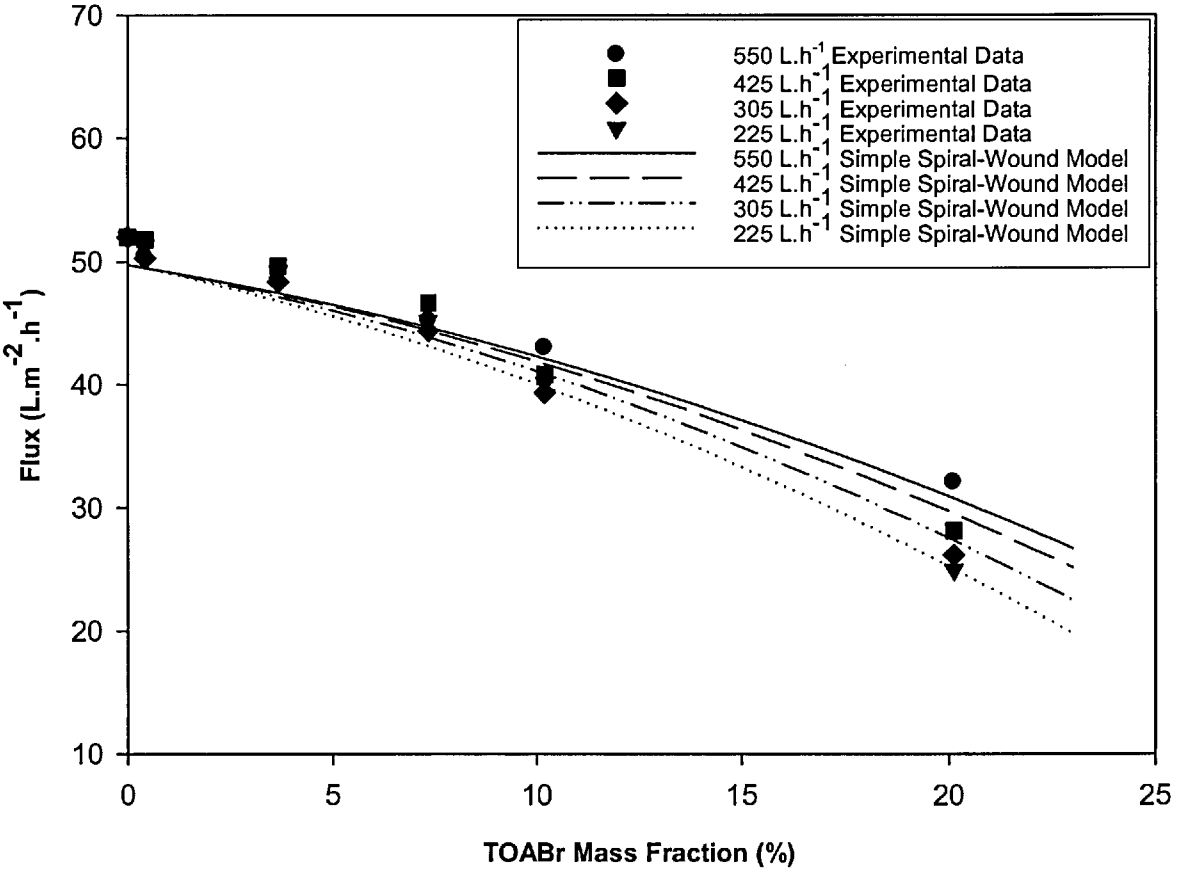

Figure 27 : Spiral-wound flux of toluene/TOABr mixtures for several feed flow rates, at 30 bar and 30 °C.

However, since equipment limitations restricted flow rates to above 200 $L.h^{-1}$, the effect is not very pronounced until high TOABr mass fractions. The predicted feed channel mass transfer coefficient (from the complex model) variation along the spiral-wound element length, for a 225 $L.h^{-1}$ flow rate, is presented in Figure 28. A linear decrease is predicted, but, this change is relatively small, and does not significantly affect flux or rejection. Therefore, the simple spiral-wound model assumption of a constant mass transfer coefficient is a good approximation, for systems with sufficiently high feed flow rates.

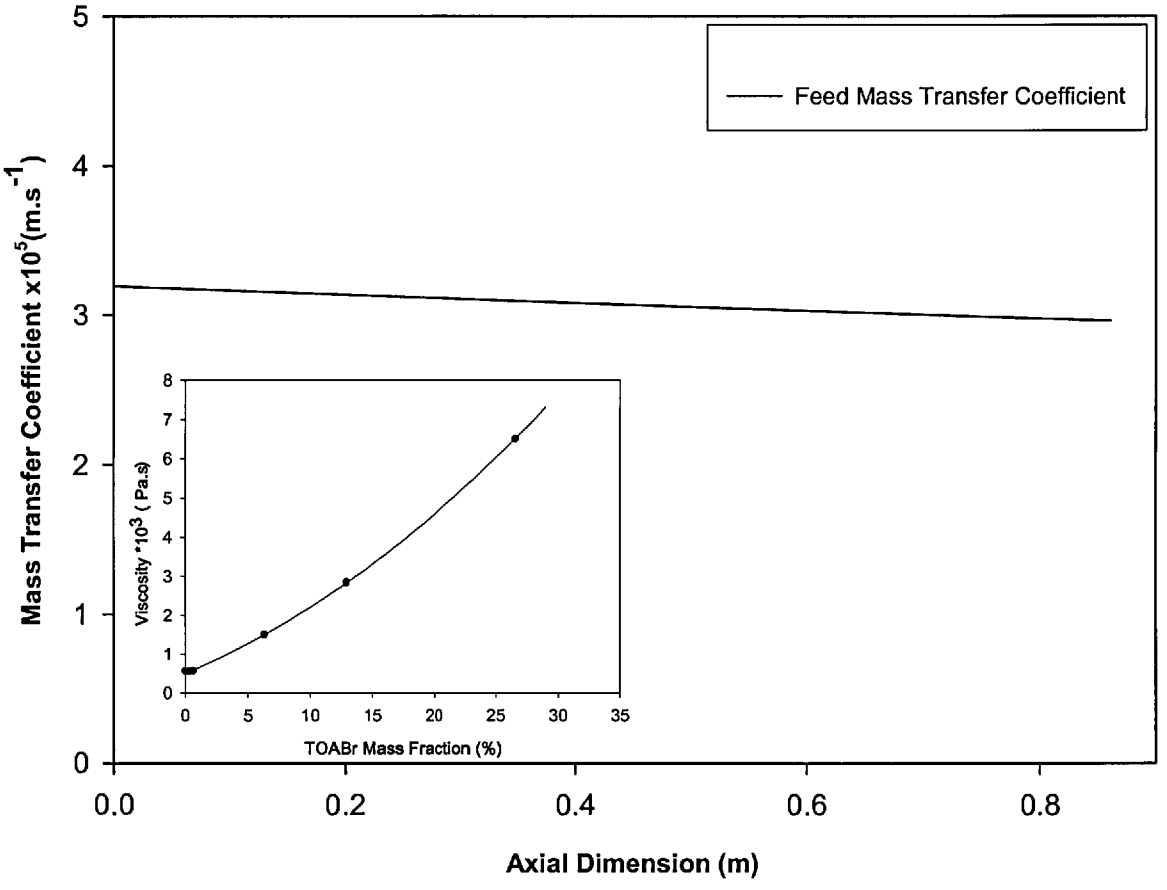

Figure 28 : Feed channel's mass transfer coefficient, at 30 bar, 30 °C, 225 $L.h^{-1}$ feed flow rate and 20 % TOABr mass fraction.

5.3.4 Pressure Drop

Pressure drop through the module is a crucial factor determining the model complexity required to simulate OSN in spiral-wound elements. Experimental feed channel pressure drop values are below the predicted ones (Figure 29) in particular for high pressure/high permeating flux systems. The similarity between complex spiral-wound model and simple spiral-wound model predictions is also an indication that the feed channel pressure drop throughout the spiral-wound element length should not be significant. Figure 29 not only confirms the low pressure drop values in this system but also shows a good agreement between experimental and model predicted feed channel's pressure drop values, proving the applicability of Schock and Miquel (1987) pressure drop correlation to this system.

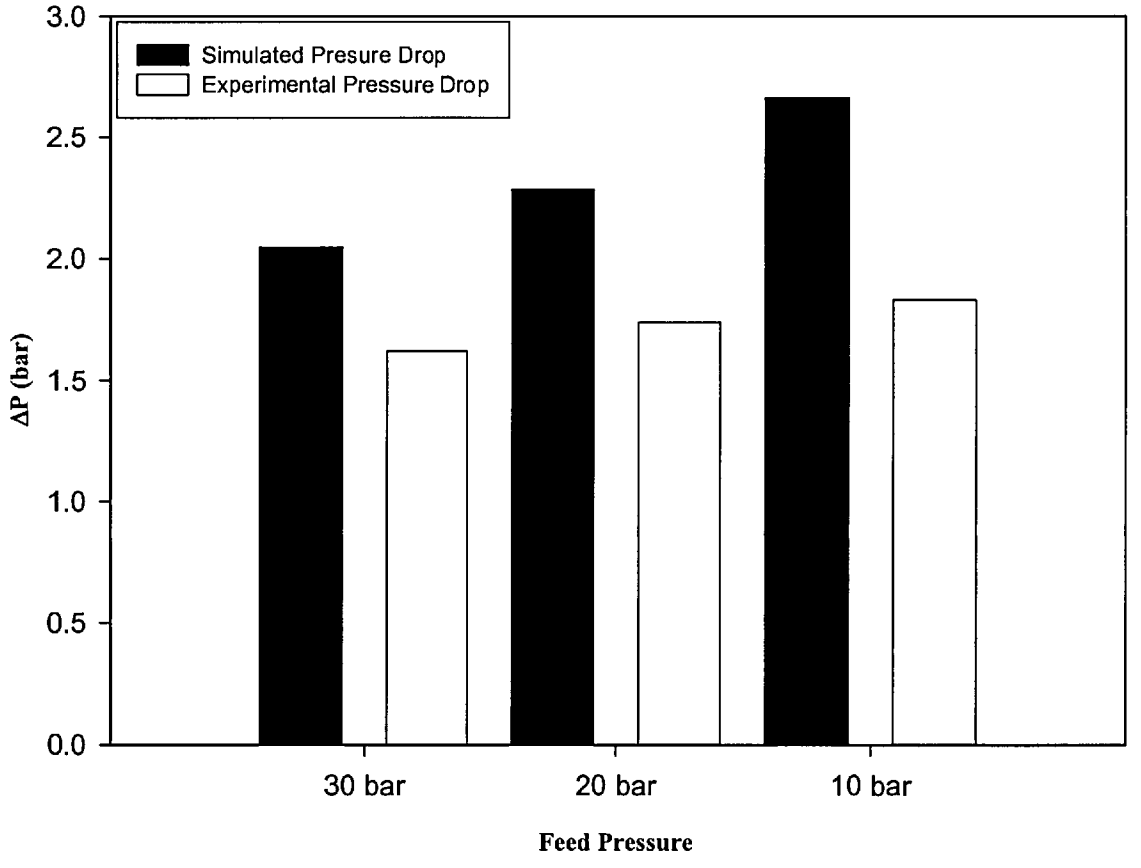

Figure 29 : Spiral-wound pressure drop at 30 °C, 550 $L.h^{-1}$ feed flow rate and 20 % TOABr mass fraction.

According to the complex spiral-wound model predictions, the permeate channel pressure drop is negligible, being always below 0.02 bar. Therefore, permeate channel pressure drop should not be a significant factor in determining the transport through the OSN spiral-wound element system presented in this study.

Although in the system tested the pressure drop values are negligible, it can be observed in Figure 30 an approximately linear relationship between the feed channel pressure drop value and the number of spiral-wound modules packed in series.

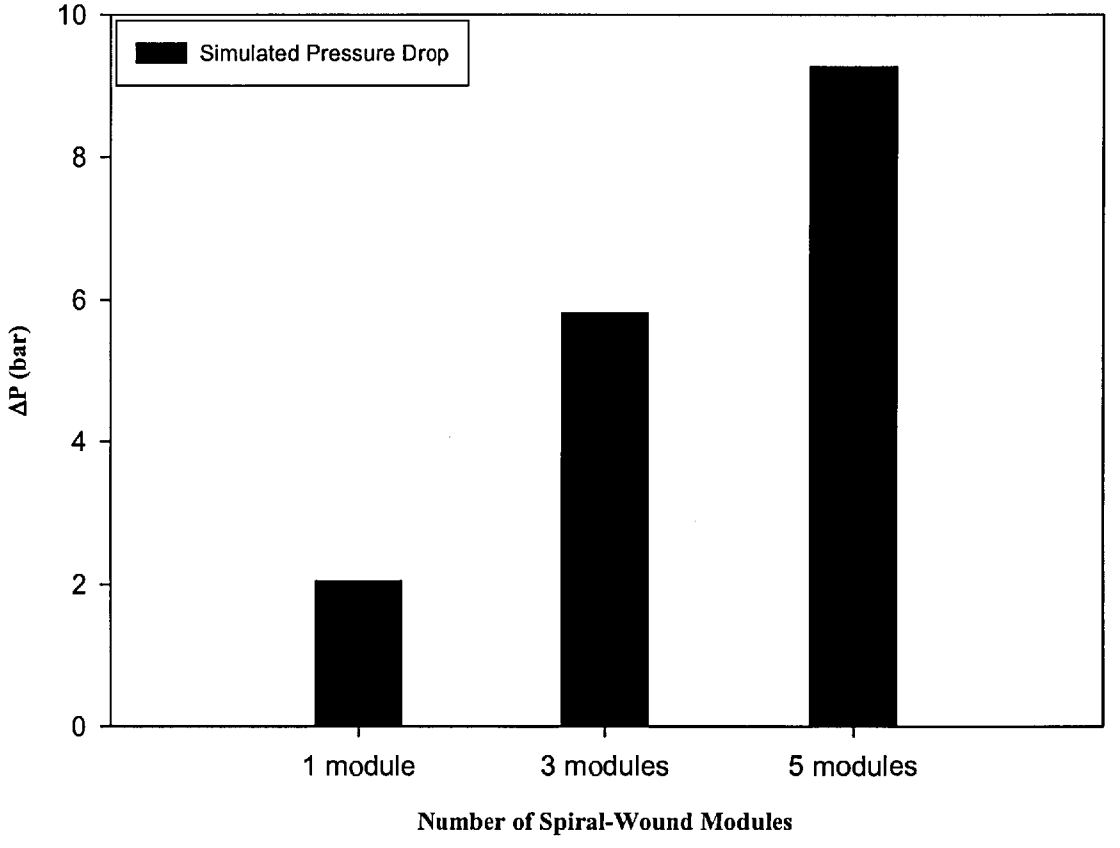

Figure 30 : Predicted spiral-wound pressure drop at 30 °C, 550 $L.h^{-1}$ feed flow rate and 20 % TOABr mass fraction.

Therefore, in industrial applications where large membrane areas are required, pressure drop might become a really important issue. For instance, for five spiral-wound elements arranged in series, the feed channel pressure drop has a value of approximately 10 bar. Such a high pressure drop value would lead to a considerable reduction in the flux, in this case the simple spiral-wound model constant pressure assumption would be less accurate and only the complex spiral-wound model would be able to give reasonable flux predictions for such a system, as it can be seen in 1 and 2 of Figure 31.

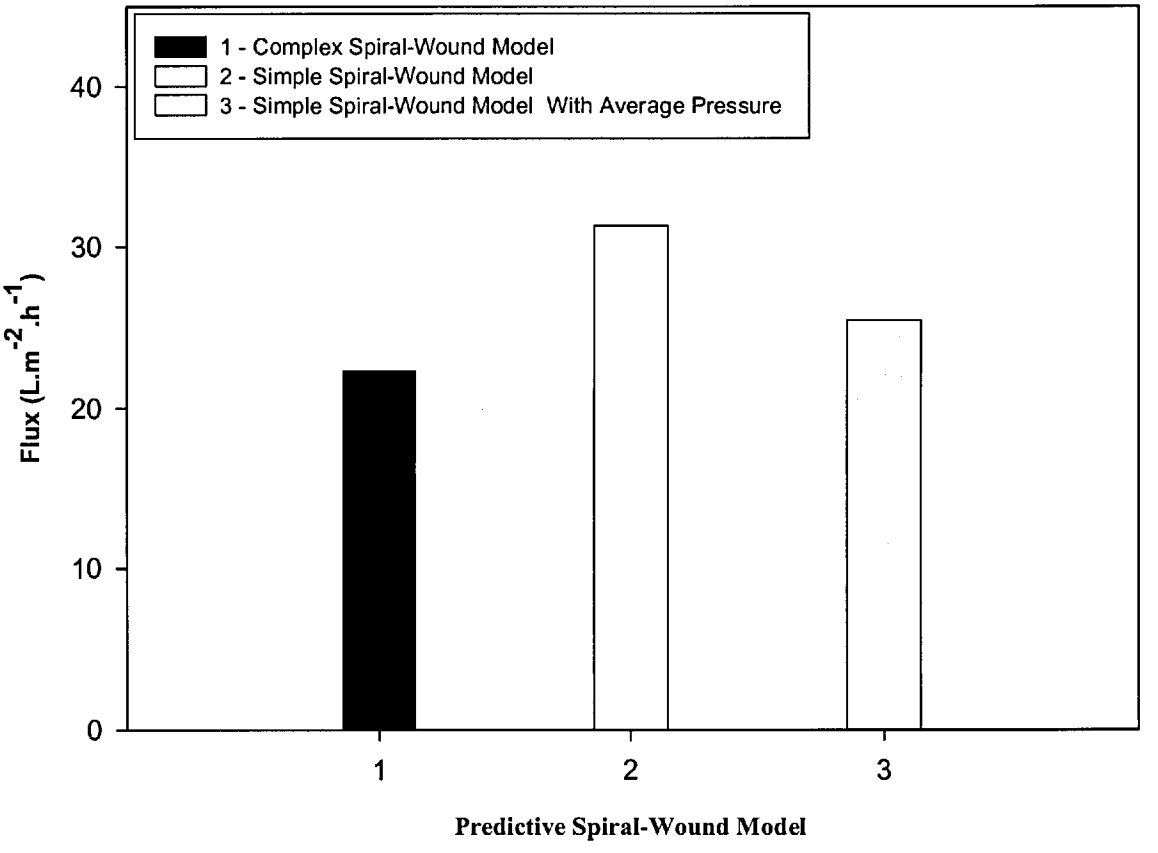

Figure 31 : Predicted spiral-wound fluxes at 30 °C, 30 bar, 550 $L.h^{-1}$ feed flow rate and 20 % TOABr mass fraction.

However, assuming that the feed channel pressure drop in our experimental system is known, and approximately 10 bar (complex spiral-wound model prediction), the simple spiral-wound model can still be used, to perform accurate predictions, as long as the arithmetic average of trans membrane pressure difference (25 bar) is used instead of the feed side pressure value (30 bar). As can be observed in 3 of Figure 31, when using this approach complex spiral-wound model values and simple spiral-wound model values differ by less than 15 %.

5.4 Conclusion

The flux/rejection profiles for the permeation of highly concentrated solutions of TOABr in toluene were reasonably predicted by using flat-sheet membrane transport parameters. Both complex (Table 18) and simple spiral-wound models (Table 17) gave an accurate description of the experimental results. However, the simple spiral-

wound model gave slightly better predictions due to the negligible pressure drop assumption and the consequently higher flux predictions generated when considering one single maximum pressure over the whole membrane area. Moreover, although the simple spiral-wound model predictions worked quite well for the system under study, where both pressure and mass transfer coefficient constancy were verified, the pressure drop predictions indicate that such a simple model would not give accurate predictions when the number of spiral wound elements starts to increase, due to the significantly higher pressure drop values generated in such systems. However, even in this case an improved simple spiral-wound model that makes use of the experimental pressure drop value is still able to provide reasonably accurate results. As general lesson from this modelling work, it is clear that for spiral-wound module systems, with high feed side pressures and reasonably high solvent permeation flux, neglecting the pressure drop and the decrease in the mass transfer coefficient along the module is a good assumption. Therefore, for such systems a simple spiral-wound model will be able to accurately describe the results. On the other hand, spiral-wound systems with low feed side pressures and low solvent permeation flux are likely to present high pressure drop values and significant mass transfer coefficient decrease along the module. In this case the simple spiral-wound model assumptions will not be verified and a complex spiral-wound model should be employed to model such type of systems.

Although, the membrane transport model used in this work was the solution-diffusion model, Bowen's pore flow model of membrane transport, Eq. (29), could also have been employed. As long as flat-sheet experiments were performed in order to determine the membrane pore radius, r_p Eq. (29). However, as it was seen in chapter 4 this model is likely to perform poorly in the high solute concentration zone, where the solute-solvent distinction starts to vanish.

6. New Approach to Organic Solvent Nanofiltration (OSN) Modelling

6.1 Aim and Scope

The broad applicability of semi-empirical models developed to describe solvent permeability through OSN membranes (chapter 2.4) seems to indicate that solvent flux depends on viscosity, molecular size and the difference in surface tension between the membrane and the solvent. This work is quite interesting; however it is important to notice that:

- A weakness of these semi-empirical models is the absence of predictive power caused by the lack of physical interpretation of fitting parameters. Furthermore, in comparison of models with data, it is often not clear how one can use the data presented to make predictions.
- Although the major solvent/membrane properties affecting transport have been found, there are few attempts on trying to identify the reasons why a determined property is important to transport. It would be interesting to perform experiments able to independently measure the influence of a certain physical property on the thermodynamic transport parameters or to construct/analyse physically meaningful transport models.

In this work, a complete deterministic physically meaningful model able to predict solvent flux through OSN membranes is derived. The elaboration of the model is based on literature data about the influence of different membrane/solvent properties on the transport trough OSN membranes and the predictive power of the model will be tested on cross-flow experimental data for the permeation of ethanol, ethyl acetate, methanol, toluene and water through the commercially available OSN membrane STARMEM^{TM} 122.

6.2 Model Derivation

Most of the work presented in modelling solvent nanofiltration deals with rubbery polymers; however the most promising polymers for OSN applications, due to their chemical stability and temperature resistance are the glassy ones. There are distinctive property differences between these different types of polymers: rubbery polymers are in a thermodynamic equilibrium liquid state where their sorption properties obey Henry's law of dissolution. On the other hand, glassy polymers are typically encountered in a non-equilibrium state containing two phases; a liquid one presenting Henry's type dissolution of species and a solid one presenting Langmuir's type sorption in the microvoids that form her. This well known dual-sorption model (Barrer et al., 1958; Michaels et al., 1963; Vieth et al., 1966) can be expressed by:

$$C = C_D + C_H = K_D a + \frac{C_H' k a}{1 + k a} \tag{54}$$

Where C is the total specie concentration in the polymer, C_D the Henry sorption specie concentration, K_D the Henry's law coefficient, k the Langmuir hole affinity parameter, C_H' the Langmuir capacity parameter, and a the specie activity in solution. Over the pass three decades this dual sorption model was successfully used to describe the sorption of gas molecules by glassy polymers. In this study there is an intention to demonstrate that this model holds the key for a generalized transport model in solvent permeation through OSN membranes. In rubbery membranes C_H' is zero, therefore there is a linear (Henry's law type) relation between specie activity in solution and specie activity in the membrane, also, in such type of membranes with liquid type behaviour no pressure gradient can exist. Putting these statements together with Fick's law of transport the solution-diffusion model of membrane transport can be derived (Wijmans and Baker, 1995):

$$N_i = \frac{C_i D_{im} K_i}{l}\left(x_{if} - x_{ip}\exp\left(-\frac{\overline{V}_1 \Delta p}{RT}\right)\right) \tag{55}$$

Where C_i is the total concentration inside the membrane, D_{im} the specie diffusion coefficient inside the polymeric phase, K_i the specie's partition coefficient and $\overline{V}_i$ the specie's partial molar volume.

This model has been widely used by Paul in the seventies (Paul and Ebra-Lima, 1970) and proved to correctly describe the transport of organic solvents through rubbery type membranes, where the most important parameters describing the flux were solvent viscosity, molar volume and membrane swelling.

On the other hand for glassy polymers, as the polymer glass transition temperature (T_g) increases, the non-equilibrium excess free volume (microvoids) increases. It is reasonable to assume that for glassy polymers with high T_g the sorption process is dominated by the Langmuir regime. In fact this has been proven for gas permeation in high T_g polymers (Kanehashi and Nagai, 2005):

$$C = C_H = \frac{C_H' ka}{1 + ka} \tag{56}$$

In this work polyimide based commercial membranes, known for their high T_g are used, therefore Eq. (56) seems a good approximation.

It is clear that if a predictive permeation model, based on Eq. (56), is to be derived, relations between the sorption parameters C_H', k and the membrane/solvent properties must be found.

C_H' is proportional to the fractional unrelaxed volume of the glassy state (Barbari et al., 1998). Since this value changes with the different permeating solvent characteristics: being higher for high interacting solvents and lower for low interacting solvents. Therefore, a good approximation for C_H' is to set it directly proportional to the swelling degree of the membrane, for a specific solvent:

$$C'_{Hi} = bSW_i \tag{57}$$

Where C'_{Hi} is the Langmuir capacity parameter for the solvent i, SW_i is the membrane swelling in the presence of solvent i, and b a proportionality constant.
k represents the ability for a penetrant molecule to cross the polymer-solvent interface and sorb into the microvoids of the polymer phase. Using the same approach as the one developed for sorption of gases in liquids (Uhligh, 1937), the assumption that the energetic barrier for the sorbing molecule will be mainly determined by the solvent-polymer interface breaking was made. Therefore, for a mole of spherical molecules of radius r to enter the polymer, a cavity in the interface will be produced, the energy of this cavity is given by:

$$\Delta u = N_a \pi r^2 \sigma^{SL} \tag{58}$$

Where N_a is the Avogadro number and σ^{SL} is the solid-liquid surface tension. On the equilibrium (Uhligh, 1937):

$$\Delta u = -RT \ln(k) \tag{59}$$

From the Young equation (section 2.3.2):

$$\sigma^{SL} = \sigma^{SG} - \sigma^{LG} \cos\theta \tag{60}$$

Where σ^{SG} is the solid-gas surface tension and σ^{LG} is the liquid-gas surface tension. Therefore, for a liquid wetting the whole membrane surface area, the Langmuir affinity parameter can be given by:

$$k = \exp\left(-\frac{N_a \pi r^2}{RT} \left(\sigma^{SV} - \sigma^{LV} \right) \right) \tag{61}$$

By now, a fully predictive solvent sorption model that only requires the membrane solid-vapour surface tension determination was built.

Determination of solid surface tensions it is not a trivial matter and several methods have been proposed in the literature. In this work the method proposed by Fowkes (1964), Owens and Wendt (1969) was adopted (section 2.3.2):

$$\left(\sigma_d^{LV} + \sigma_p^{LV}\right)(1+\cos\theta) = 2\sqrt{\sigma_d^{LV}\sigma_d^{SV}} + 2\sqrt{\sigma_p^{LV}\sigma_p^{SV}} \tag{62}$$

By measuring the contact angles of two different liquids on the membrane surface the membrane's surface tension value can be obtained.

A sorption model formed by Eqs. (56), (57), (61) and Eq. (62) was derived, however in constructing a predictive transport model, a mechanism for solvent transport through the membrane must be included. Since the permeation in glassy membranes is dominated by sorption and diffusion through rigid nano-sized microvoids, the transport mechanism should be analogous to the transport through zeolite membranes (Krishna and Wesselingh, 1997) therefore, from the Maxwell-Stefan equations and adopting the glassy membrane formalism, the transport equation can be written as:

$$N_i = -\frac{\rho_p C_H' D_{iV}^S}{1-\theta_i}\frac{d\theta_i}{dz} \tag{63}$$

Where N_i is the molar flux, ρ_p the polymer density θ_i the fraction of microvoids occupied by the penetrant i and D_{iV}^S is the solvent Maxwell-Stefan diffusivity, for zeolites this diffusivity should be dependent on the self-diffusivity of the solvent, the loading and solvent-membrane interactions (Krishna and Wesselingh, 1997). For glassy polymers it will be assumed that the membrane-solvent interactions are mostly important in determining the sorption behaviour, therefore, their influence in the diffusion coefficient will be neglected and due to the low values of sorption in this type of membranes the Maxwell-Stefan diffusivity of the solvent will be approximated by the self-diffusivity of the solvent:

$$D_{1V}^S \approx D_{10} = \frac{RT}{N_a 6\pi r_1 \eta} \tag{64}$$

Substituting Eqs. (57), (61) and (64) in Eq. (63) and integrating under the boundary conditions of Figure 32.

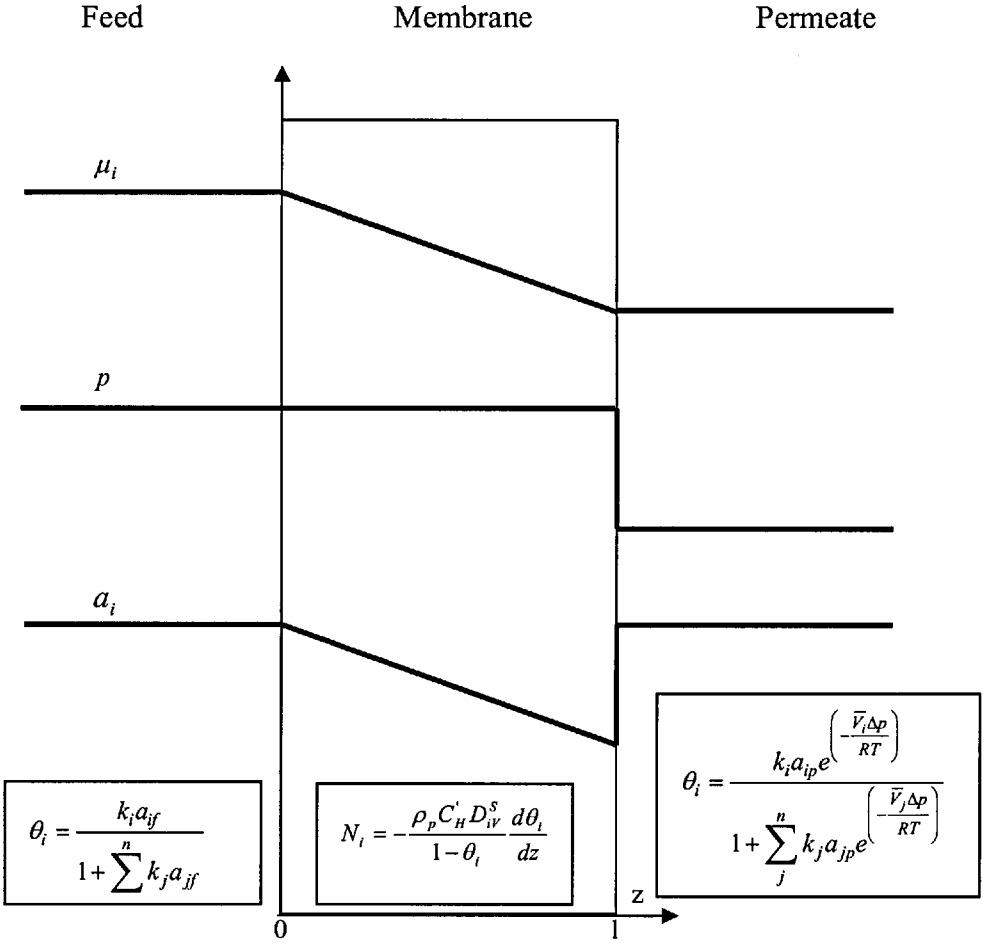

Figure 32 : Gradients across the membrane plus transport model and sorption model equations.

A sorption-diffusion predictive model for OSN solvent transport is obtained. For a pure solvent it will be given by:

$$N_i = \frac{SW_i D_{i0}}{l_{eff}} \ln\left((k+1)\left(1 - \frac{e^{\left(-\frac{\bar{V}_i \Delta p}{RT}\right)}}{\frac{1}{k} + e^{\left(-\frac{\bar{V}_i \Delta p}{RT}\right)}}\right)\right) \tag{65}$$

The justification for the use of these boundary conditions results from the fact that transport through nanosized microvoids must be purely diffusive.

In this work the predictive power of this model will be tested against experimental solvent permeation data. Most of the parameters in Eq. (65) related to solvent properties could be found in the literature (Weast, 1970; Daubert and Danner, 1989; Kirk and Othmer, 1984; McClellan, 1989), with exception of the molecular radius that was determined using molecular modelling software. Membrane solid-vapour surface tension was determined by the sessile-drop contact angle measurement of diiodomethane and water on the membrane surface. Membrane swelling was determined using dynamic vapour sorption (DVS) on a dense polymer film prepared from polyimide P84 (a polymer having very similar properties to the material that constitutes the commercial membrane STARMEM^{TM} 122). Finally, the membrane effective thickness (l_{eff}) was determined by fitting the experimental value for the flux of one of the solvents (methanol was chosen since it is a widely used test solvent for this membrane). The value obtained was then used to predict the flux of all the other tested solvents.

6.3 Materials and Methods

6.3.1 Chemicals

Four organic solvents, toluene, ethyl acetate, methanol, ethanol (analytical grade) were used in this study as these are commonly used in the pharmaceutical and chemical industries. The solvents were obtained from Aldrich, UK. High purity water was also tested for comparison. Table 1 lists the physical properties of the solvents used in this work.

For preparing dense polymer films analytical grade N,N-dimethylformamide (DMF) was used, dioxane and Lenzing P84 co-polyimide polymer. The solvents were obtained from Aldrich, UK and the polymer from HP polymers GmbH, Austria.

For the contact angle experiments deionised water, and diiodomethane (> 99 %, Acros Organics) were used as probe liquids.

Table 21: Physical properties of the solvents used in permeation experiments.

Properties*	Toluene	Ethyl acetate	Methanol	Ethanol	Water
Molar volume ($m^3.mol^{-1}$)x 10^6	106.00	98.23	40.46	58.39	18.00
Density ($g.cm^3$)	0.87	0.90	0.79	0.79	1
Molecular weight ($g.mol^{-1}$)	92.14	88.11	32.04	46.07	18.00
Viscosity (cP)	0.56	0.43	0.54	1.08	1
Surface Tension ($dyn.cm^{-1}$)	27.9	23.75	22.60	23.3	72.8
Dielectric constant ($C^2.N^{-1}.m^{-2}$)	2.40	6.02	32.6	24.53	78.2
Dipolar moment (D)	0.32	1.68	2.92	3.01	3.11

* - Weast (1970); Kirk and Othmer (1984); Daubert and Danner (1989); McClellan (1989)

6.3.2 Membrane

STARMEM^{TM} 122 is an asymmetric OSN membrane with an active layer of polyimide and a nominal MWCO of 220 $g.mol^{-1}$ (manufacturer's data). It was supplied by Membrane Extraction Technology Ltd. (UK) in a "dry" form but containing lube oil as a preserving agent. Table 22 lists the physical properties of the membrane used in this study.

Table 22: STARMEM^{TM} 122 properties.

Manufacturer	MWCO	Nature	Dielectric constant ($C^2.N^{-1}.m^{-2}$)	T_g (^oC)
W.R. Grace	220	Hydrophobic	3.5	315

6.3.3 Contact Angle Measurements

Sessile-drop contact angles were obtained with a Krüss drop shape analyzer (DSA 10, Krüss GmbH, Hamburg, Germany). Initial drops of about 5 μL were dispensed onto the solid surface. By use of a motor-driven syringe, the test liquid was added onto the droplet, allowing the advancing contact angles to be obtained. The needle remained immersed within the top half of the droplet, and the advancing contact angles were determined with a slowly advancing wetting line. The droplet was monitored with a CCD camera and analyzed by Drop Shape Analysis software (DSA version 1.0, Krüss). The droplet contour was fitted by the tangent method (function $f(x) = a + bx + cx^{0.5} + d/\ln x + e/x^2$) at both the left and right sides of the drop. The function is differentiated and the slope at the three phase contact point gives the contact angle. At least 7 contact angle measurements were taken for each liquid. Measurements were obtained in the open air at ambient conditions ($T = 20 \pm 2^0 C$). Although slip/stick behaviour is often reported for contact angle measurements with diiodomethane, this behaviour was not significant in this study. In cases when it was observed, these data were not included in the analysis reported. Table 23 contains the contact angles for diiodomethane and water in the tested films and Table 24 gives us the calculated solid-vapour surface tension values. It is interesting to notice that the P84 surface tension values are very similar to the ones obtained for STARMEM™ 122. This indicates that polyimide P84 is a good approximation of the polymer material that constitutes the commercial OSN membrane STARMEM™ 122.

Table 23: Contact angles.

	Contact angles (°)	
Solvent	P84 dense film	STARMEM™ 122
Diiodomethane	20	18
Water	77	77

Table 24: Solid-vapour surface tensions.

Properties	P84 dense Film	STARMEM™ 122
σ^{SV} (mJ.m^{-2})	50.80	51.20
σ_d^{SV} (mJ.m^{-2})	47.80	48.30
σ_p^{SV} (mJ.m^{-2})	2.97	2.90

6.3.4 Polymer Film Preparation

Dense polymer films were fabricated by using a 22 wt. % polymer 21 wt. % dioxane and 57 wt. % DMF casting solution. The polymer was fully dissolved in DMF and dioxane, by mixing for 24 h, and then the solution was poured onto a levelled glass plate. The solvent was slowly evaporated and the resultant film was dried under vacuum with temperature gradually increased to 250 °C at a rate of 10 °C/20 min and held there for 24 h to remove the residual solvents. These polymer films were used to in the sorption measurements.

6.3.5 Filtration Experiments

Cross-flow permeations were performed for the solvents listed in Table 21 in order to test the predictive power of the model derived in this work. The experiments were conducted at 30 °C and 30 bar pressure. Figure 7 shows the diagram of the cross-flow nanofiltration rig. It consists of four cross-flow nanofiltration cells connected in series, a solution reservoir, a backpressure regulator, and a piston pump. Each cell had a membrane area of 1.4×10^{-3} m^2 and the height of the chamber from the surface of the membrane was 5 mm, giving a fluid volume of 7 ml. At a flow rate of 60 $L.h^{-1}$ the solution enters the cross-flow cell tangentially from the cell wall and exits the cell from the top centre, providing turbulent hydrodynamic conditions. The applied pressure was controlled using a backpressure regulator and the temperature at 30±0.5 °C using a water bath and heat exchanger. During filtration the solvent flux was obtained by:

$$N_V = \frac{V}{A.t} \tag{66}$$

Where V is the sampling volume in the permeate, A the effective membrane area and t is the sampling time.

6.4 Results and Discussion

6.4.1 Pure Solvent Model Predictions

To predict solvent flux using the proposed model; solvent viscosity, solvent molar volume, solvent liquid-vapour surface tension, solvent molecular radius, membrane density, membrane glass transition temperature, membrane solid-vapour surface tension and membrane effective thickness are required. All these parameters with exception of the last one can be determined from independent measurements:

- Data on the solvent molar volumes, liquid-vapour surface tensions and viscosities are available in the literature (Table 21). To calculate solvent molecular radius Gaussian 3.0 molecular modelling software was used (within Gaussian, the ground state DFT, B3LY method with a 6−31*G*+ (*d*, *p*) basis set was used (Frisch et al., 2004)). Drawings of the optimized molecular structures obtained (Figure 33) and the corresponding molecular dimensions were determined (Table 25).

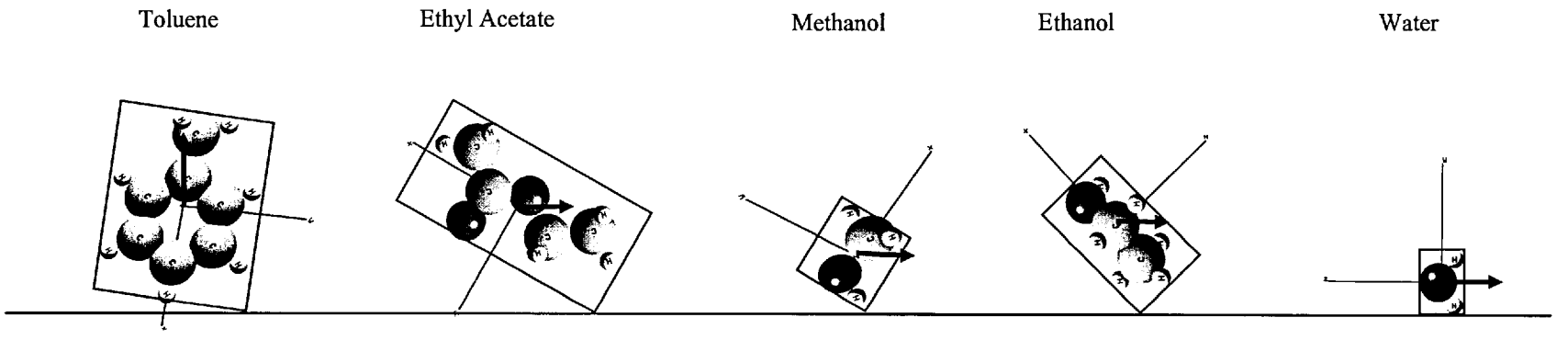

Figure 33 : Solvent molecules with the preferred dipole orientation near membrane-solvent interface.

Table 25: Molecular dimensions determined by molecular modelling.

Solvent	D (Å)	H(Å)	Minimum Radius(Å)	Orthogonal Projecion Radius(Å)
Toluene	6.66	8.17	3.33	3.87
Ethyl acetate	5.60	8.96	2.80	5.28
Methanol	4.13	4.61	2.06	2.96
Ethanol	4.98	6.05	2.49	3.90
Water	3.29	3.96	1.65	1.65

- Membrane swelling for the different solvents was obtained by performing DVS on dense P84 polyimide films (Figure 34). For the model derived in this work, the liquid phase swelling values are required, these were obtained by extrapolating the vapour sorption isotherms to the saturation pressure value (P/P0=1), where thermodynamically we should have a liquid phase (Table 26).

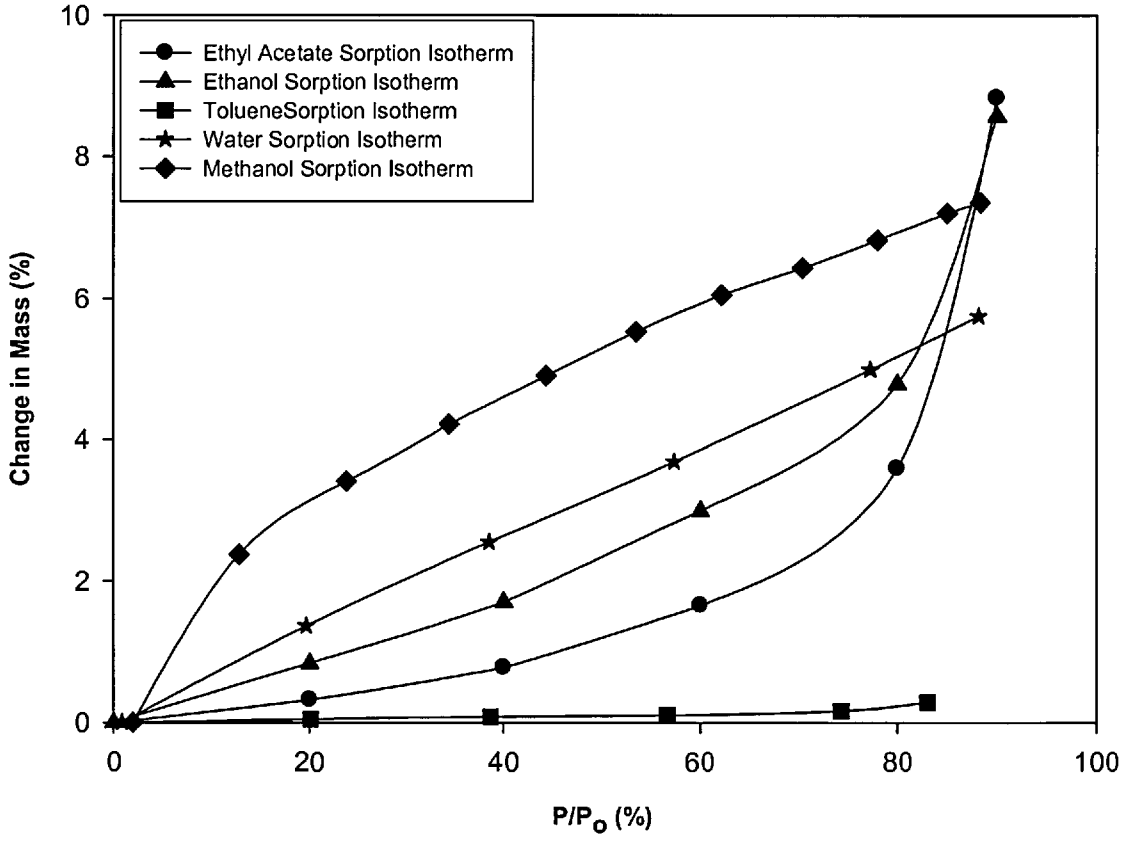

Figure 34 : Sorption isotherms in polyimide P84 at 30 °C.

Table 26 : Solvent swelling for P84 polyimide.

Solvent	Degree of Swelling (%)
Toluene	0.53
Ethyl acetate	11.44
Methanol	8.33
Ethanol	12.35
Water	6.57

- For the effective membrane thickness, reflecting the equilibrium compaction thickness, porosity and tortuosity of the nanovoid layer, one single experimental solvent flux is required to obtain it. However, after obtaining a value for one solvent, this value can be used to predict the flux of all the other solvents, assuming that at the low sorption levels, characteristic of the glassy membrane used, there is no significant change of the membrane's nanovoid structure, with the change of solvent. In this study pure methanol flux was used to determine the effective membrane thickness, due to the high reproducibility of flux values for a series of experiments performed with different membrane batches.

In the first attempt to predict solvent fluxes, the smallest possible molecular radius was used for each molecule (Table 25). This choice was based in the belief that at the interface the molecules should adopt the orientation that leads to minimal interface breaking energy. Using this approach and methanol as the model calibration solvent a value of l_{eff}=34 nm was obtained. Before discussing the predicted results in detail, it is interesting to notice that all model parameters and all predicted flux values are physically meaningful. In general, the predicted flux values are in agreement with the experimental ones (Figure 35), With the exception of toluene and ethyl acetate.

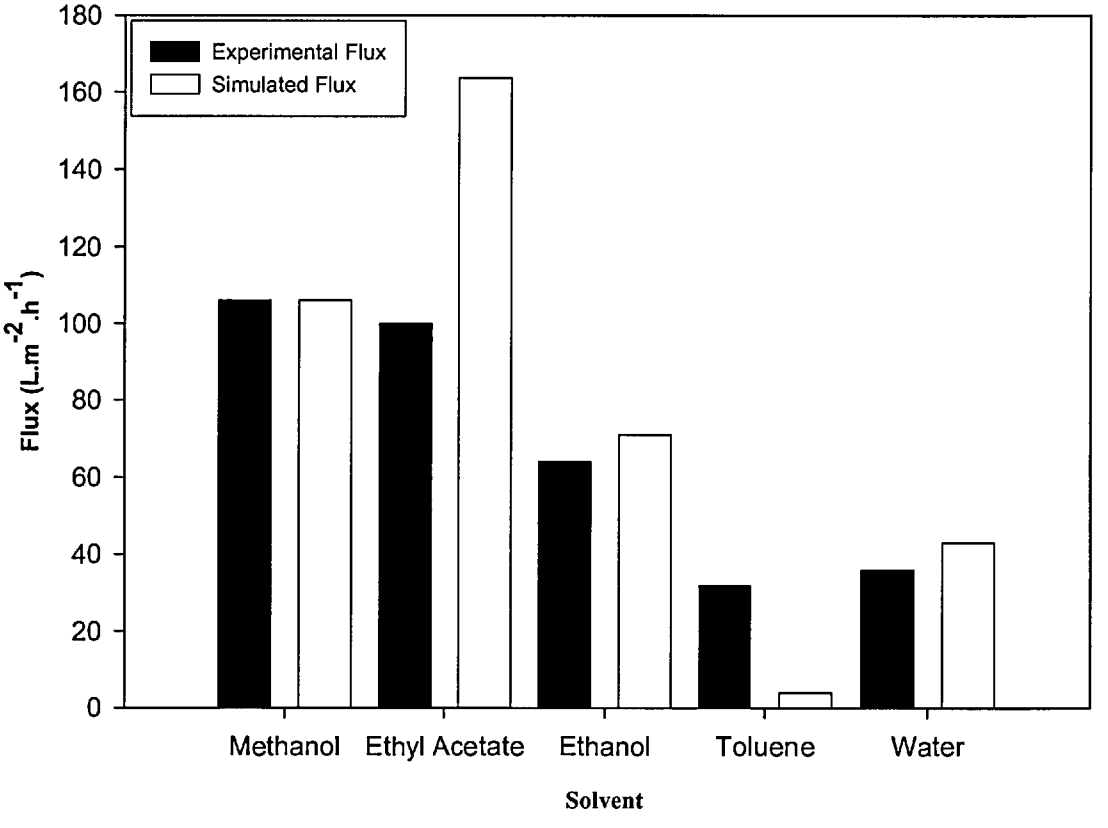

Figure 35 : Solvent flux predictions using the minimum molecular radius.

Experimentally, toluene flux is much higher and ethyl acetate flux is lower. In an attempt to improve model predictions and in the belief that the model requires more membrane/solvent information to be able to predict all solvent flux values, the work of Geens et al. (2006) where it was suggested that polarity is a crucial parameter in OSN permeation, was analysed. In the pursuit of an extra membrane/solvent

parameter able to improve the predictive capabilities of the model, having in mind that this extra descriptor might be related to, solvent polarity, solvent dielectric constant or dipole orientation of the solvent molecule, an interesting expression, reflecting the influence of all the possible factors, was found (Teixeira and telo da Gama, 2002):

$$E = -\frac{\mu^2(\varepsilon_2 - \varepsilon_1)(1+\cos^2(\theta))}{16\varepsilon_1(\varepsilon_2 + \varepsilon_1)z^3} \tag{67}$$

This expression gives us the energy required to place a dipole of strength μ at a distance $z > 0$ from a sharp interface at $z = 0$ separating two mediums of dielectric constants ε_1 and ε_2. θ is the dipole angle with the normal. It is easy to show that the preferred orientation of the dipole is perpendicular to the interface if it is located in the medium of smaller permittivity or parallel to the interface if it is located in a medium with larger permittivity (Teixeira and telo da Gama, 2002). Knowing the membrane dielectric constant (Table 22) and calculating the solvent dipole moment vector using Gaussian 3.0 molecular modelling software (Frisch et al., 2004), the preferred dipole orientation near membrane solvent interface was determined (Figure 33). Then there was an attempt to use the radius derived from the orthogonal projection of the molecules into the membrane surface (Table 25), for r_p in the model, Eq. (29), and it was found that the model predicted values were much worse (Figure 36).

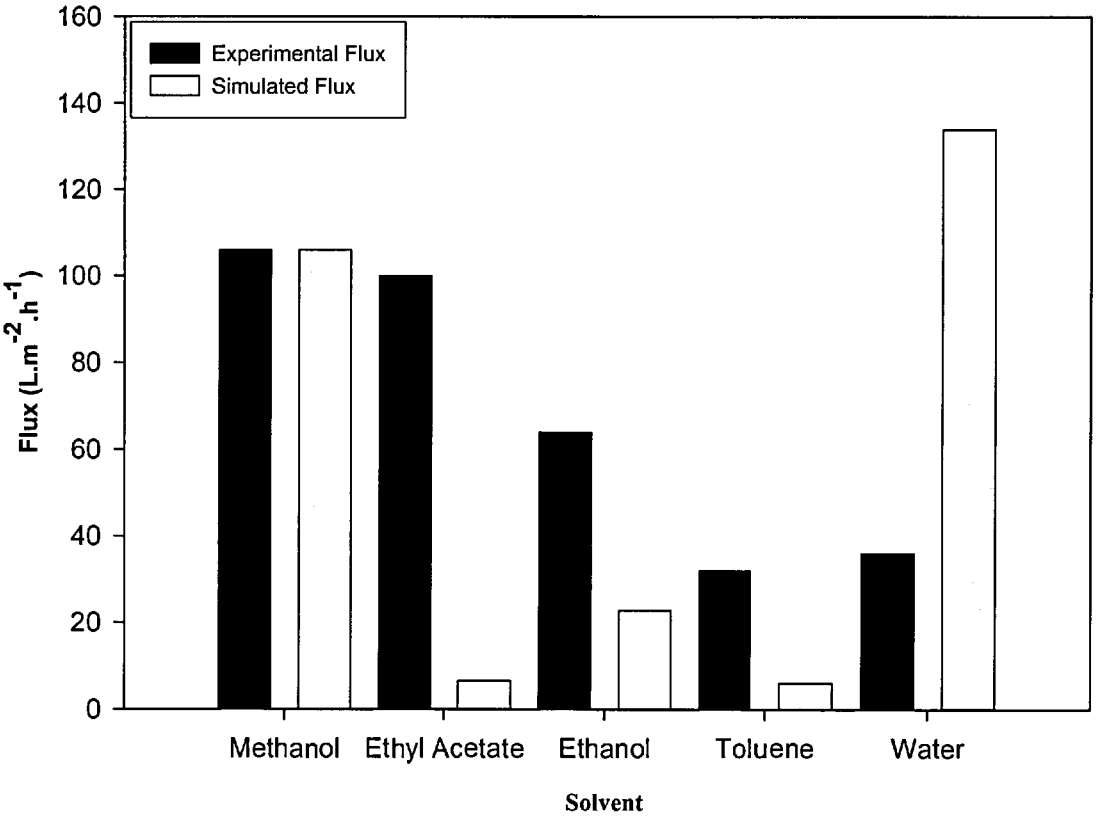

Figure 36 : Solvent flux predictions using the orthogonal projection molecular radius.

Therefore, it seems more likely that molecule orientation at the interface is determined by minimal interface breaking energy instead of by dipole moment alignment. Moreover, the explanation for the low flux value predicted by the model, for toluene (Figure 35) probably lies in the very low swelling value obtained for this solvent. Searching the literature for P84 swelling data in toluene it was found a reported 2.7 wt. % value for P84 swelling in liquid toluene (Beerlage, 1994). This value is five times higher than the value obtained with DVS. Actually, if this value was used instead of the one obtained by DVS, the predicted toluene flux would be very close to the experimental value (21.1 $L.m^2.h^{-1}$). For the high ethyl acetate flux predicted by the model the explanation may also lie in the difference between the DVS determined P84 swelling value and the P84-liquid ethyl acetate true swelling value since Beerlage (1994) also reported a very different value for P84 swelling in liquid ethyl acetate (2.8 wt. %). In this work the DVS technique was chosen to determine solvent swelling because this method is more accurate than the common polymer immersion in liquid technique. However, it is important to point out the literature data reporting

differences between vapour-polymer and liquid-polymer swelling behaviour (a phenomena known as Schroeder's paradox (Vallieres, et al. 2006)). These differences might have reduced the model predictive power for some of the solvents tested. Moreover, being swelling a crucial factor determining the solvent flux predictions, for a broader implementation of the model, derived in this work, in OSN, it is necessary to develop accurate liquid-polymer swelling determination techniques.

Although the model cannot be used to predict other literature data concerning solvent permeation through OSN membranes, since, in order to do so, it would be required swelling data for the different membrane films used. Looking at Geens et al. (2005), where different OSN membranes were tested with water, methanol and ethanol binary mixtures, it can observed that the N30F membrane has a solid-vapour surface tension value close to the one determined for STARMEM^{TM} 122. Assuming that this similar surface tension also implies similar sorption behaviour the methanol, ethanol and water flux trends predicted by our model, Figure 35 (methanol flux = 1.49 ethanol flux = 2.43 water flux) should be similar to the one presented in the previously mentioned paper (methanol flux = 1.42 ethanol flux = 3.8 water flux). In fact they are, indicating a successful application of the model to other OSN systems present in the literature. Moreover, it is interesting to note that performing a sensitivity analysis to the model proposed in this work a very similar behaviour to the model proposed by Geen et al. (2006) is observed, indicating that the successful semi-empirical approach of this author might have a physical meaningful explanation given by the model derived in this thesis.

6.4.2 Solvent Mixtures Model Predictions

The sorption-diffusion model developed in this work can be extended to predictions of solvent mixture flux. In order to do so, solvent mixture activity, surface tension, and viscosity are required.

Using the modified UNIFAC for solution activity (Larsen et al., 1987), a Wilson based model for surface tension of solvent mixtures (Chunxi et al., 2000) and the experimental data for the viscosity of methanol-toluene mixtures (Silva et al., 2005) the predictions of the model for the system methanol-toluene are given in Figure 37.

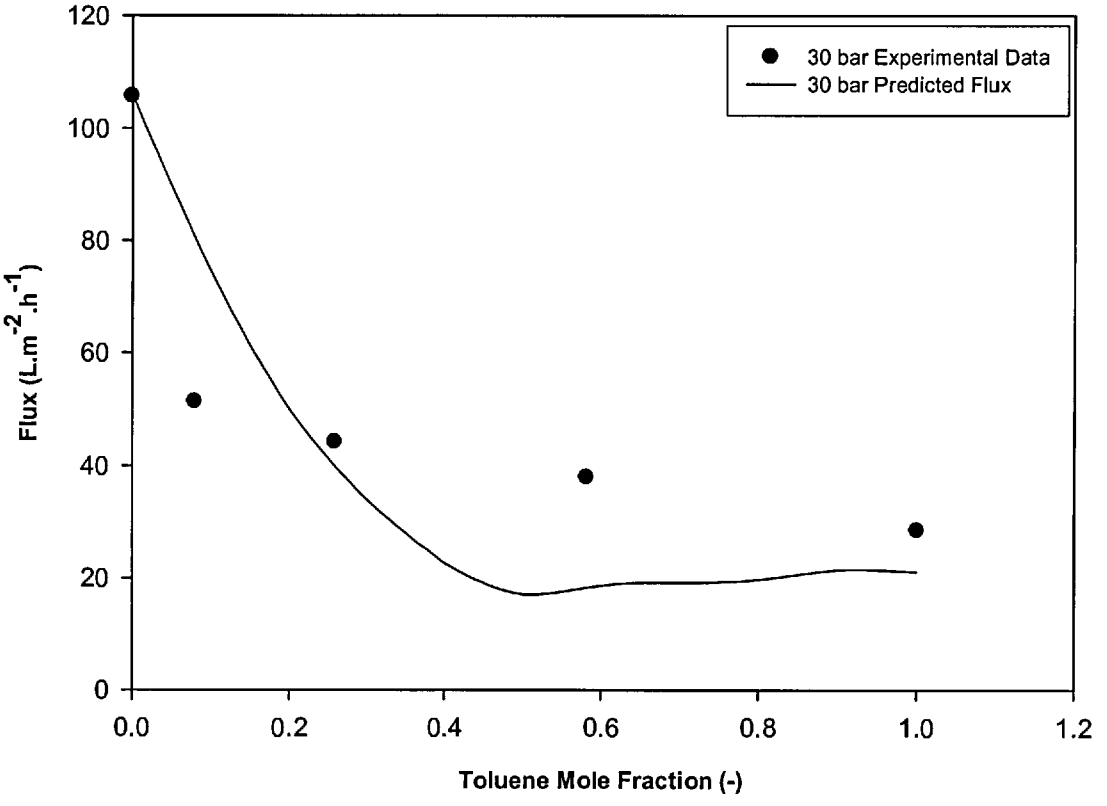

Figure 37 : Model predictions for methanol-toluene mixture permeation through STARMEM^{TM} 122 at 30 ^{0}C and 30 bar.

Model predictions are relatively good for a single fitting parameter model. It is clear that a flux minimum is predicted by the model, for a 0.5 toluene mole fraction. Minimums in solvent mixture flux have been reported in the OSN literature (Machado et al., 2000), however the experimental data for this system (toluene-methanol in STARMEM^{TM} 122) does not seem to indicate the presence of such minimum.

6.5 Conclusion

Solvent fluxes for methanol, ethanol, water, ethyl acetate, and toluene in STARMEM^{TM} 122 can be well described by the sorption-diffusion model developed in this work, as long as the smallest penetration radius possible is used as the molecular dimensions in calculating the energy required to move a molecule across the interface. The difference between predicted and experimental values for ethyl acetate and toluene are probably explained by the inaccuracies of the polymer swelling values for these solvents. Therefore, developing accurate techniques to determine polymer-liquid solvent swelling is a crucial step for broader model implementation. Moreover the model can be easily extended to solvent mixtures, giving reasonably accurate results with the use of a single fitting parameter.

7. Conclusions and Future Work

In this thesis, the extension of the principles of aqueous nanofiltration to non-aqueous systems has been investigated. OSN long term performance studies (involving both solvent-solvent and solvent-solute systems) were conducted on commercially available nanofiltration membranes in order to assess the factors determining specie transport in OSN. Simple methodologies based on the solution-diffusion and pore-flow models were developed. These were successfully employed to predict solvent flux during solvent mixture permeation, and flux/rejection behaviour during the permeation of highly concentrated solutions through OSN membranes. Moreover, using parameters determined for flat-sheet, these methodologies were successful in predicting OSN behaviour in spiral-wound element systems. Finally a physically meaningful model able to predict OSN solvent fluxes using independently determined solvent/membrane characteristics was developed.

In the first part of this study, continuous cross-flow experiments involving toluene-methanol and toluene-ethyl acetate solvent mixture permeation through STARMEM^{TM} and MPF-50 OSN membranes were performed. Firstly it is important to mention that the MPF-50 data was not analysed due to the lack of reproducibility of this membrane. For STARMEM^{TM} 122 it was shown that when toluene and methanol are swapped, using the same membrane discs, after a few swaps, the fluxes are stable at 25-30 $L.m^{-2}.h^{-1}$ for toluene and 60-70 $L.m^{-2}.h^{-1}$ for methanol. This suggests that solvent fluxes in STARMEM^{TM} 122, are independent of "membrane history". Moreover, it was demonstrated that compaction is a slow process (usually taking about 3 days to reach steady state), leading us to question the reliability of data collected in dead-end cell testing, where the data collection period is limited (typically 1-3 hours). In relation to solvent fluxes it was verified that the membrane-solvent interaction parameter is an important descriptor to assess solvent transport in a particular system. However this factor alone seems to be unable to explain the difference in flux between toluene and ethyl acetate in STARMEM^{TM}122. This difference in flux is probably due to different solvent diffusivities in the membrane matrix, caused by different solvent molecule shape and/or specific solvent-membrane matrix interactions. Solvent mixture viscosity alone does not describe flux behaviour

leading us to question the pore-flow mechanism of transport. However, both solution-diffusion and pore-flow (two parameter Hagen-Poiseuille model) transport models were able to describe quite well solvent fluxes for methanol/toluene and ethyl acetate/ toluene mixtures in STARMEM^{TM} 122, with the solution-diffusion model giving moderately better results. The key conclusion in this part of the study is that it is possible to predict solvent fluxes for solvent mixtures using pure solvent data. To do this for polyimide membranes, this work recommends measuring steady fluxes of pure solvents, and using these to determine membrane permeabilities. These permeabilities, together with the simple solution-diffusion model presented in this work, should be used to make design calculations for solvent mixtures.

In the second part of this research, the binary system methanol/dimethyl-methylsuccinate was used to investigate solute transport mechanism in OSN membranes, and to clarify the effect of solute concentration on the flux/rejection profiles, for partially rejected species. In order to do so, continuous cross-flow experiments involving methanol/dimethyl-methylsuccinate solution permeation through STARMEM^{TM}122 and MPF-50 OSN membranes were performed. As a first conclusion of this study it should be pointed out that long term continuous pressurization seems to be a requirement for obtaining reliable, time invariant flux and rejection data.

As solute concentration increases the flux decreases due to a build up in osmotic pressure and concentration polarization. It is interesting to notice that both solution-diffusion and pore-flow models can explain solvent flux dependence on concentration, for the tested membranes. Moreover, all model fitted parameters; the solution-diffusion solute permeability, the pore-flow pore radius and the film-theory mass transfer coefficients, are physically feasible values in agreement with data reported in the literature. The solute rejection analysis in this study focused on the STARMEM^{TM} 122 performance, due to the constancy of the MPF-50 rejection values, explained by the high MWCO of this membrane. It was concluded that the solution mass transfer characteristics of the nanofiltration setup in use are a crucial factor determining how rejection profile changes with concentration. Moreover, it was found that the solution-diffusion model coupled with film-theory for solution mass transfer provided the best fit for the solute rejection profile in STARMEM^{TM} 122. This superior performance of

the solution-diffusion model is more evident in the high solute concentration domain and it is probably explained by the fact that, contrary to the pore-flow model, the solution-diffusion model does not make any distinction between "solvent" and "solute" for the permeating species, being intrinsically a broader model. It is important to point out that previously, solvent mixtures were investigated and the solution-diffusion model was found to describe their permeation behaviour (Silva et al., 2005). Highly rejected species where the distinction between solvent and solute is clear were also investigated. Once again the solution-diffusion approach gave a good description of the experimental data (Peeva et al., 2004). And now, in this part of the study it was shown that for a partially rejected specie system the solution-diffusion model coupled with the film theory for solution mass transfer is able to describe quite well the flux and rejection trends for a broad range of concentration and pressure. Therefore, it seems clear that the solution-diffusion model has a successful applicability in a broad range of OSN systems (solvent mixtures, highly rejected solutes, partially rejected solutes). Moreover, this general predictive capability is achieved by the means of three experimentally determined parameters (solvent permeability, solute permeability and solute mass transfer coefficient).

After proving the applicability of the solution-diffusion model for a broad range of flat-sheet cross-flow OSN systems, in the third part of this study a pilot plant apparatus was used to determine the flux and rejection behaviour of a spiral-wound STARMEM^{TM} 122 module. The binary system toluene/TOABr was used to investigate the mechanisms that determine solvent flux and solute rejection, by establishing comparisons with flat-sheet cross-flow nanofiltration results. It was concluded that by using membrane transport parameters, obtained from flat-sheet experiments it was possible to accurately predict the flux/rejection trends for OSN with spiral-wound elements. Moreover, a simple spiral-wound model considering uniform pressure and concentration on each side of the membrane, coupled with the solution-diffusion model for membrane transport and the film theory for solution mass transfer was able to give accurate flux and rejection predictions for the system in study. The success of this simple model requires low pressure drop values and low mass transfer resistances. In industrial applications where large membrane areas are required, pressure drop might become a really important issue and for these cases only a complex spiral-wound model, taking into account radial and axial variation of:

pressure, cross-flow velocity, and concentration, or a simple spiral-wound model that makes use of the experimental pressure drop value will be able to provide accurate flux/rejection predictions.

Lastly, in the fourth part of this work there was a concern with the development of a generalized model based on physiochemical interactions, rather than semi-empirical relations, able to explain solvent transport in OSN. As solvent properties important to transport, the derived model takes into account; solvent viscosity, solvent molecular dimension, solvent molar volume, solvent swelling capability and solvent liquid-vapour surface tension. The membrane property determining transport is the membrane's solid-vapour surface tension. Although this model is still in its early stages, and more experimental work is required to test the broadness of its applicability, it is interesting to notice that all model parameters used in the flux predictions are physically meaningful values. Moreover, the model can be successfully extended to the permeation of solvent mixtures, with the use of one single fitting parameter.

Specific achievements of the research and corresponding future work can be outlined as follows:

1. This work established the importance of polymer-solvent interactions for non-aqueous systems. Evaluated several parameters such as the Flory-Huggins interaction parameter and membrane surface energy which can be used for quantifying such interactions. More research should be developed in order to construct precise equipment/techniques able to measure sorption and diffusion coefficients in asymmetric structured OSN membranes.

2. Traditional transport theories (solution-diffusion and Pore-flow models) have been extended to non-aqueous systems to explain separation behaviour; however, they only impart a physical interpretation of the transport mechanism.

3. A simple model (coupling the solution-diffusion model for membrane transport and film theory for solution mass transfer) able to predict the permeation of; solvent mixtures, highly concentrated solutions of highly rejected species, and highly

concentrated solutions of partially rejected species, through OSN membranes. The general predictive capability of the model is achieved by the means of three experimentally determined parameters (solvent permeability, solute permeability and solute mass transfer coefficient). More research should be carried out in order to obtain, physiochemical model/correlations able to predict solvent/solute permeabilities by the means of solvent, solute and membrane characteristics. Since this would be the crucial step in achieving the ultimately desired, OSN fully predictive models.

4. Developed and verified models able to predict the performance of OSN with spiral-wound elements. Using membrane transport parameters obtained from flat-sheet experiments. Assessed spiral-wound model complexity required to model a specific system. It would be interesting to carry out more spiral-wound experiments for several solvent-solute-membrane systems, in order to generalize this technique

6. Developed a diffusion-based transport theory using a fundamental chemical potential gradient approach coupled with a Langmuirian sorption isotherm controlled by an interface breaking energy concept. This model uses solvent and membrane physical properties to explain permeation behaviour and can be easily extended to the analysis of solvent mixture permeation. More experiments involving different solvent-membrane systems are required to assess the broadness of this model, as well as to prove the validity of the physical concepts behind the model development.

This research contributed to fundamental understanding of the membrane processes that are well-established for aqueous systems to non-aqueous systems, both experimentally and theoretically.

References

Adam,W.J., Luke, B., & Meares, P. (1983).
The separation of mixtures of organic liquids by hyperfiltration.
J. Membr. Sci., 13, 127–149.

Aithal, U.S., Aminabhavi, T.M., & Cassidy, P.E. (1990).
Interaction of organic halides with polyurethane elastomer.
J. Membr. Sci., 50, 225.

Alberino, L.M. (1971).
Mischpolyimide, Ger. DE 2143080

Almquist, C.B., & Hwang, S. (1999).
The permeation of organophosphorus compounds in silicone rubber membranes. *J. Membr. Sci.*, 153, 57

Barbari, T.A., Koros, W.J., & Paul, D.R. (1988).
J. Polym. Sci. Phys., Ed. 26, 709 and 729.

Barrer, R.M., Barrie, J.A., & Slater, J. (1958).
Sorption and diffusion in ethyl cellulose. Part III. Comparison between ethyl cellulose and rubber.
J. Polym. Sci., 27, 177–197.

Barton, A.F.M. (1983).
Handbook of Solubility Parameters and Other Cohesion Parameters. CRC Press, Boca Raton, FL.

Bateman, J., & Gordon, D.A. (1974).
Soluble polyimides derived from phenylindane diamines and Dianhydrides, US 3.856.752.

Bhanushali, D., Kloos, S., Kurth, C., & Battacharyya, D. (2001).
Performance of solvent-resistant membranes for non-aqueous systems: solvent permeation results and modelling.
J. Membr. Sci., 189, 1-21.

Bhanushali, D., Kloos, S., & Battarcharyya, D. (2002).
Solute transport in solvent-resistant nanofiltration membranes for non-aqueous systems: experimental results and the role of solute-solvent coupling.
J. Membr. Sci., 208, 343-359.

Beerlage, M.A.M. (1994).
Polyimide ultrafiltration membranes for non-aqueous systems, PhD dissertation, University of Twente, the Netherlands.

Bearman, R.J., & Kirkwood, J.G. (1958).
Statistical mechanics of transport processes. XI. Equations of transport in multicomponent systems.
J. Chem. Phys., 28, 136.

Bearman, R. J. (1959).
On the linear phenomenological equations. II. The linear statistical mechanical theory.
J. Chem. Phys., 31, 751.

Bearman, R.J. (1985).
On the linear phenomenological equation.
J. Chem. Phys., 28, 136.

Boudinar, M.B., Hanbury, W.T., & Avlonitis, S. (1992).
Numerical simulation and optimisation of spiral-wound modules.
Desalination, 86, 273.

Bowen, W.R., & Mukhtar (1996).
Characterization and prediction of separation performance of nanofiltration membranes.
J. Membr. Sci., 112, 263-274.

Bowen, W.R., Mohammad, A.W., & Hilal, N. (1997).
Characterization of nanofiltration membranes for predictive purposes — use of salts, uncharged solutes and atomic force microscopy.
J. Membr. Sci., 126, 91– 105.

Bowen, W.R., & Welfoot, J.S. (2002).
Modelling the performance of membrane nanofiltration — critical assessment and model development.
Chem. Eng. Sci., 57, 1121–1137.

Burghoff, H.G., Lee, K.L., & Pusch, W. (1980).
Characterization of Transport Across Cellulose Acetate Membrane in the Presence of Strong Solute-Membrane Interactions.
J. Applied Polymer Science, 25, 323-347.

Chiolle, Gianotti, G., Gramondo, M., & Parrini, G. (1978).
Mathematical model of reverse osmosis in parallel-wall channels with turbulence promoting nets.
Desalination, 26, 3.

Chunxi, L., Wenchuang, W., & Zihao, W. (2000).
A surface tension model for liquid mixtures based on the Wilson equation.
Fluid Phase Equilibr., 175, 185-196.

Clark, J. H. (1999).
Green chemistry: challenges and opportunities.
Green Chem., 1(1), 1-8.

Clément, R., Jonquiéres, A., Sarti, I., Sposata, M.F., Teixidor, M.A.C., & Lochon, P. (2004)
Original structure-property relationships derived from a new modeling of diffusion of pure solvents through polymer membranes.
J. Membr. Sci., 232, 141.

Critchley, J.P., Knight, G.J., & Wright, W.W. (1983).
Heat resistant polymers, Plenum, New York.

Curzons, A.D., Constable, J.C., Mortimer, D.N., & Cunningham, V. L. (2001)
So you think your process is green, how do you know? Using principles of sustainability to determine what is green a corporate perspective.
Green Chem., 2001, 1-6.

Danner, R. P., & High, M. S. (1993)
Handbook of Polymer Solution Thermodynamics, Design Institute for Physical Property Data. American Institute of Chemical Engineers, New York.

Datta, K., Ebert, H., & Plenio (2003).
Nanofiltration for homogeneous catalysis separation: soluble polymer-supported palladium catalysts for Heck, Sonogashira, and Suzuki coupling of aryl halides. *Organometallics,* 22, 4685–4691.

Daubert, T.E., & Danner, R.P. (1989).
Physical and thermodynamic properties of pure chemicals: Data compilation. Hemisphere Publishing Corporation, Pennsylvania.

De Smet, K., Averts, S., Cuelemans, E., Vankelecom, I.F.J., & Jacobs, P.A. (2001).
Nanofiltration-Coupled Catalysis to Combine the Advantages of Homogeneous and Heterogeneous Catalysis.
Chem. Comm.,7, 597-598.

Deen, W.M. (1987).
Hindered transport of large molecules in liquid-filled pores.
AIChE J., 33, 1409–1425.

del Castillo, L.F., & Mason, E.A. (1980).
Statistical-mechanical theory of passive transport through partially sieving or leaky membranes.
Biophys. Chem., 12, 223.

Dijkstra, H.P., Van Klink, G.P.M., & Van Koten, G. (2002).
The use of ultra- and nanofiltration techniques in homogeneous catalyst recycling.
Acc. Chem. Res. 35, 798–810.

Evangelista, F., & Jonsson, G. (1988).
Optimal design and performance of spiral wound modules. I. Numerical method.
Chem. Eng. Comm.,72, 69.

Fowkes, F.M. (1964)
Attractive Forces at Interfaces.
Ind. Eng. Chem. 56, 40-52.

Frisch, M.J., Trucks, G.W., Schlegel, H.B., Scuseria, G.E., Robb, M.A., Cheeseman, J.R., Montgomery Jr., J.A., Vreven ,T., Kudin, K.N., Burant, J.C., Millam, J.M., Iyengar, S.S., Tomasi, J., Barone, V., Mennucci, B., Cossi, M., Scalmani, G., Rega, N., Petersson, G.A., Nakatsuji, H., Hada, M., Ehara, M., Toyota, K., Fukuda, R., Hasegawa, J., Ishida, M., Nakajima, T., Honda, Y., Kitao, O., Nakai, H., Klene, M., Li, X., Knox, J.E., Hratchian, H.P., Cross, J.B., Bakken, V., Adamo, C., Jaramillo, J., R., R.E. Stratmann, O. Yazyev, A.J. Austin, R. Cammi, C. Pomelli, J.W. Ochterski, Gomperts, Ayala, P.Y., Morokuma, K., Voth, G.A., Salvador, P., Dannenberg, J.J., Zakrzewski, V.G., Dapprich, S., Daniels, A.D., Strain, M.C., Farkas, O., Malick, D.K., Rabuck, A.D., Raghavachari, K., Foresman, J.B., Ortiz, J.V., Cui, Q., Baboul, A.G., Clifford, S., Cioslowski, J., Stefanov, B.B., Liu, G., Liashenko, A., Piskorz, P., Komaromi, I., Martin, R.L., Fox, D.J., Keith, T., Al-Laham, M.A., Peng, C.Y., Nanayakkara, A., Challacombe, M., Gill, P.M.W., Johnson, B., Chen, W., Wong, M.W., Gonzalez, C., Pople, J.A. (2004)
Gaussian 03, Revision B.04
Gaussian, Inc., Wallingford CT.

Dotremont, C., den Ende, S.V., Vandommele, H., & Vandecasteele, C. (1994)
Concentration polarization and other boundary layer effects in the pervaporation of chlorinated hydrocarbons.
Desalination, 95, 91.

Gebben, B. (1988).
Thermally Stable and Chemically Resistant Polymer Membranes; Aromatic Polyoxadiazoles and Polytriazoles, PhD dissertation, University of Twente, the Netherlands.

Geens, J., Peeters, K., Van der Bruggen, B., & Vandecasteele, C. (2005).
Polymeric nanofiltration of binary water–alcohol mixtures: influence of feed composition and membrane properties on permeability and rejection.
J. Membr. Sci., 255, 255–264.

Geens, J., Van der Bruggen, B., & Vandecasteele, C. (2006)
Transport model for solvent permeation through nanofiltration membranes.
Sep. Purif. Technol. 48, 255-263.

Gekas, V., & Hallstrom (1987).
Mass transfer in the membrane concentration layer under turbulent cross flow I. Critical literature review and adaptation of existing Sherwood correlations to membrane operations.
J. Membr. Sci., 30, 153.

Gevers, L.E.M., Meyen, G., De Smet, K., Van De Velde, P., Du Prez, F.,Vankelecom, I.F.J., & Jacobs, P.A. (2006).
Physico-chemical interpretation of the SRNF transport mechanism for solutes through dense silicone membranes.
J. Membr. Sci., 274, 173–182.

Gibbins, E., Antonio, M.D., Nair, D., White, L.S., Freitas dos Santos, L.M., Vankelecom, I.F.J., & Livingston, A.G. (2002).
Observation on solvent flux and solute rejection across solvent resistant nanofiltration membranes.
Desalination, 147, 307-313.

Gilron, J.; Gara, N., & Kedem, O. (2001).
Experimental analysis of negative salt rejection in nanofiltration membranes.
J. Membr. Sci., 185, 223-236.

Gosser, L.W., Knoth, W.H., & Parshall G.W. (1997).
Reverse osmosis in homogeneous catalysis.
J. Mol. Catal., 2, 253–263.

Groß., A., & Heintz, A. (2000).
Diffusion coefficients of aromatics in nonporous PEBA membranes.
J. Membr. Sci., 168, 233.

Harris, F.W., & Lanier, L.H. (1977).
Structure-solubility relationships in polyimides. Harris, F.W, & Seymour, R.B. (Eds.), *Structure-solubility relationships in polymers*. Academic Press, New York, 1977, p. 183

Herath, G., Yamamoto, K., & Urase, T. (2000).
The effect of suction velocity on concentration polarization in microfiltration membranes under turbulent flow conditions.
J. Membr. Sci., 169, 175.

Hirata, O., & Nagahama (1975).
Computer aided data book of vapour-liquid equilibria.
Kodansha Limited Elsevier Scientific Publishing Group, Japan, 1975.

Ho, W.S.W., & Sirkar, K.K. (1992).
Membrane Handbook.
Van Nostrand Reinhold, New York, 239-240.

Hori, H., & Tanaka, I. (1998).
Equilibrated vapour concentrations for bicomponent organic solvents.
J. Occup. Health., 40, 132.

Jagur-Grodzinski, J., & Kedem, O. (1966).
Transport coefficients and salt rejection in hyperfiltration membranes.
Desalination, 1, 327.

Jain, S., & Gupta, S.K. (2004).
Analysis of modified surface pore flow model with concentration polarization and comparison with Spiegler-Kedem model in reverse osmosis systems.
J. Membr. Sci., 232, 45.

Jonsson, G., & Boesen, C.E. (1977).
Concentration polarization in a reverse osmosis test cell.
Desalination, 21, 1.

Kedem, O. & Katchalsky, A. (1958).
Thermodynamic analysis of the permeability of biological membranes to non-electrolytes.
Biochim. Biophys. Acta., 27, 229.

Kanehashi, S., & Nagai, K. (2005).
Analysis of dual-mode model parameters for gas sorption in glassy polymers.
J. Membr. Sci., 253, 117-138.

Katchalsky, A., & Kedem, O. (1962).
Thermodynamic of flow processes in biological systems.
Biophys. J., 2, 53.

Kim, J.Y.; Lee, H.K., Baik, K.J., & Kim, S.C. (1997).
Liquid-Liquid Phase Separation in Polysulfone/ Solvent/ Water Systems.
J. Applied Polymer Science, 65, 2643-2653.

Kim, D., Caruthers, J.M., & Peppas, N.A. (1993).
Penetrant transport in cross-linked polystyrene.
Macromolecules, 26, 1841.

Kirk & Othmer (1984).
Encyclopedia of chemical technology, 3rd Ed., Wiley-Interscience, Volume 1-24.

Krishna, R., & Wesselingh, J.A. (1997).
The Maxwell-Stefan approach to mass transfer.
Chem. Eng. Sci., 52, 861-911.

Krockel, J., & Kragl, U. (2003).
Nanofiltration for the separation of non-volatile products from solutions containing ionic liquids.
Chem. Eng. Technol. 26, 1166–1168.

Kwok, D.Y., & Neumann, A.W. (1999).
Contact angle measurement and contact angle interpretation.
Advances in Colloid and Interface Science, 81, 167-249.

Larsen, B.L., Rasmussen, P., & Fredenslund, A.A. (1987).
A modified UNIFAC group contribution model for prediction of phase equilibria and heat of mixing.
Ind. Eng. Chem. Res., 26, 2274–2286.

Lightfoot, E.N. (1974).
Transport phenomena and living systems.
Willey-Interscience, New York, 1974, 175-177.

Linder, C., Nemas, M., Perry, M., & Katraro, R. (1993).
Silicone-derived solvent stable membranes.
US Patent 5,205,934 .

Livingston, A.G., Peeva, L., Han, S., Nair, D., Luthra, S.S., White, L.S., & Santos, L.M.F. (2003).
Membrane separation in green chemical processing; Solvent nanofiltration in liquid phase organic synthesis reactions.
Ann. N.Y. Acad. Sci., 984,123-141

Lonsdale, H.K., Merten, U., & Riley, R.L. (1965).
Transport properties of cellulose acetate osmotic membranes.
J. Appl. Polym. Sci., 9, 1341.

Luthra, S.S., Yang, X., Freitas dos Santos, L.M., White, L.S., & Livingston, A.G. (2000).
Phase-Transfer Catalyst Separation and Re-Use by Solvent Resistant Nanofiltration Membranes.
Chem. Commun., 16 , 1468-1469.

Luthra, S.S., Yang, X., Freitas dos Santos, L.M., White, L.S., & Livingston, A.G. (2002)
Homogeneous phase transfer catalyst recovery and re-use using solvent resistant membranes.
J.Membr. Sci., 201, 65-75.

Mark, J.E.(1999).
Polymer Data Handbook.
Oxford University Press, Oxford, 1999.

Machado, D.R., Hasson, D., & Semiat, R. (1999).
Effect of solvent properties on permeate flow through nanofiltration membranes. Part I. Investigation of parameters affecting solvent flux.
J. Membr. Sci., 163, 93-102.

Machado, D.R., Hasson, D., & Semiat, R. (2000).
Effect of solvent properties on permeate flow through nanofiltration membranes, Part II. Transport model.
J. Mem. Sci., 166, 63-69.

Mason, E.A., & del Castillo, L.F. (1985).
The role of viscous flow in theories of membrane transport.
J. Membr. Sci., 23, 199.

Mason, E.A., & Viehland, L.A. (1978).
Statistical-mechanical theory of membrane transport for multicomponent systems: Passive transport through open membranes.
J. Chem. Phys., 68, 3562.

Mason, E.A., & Lonsdale, H.K. (1990).
Statistical-mechanical theory of membrane transport.
J. Membr. Sci., 51, 1-81.

Matsui, S. & Paul, D.R. (2004).
A simple model for pervaporative transport of binary mixtures through rubbery polymeric membranes.
J. Membr. Sci., 235, 25

McCarthy, R.A. (1985).
Encyclopaedia of polymer science and engineering.
J. Wiley, New York.

McClellan, A.L. (1989).
Tables of experimental dipole moments.
Volume 3. Rahara Enterprises, El Cerrito,1455.

Merten, U. (1966).
Transport properties of osmotic membranes.
U. Merten (Ed.), Desalination by reverse osmosis, MIT Press, Cambridge, MA, Chapter 2, 15-54.

Michaels, A.S., Vieth, W.R., & Barrie, J.A. (1963).
Solution of gases in polyethylene terephthalate.
J. Appl. Phys., 34, 1–12.

Michaels, A.S. (1968).
New separation techniques for the CPI.
Chem. Eng. Prog., 64, 31.

Mulder, M. (1997).
Basic principles of membrane technology, sec. ed.
Kluwer Academic Publishers.

Murthy, Z.V.P., & Gupta, S.K. (1997).
Estimation of mass transfer coefficients using a combined nonlinear membrane transport and film theory model.
Desalination, 109, 39.

Nair, D., Scarpello, J.T., White, L.S., Freitas dos Santos, L.M., Vankelecom, I.F.J., & Livingston, A.G. (2001).
Semi-continuous nanofiltrationcoupled Heck reactions as a new approach to improve productivity of homogeneous catalysts.
Tetrahedron Lett., 42, 8219–8222.

Nakao, S., & Kimura, S. (1981).
Analysis of solutes rejection in ultrafiltration.
J. Chem. Enj. Jpn., 14, 32.

Nakao, S., Wijmans, J.G., & Smolders, C.A. (1986).
Resistance to the permeate flux in unstirred ultra-filtration of dissolved macromolecular solutions.
J. Membr. Sci., 26, 165.

Nakao, S. (1994).
Determination of pore size and pore size distribution. Part 3. Filtration membranes.
J. Membr. Sci., 96, 131–165.

Noordman, T.R., & Wesselingh, J.A. (2002).
Transport of large molecules through membranes with narrow pores, the Maxwell-Stefan description combined with hydrodynamic theory.
J. Membr. Sci., 210, 227.

Owens, D.K., & Wendt, R.C. (1969).
Estimation of the surface free energy of polymers.
J. Appl. Polym. Sci., 13, 1969, 1741-1747.

Park, J.S., Kim, S.K., & Lee, K.H. (2000).
J. Ind. Eng. Chem., 6, 93-99.

D.R., Paul, & Ebra-Lima, O.M. (1970).
Pressure induced diffusion of organic liquids through highly swollen polymer membranes.
J. Appl. Polym. Sci., 14, 2201–2224.

Paul, D.R., Garcin, M., & Garmon, W.E. (1976).
Solute diffusion through swollen polymer membranes.
J. Appl. Polym. Sci., 20, 609– 625.

Paul, D.R. (2004).
Reformulation of the solution-diffusion theory of reverse osmosis.
J. Membr. Sci., 241, 371–386.

Peeva, G.L., Gibbins, E., Luthra, S.S., White, L.S., Stateva, R.P., & Livingston, A.G. (2004).
Effect of concentration polarization and osmotic pressure on flux in organic solvent nanofiltration.
J. Membr. Sci., 236, 121-136.

Perry, R.H., & Green, D.W. (1998).
Perry's Chemical Engineers Handbook.
Seventh ed., McGraw-Hill.

Poling, B., Prausnitz, J., & O' Connell, J. (2001).
The properties of gases and liquids.
Mcgraw-Hill; London.

Process Systems Enterprise Ltd. (2002).
gPROMs Introductory User Guide.
Process Systems Enterprise Ltd., London.

Raman, L.P., Cheryan, M., & Rajagopalan, N. (1996).
Deacidification of soybean oil by membrane technology.
JAOSC, 73, 219–224.

Rautenbach, R., & Helmus, F.P. (1994).
Some considerations on mass-transfer resistances in solution-diffusion-type membrane processes.
J. Membr. Sci., 87, 171.

Rautenbach, R., & Dahm, W. (1987).
Design and optimization of spiral-wound and hollow fiber RO-modules.
Desalination, 65, 259.

Reid C.R., Prausnitz, J.M., & Poling (1987)
The properties of gases and liquids, forth. ed.,
McGraw-Hill, London.

Rezac, M.E., John, T., & Pfromm, P.H. (1997)
Effect of copolymer composition on the solubility and diffusivity of water and methanol in a series of polyether am-ides.
J. Appl. Polym. Sci., 65, 1983.

Robinson, J.P., Tarleton, E.S., Millington, C.R., & Nijmeijer, A. (2004).
Solvent flux through dense polymeric nanofiltration membranes.
J. Membr. Sci., 230, 29–37.

Scarpello, J.T., Nair, D., Freitas dos Santos, L.M., White, L.S., & Livingston, A.G. (2002).
The separation of homogeneous organometallic catalysts using solvent resistant nanofiltration.
J. Membr. Sci., 203, 71.

Scattergood, E.M., & Lightfoot, E.N. (1968).
Diffusional interactions in ion-exchange membranes.
Trans. Faraday Soc., 64, 1135.

Schock, G., & Miquel, A. (1987).
Mass transfer and pressure loss in spiral wound modules.
Desalination, 64, 339.

She, M., & Hwang, S.-T. (2004).
Concentration of dilute flavor compounds by pervaporation: permeate pressure effect and boundary layer resistance modeling.
J. Membr. Sci., 236, 193.

Sheldon, R.A. (1997).
Catalysis: The Key to Waste Minimization.
J. Chem. Tech. Biotechnol., 68, 381.

Sheth, J.P., Qin, Y.,Sirkar, K.K., & Baltsis, B.C. (2003).
Nanofiltration-based diafiltration process for solvent exchange in pharmaceutical manufacturing.
J. Membr. Sci., 211, 251-261.

Silva, P., Han, S., & Livingston, A.G. (2005).
Solvent transport in organic solvent nanofiltration membranes.
J. Membr. Sci., 262, 49–59.

Silva, P., & Livingston, A.G. (2006).
Effect of solute concentration and mass transfer limitations on transport in organic solvent nanofiltration-partially rejected solute.
J. Membr. Sci., 280, 889-898.

Snell, F.M., Aranow, R., & Spangler, R.A. (1967).
Statistical-mechanical derivation of the partial molecular stress tensors in isothermal multicomponent systems.
J. Chem. Phys., 47, 4959.

Soltanieh, M., & Gill, W.N. (1981).
Review of reverse osmosis membranes and transport models.
Chem. Eng. Commun., 12, 279.

Sourirajan, S., & Matsuura, T. (1985).
Reverse Osmosis/Ultrafiltration Principles.
NationalResearch Council of Canada, Ottawa, Canada.

Spiegler, K.S., & Kedem, O. (1966).
Thermodynamics of hyperfiltration (reverse osmosis): Criteria for efficient membranes.
Desalination, 1, 311.

Stafie, N., Stamatialis, D.F., & Wessling, M. (2004).
Insight into the transport of hexane-solute systems through tailor made composite membranes.
J. Membr. Sci., 228, 103.

Schwinge, J., Neal, P.R., Wiley, D.E., Fletcher, D.F., & Fane, A.G. (2004).
Spiral wound modules and spacers-review and analysis.
J. Membr. Sci., 242, 129-153.

Tang, W., Liu, D., & Zhang, X. (2003).
Asymmetric hydrogenation of itaconic acid and enol acetate derivatives with the Rh-TangPhos catalyst.
Org. Lett., 5, 205–207.

Tarleton, E.S., Robinson, J.P., Millington, C.R., & Nijmeijer, A. (2005).
Non-aqueous nanofiltration: solute rejection in low-polarity binary systems.
J. Membr. Sci., 252, 123–131.

Teixeira, P.I.C., & telo da Gama, M.M. (2002)
Orientation and association at the liquid-vapour interface of dipolar fluids, J.
Phys. Condens. Matter, 14, 12159-12165.

Thiel, S.W., Lloyd, D.R. (1988).
Application of the Stefan-maxwell equations to the pressure-driven membrane separation of dilute multicomponent solutions of nonelectrolytes.
J. Membr. Sci., 252, 123–131.

Uhlig, H. (1937).
Solubilities. of. Gases and Surface Tension.
J. Phys. Chm., 41, 1215.

Uragami, T., Tamura, M., & Sugihara, M. (1979).
Synthesis and permeability of special polymer membranes : XIII. Ultrafiltration and adsorption characteristics of cellulose nitrate-activated charcoal membranes. *J. Membr. Sci.*, 4, 305.

Vallieres, C., Winkelmann, D., Roizard, D., Favre, E., Scharfer, P., & Kind, M. (2006). On Schroeder's paradox.
J. Membr. Sci., 278, 357-364.

Van der Berg, G. B., & Smolders, C.A. (1989).
The boundary-layer resistance model for unstirred ultrafiltration. A new approach.
J. Membr. Sci., 40, 149.

Van der Bruggen, B., Schaep, J., Wilms, D., & Vandecasteele, C. (1999).
Influence of molecular size, polarity and charge on the retention of organic molecules by nanofiltration.
J. Membr. Sci. 156, 29–41.

Van der Bruggen, B., Schaep, J., Wilms, D., & Vandecasteele, C. (2000).
A comparison of models to describe the maximal retention of organic molecules in nanofiltration.
Sep. Sci. Technol. 35, 169–182.

Van der Bruggen, B., Geens, J., & Vandecasteele, C. (2002).
Influence of organic solvents on the performance of polymeric nanofiltration membranes.
Sep. Sci. Technol. 37, 783.

Van der Bruggen, B., Geens, J., & Vandecasteele, C. (2002).
Fluxes and rejections for nanofiltration with solvent stable polymeric membranes in water, ethanol and n-hexane.
Chem. Eng. Sci., 57, 2511-2518.

Van Kreleven, D.W. (1990)
Properties of Polymers.
Elsevier, New York.

Vieth, W.R., Tam, P.M., & Michaels, A.S. (1966)
Dual sorption mechanisms in glassy polystyrene.
J. Colloid Interf. Sci., 22, 360–370.

Weast, R.C. (1970).
Handbook of chemistry and physics, 51st Ed.
The Chemical Rubber Co.,Cleveland.

Weinrotter, K. (1985).
Properties and applications of the new polyimide fiber P84; Polyimides, synthesis, characterization and application; Proc. 2nd Intern. Conf. on polyimides.
New York, p. 253.

White, L.S., Wang, I., & Minhas, B.S. (1993).
Polyimide membrane for separation of solvents from lube oil.
US Patent 5,264,166.

White, L.S. (1998).
US Patent, 6,180,008.

White, L. S., & Nitsch, A.R. (2000).
Solvent recovery from lube oil filtrates with a polyimide membrane.
J. Memb. Sci., 179, 267-274

White L.S. (2001).
Polyimide membranes for hyperfiltration recovery of aromatic solvents
US Patent 6,180,008

White, L.S. (2002).
Transport properties of a polyimide solvent resistant nanofiltration membrane.
J. Membr. Sci., 205, 191-202.

Whu, J.A., Baltzis, B.C., & Sirkar, K.K. (2000).
Nanofiltration studies of larger organic microsolutes in methanol solutions.
J. Memb. Sci., 170, 159-172.

Wijmans, J.G. & Baker, R.W. (1995).
The solution diffusion model: a review.
J. Membr. Sci., 107, 1-21.

Yang, X.J., Livingston, A.G., & Freitas dos Santos, L. (2001).
Experimental observations of Nanofiltration with Organic Solvents.
J. Membr. Sci., 190, 45-55.

Zydney, A.L. (1997).
Stagnant film model for concentration polarization in membrane systems.
J. Membr. Sci., 130, 275.

Zwijenburg, H.J., Krosse, A.M., Ebert, K., Peinnemann, K.V., & Cuperus, F.P. (1999)
Acetone-stable nanofiltration membranes in deacidifying vegetable oil.
JAOSC, 76, 83–87.

Appendix I

The starting point for the derivation of a general theory of membrane transport is the classical-mechanical Liouville equation that describes the motion of all particles in a system, in a statistical form.

The second step is the passage from the Liouville equation to the general equations of fluid transport for a flowing, diffusing, multicomponent system (Bearman 1958; Bearman and Kirkwood 1958; Bearman 1959; Snell et al, 1967).

Finally there was a need to transform the previous equations of fluid transport into the membrane transport equations (del Castillo and Mason 1980; Mason and del Castillo 1985; Mason and Viehland 1978). In the end, denoting the test species with the index i, we can write the general transport equation for these species as:

$$\sum_{j=1}^{N} \frac{c_{j(m)}}{c_{t(m)} D_{ij}} \left(u_i - u_j\right) + \frac{u_i}{D_{iM}} = -\frac{1}{RT}\left(\nabla_T \mu_i^m - F_i\right) - \frac{\alpha_i' B_0}{\eta D_{iM}}\left(\nabla p - c_{t(m)} F\right) - \sum_{j=1}^{N} \frac{c_{j(m)}}{c_{t(m)} D_{ij}} D_{ij}^T \nabla \ln T \quad (1)$$

This equation has a clear physical interpretation and it basically states that the sum of the friction forces between i and the other species j is equal to the total driving force exerted on a specie i in a mixture. The total driving force is represented in the right side of the equation and can be divided in three sets of terms: the isothermal diffusion, the viscous flow and the thermal diffusion terms.

The generality of Eq. (1) has been clearly demonstrated. It was shown (Mason and Lonsdale 1990) that all the transport models currently used to describe nanofiltration can be derived from Eq. (1), with the use of model simplifications and mathematical manipulation.

Table 27 : General model derivation from statistical mechanics equation.

General Model	Model Simplification Applied to (1)	Mathematical Manipulation Applied to (1)
Frictional	none	Use of suitable algebra to adsorb the viscous flow term in (1) into D_{ij} and D_{iM} to produce "augmented" coefficients designated as friction coefficients f_{ij} and f_{iM} (Mason and Del Castillo, 1985).
Irreversible Thermodynamics	none	Same as the frictional model but followed by matrix inversion (Mason and Del Castillo, 1985).
Stefan-Maxwell	none	Same as the frictional one but instead of friction coefficients we have effective diffusion ones (Scattergood and Lightfoot, 1968; Lightfoot, 1974)

In the current work we will be dealing with isothermal systems where there is no external force except pressure, so Eq. (1) can be simplified.

$$\sum_{j=1}^{N}\frac{c_{j(m)}}{c_{t(m)}D_{ij}}\left(u_i-u_j\right)+\frac{u_i}{D_{iM}}=-\frac{1}{RT}\left(\nabla_T\mu_i-F_i\right)-\frac{\alpha_i' B_0}{\eta D_{iM}}\left(\nabla p-c_{t(m)}F\right) \qquad (2)$$

The number of transport parameters required to completely describe this kind of transport phenomena is given by:

Table 28 : Number of transport parameters.

Type	Number
D_{ij}	$\frac{N(N-1)}{2}$
D_{iM}	N
$\alpha_j' B_0$	N
Total	$\frac{N(N+3)}{2}$

It is clear that even for a small number of components for instance a binary mixture, a high number of transport parameters is required, 5 to be exact. But, for a binary system Eq. (2) can be mathematically manipulated and by lumping parameters we can obtain an expression with one less transport parameter so, for a binary mixture we will have:

$$\begin{aligned} N_1 &= c_{1(m)}u_1 = L_{11}^c \nabla\mu_1^m - L_{12}^c \nabla\mu_2^m - \alpha_1 c_{1(m)} L_0 \nabla p \\ N_2 &= c_{2(m)}u_2 = L_{21}^c \nabla\mu_1^m - L_{22}^c \nabla\mu_2^m - \alpha_2 c_{2(m)} L_0 \nabla p \end{aligned} \tag{3}$$

where:

$$L_{11}^c = \frac{c_{1(m)}}{\Lambda RT}\left(\frac{c_{1(m)}}{c_{t(m)}D_{12}} + \frac{1}{D_{2m}}\right) \tag{4}$$

$$L_{12}^c = L_{21}^c = \frac{1}{\Lambda RT}\frac{c_{1(m)}c_{2(m)}}{c_{t(m)}D_{12}} \tag{5}$$

$$\alpha_1 = \frac{\alpha_1'}{\Lambda D_{1M}}\left(\frac{c_{1(m)}}{c_{t(m)}D_{12}} + \frac{1}{D_{2m}}\right) + \frac{\alpha_2'}{\Lambda D_{2M}}\frac{c_{2(m)}}{c_{t(m)}D_{12}} \tag{6}$$

$$L_0 = \frac{B_0}{\eta} \tag{7}$$

$$\Lambda = \frac{1}{c_{t(m)}D_{12}}\left(\frac{c_{1(m)}}{D_{1M}} + \frac{c_{2(m)}}{D_{2M}}\right) + \frac{1}{D_{1M}D_{2M}} \tag{8}$$

If we assume component 1 to be the solvent and 2 the solute we obtain the commonly used expressions:

$$\begin{aligned} N_v &= \overline{V}_1 N_1 + \overline{V}_2 N_2 = -L_p(\nabla p - \sigma_v \nabla \pi^a) \\ N_2 &= -c_{1(m)}\overline{V}_1 \omega \nabla \pi^a + c_{2(m)}\left(1 - c_{1(m)}\overline{V}_1\sigma_s\right)N_v \end{aligned} \tag{9}$$

Where:

$$L_p = \overline{V}_1^2 L_{11}^c + \overline{V}_2^2 L_{22}^c + 2\overline{V}_1\overline{V}_2 L_{12}^c + c_{t(m)}\overline{V}_1\overline{V}_2 L_0\left(\alpha_1 c_{1(m)} + \alpha_2 c_{2(m)}\right) \tag{10}$$

$$\sigma_v = \frac{\overline{V}_1 L_{11}^c + \overline{V}_2 L_{12}^c}{c_{1(m)}L_p} - \frac{\overline{V}_2 L_{22}^c + \overline{V}_1 L_{12}^c}{c_{2(m)}L_p} \tag{11}$$

$$\sigma_s = \sigma_v + \frac{(\alpha_1 - \alpha_2)L_0}{L_p} \tag{13}$$

$$\omega = c_{2(m)}\left(\frac{L_{11}^{c}}{c_{1(m)}^{2}}+\frac{L_{22}^{c}}{c_{2(m)}^{2}}+\frac{2L_{12}^{c}}{c_{1(m)}c_{2(m)}}\right)+\frac{c_{t(m)}L_0}{c_{1(m)}}\left(\alpha_1 c_{1(m)}+\alpha_2 c_{2(m)}\right)-c_{2(m)}\sigma_v\sigma_s L_p \qquad (14)$$

In the next table the most commonly applied nanofiltration models are shown along with the correct way to deduce them starting from the general equations.

Table 29 : Usually applied nanofiltration models and their deduction.

Model	General Equations*	Usually Applied Equations**	Assumptions
Solution-Diffusion (Lonsdale et al, 1965)	$N_1 = -\frac{D_{1M}}{RT} c_{1(m)} \nabla \mu_1^m$ $N_2 = -\frac{D_{2M}}{RT} c_{2(m)} \nabla \mu_2^m$	$N_1 \approx -\frac{D_{1M}^e}{RT} \frac{(\Delta p - \Delta \pi)}{\Delta z} = P(\Delta p - \Delta \pi)$ $N_2 \approx -D_{2M}^e \frac{\Delta c_{2(m)}}{\Delta z}$ $R = 1 - \frac{c_{1P} N_2}{c_{2F} N_1} \approx 1 - \frac{c_{1P} RT D_{2M}^e}{c_{2F} D_{1M}^e} \left(\frac{\Delta c_{2(m)}}{\Delta p - \Delta \pi} \right)$	* The 2 components do not interact with each other. ** Dilute ideal solutions, finite difference approximation and constant transport coefficients.
Kedem-Katchalsky (Kedem and Katchalsky, 1958,1962)	Eq. (9)	$N_v = \frac{L_p}{\Delta z} \left(\lvert \Delta p \rvert - \sigma \lvert \Delta \pi^a \rvert \right)$ $N_2 = \frac{\omega}{\Delta z} \lvert \Delta \pi^a \rvert + \langle c_{2(m)} \rangle (1-\sigma) N_v$ $R = 1 - \frac{N_2}{c_{2F} N_v} \approx \frac{\langle c_{2(m)} \rangle}{c_{2F}} (\sigma - 1) - \frac{\omega \lvert \Delta \pi^a \rvert}{c_{2F} N_v \Delta z} + 1$ $\langle c_{2(m)} \rangle \approx \frac{c_{2F} - c_{2P}}{\ln \left(\frac{c_{2F}}{c_{2P}} \right)}$	* None ** Dilute ideal solutions, finite difference approximation, constant transport coefficients and $\alpha_1 = \alpha_2$.
Spiegler-Kedem (Spiegler and Kedem, 1966)	Eq. (9)	Same as the previous one except for $\langle c_{2(m)} \rangle$ that is rigorously calculated from the differential equation: $\langle c_{2(m)} \rangle = \frac{c_{2F} e^{Pe} - c_{2P}}{e^{Pe} - 1} - \frac{c_{2F} - c_{2P}}{Pe}$ $P_e = \frac{(1-\sigma) N_v \Delta z}{wRT}$	* None ** Dilute ideal solutions, finite difference approximation, constant transport coefficients and $\alpha_1 = \alpha_2$.
Pore Flow (Merten, 1966)	$N_1 = \frac{c_{1(m)} \alpha_1' \beta_0}{\eta} \nabla p$ $N_2 = \frac{c_{2(m)} \alpha_2' \beta_0}{\eta} \nabla p$	$N_v = \frac{\varepsilon r_p^2}{8 \eta \tau} \frac{\Delta p}{\Delta z}$	* No diffusion coupling of the fluxes and no activity gradient ** β_0 can be described by Poiseuilles's law , finite difference approximation, constant transport coefficients and $\alpha_1' = \alpha_2' = 1$.

There are many other models that can be applied for nanofiltration (Soltanieh and Gill, 1981) but all them are based in the ones shown in the previous Table. After showing that all membrane transport models can be derived from one single general equation of transport, the models used in this thesis will be derived in detail.

Solution-Diffusion Model

For the solution-diffusion (Wijmans and Baker, 1995) the following profiles are expected:

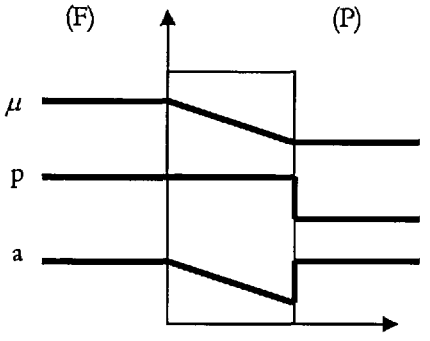

Figure 38 : Theoretical membrane profiles for the solution-diffusion mechanism.

It is clear that the solution-diffusion model assumption states that the activity gradient is the only responsible in the transport process. To fully derive this model the one dimensional version of Eq. (16) in chapter 2 is a good start:

$$N_i = -\frac{c_{i(m)} D^e_{i(m)}}{x_m} \frac{dx_{i(m)}}{dz} \tag{15}$$

Assuming constant x_m, $D^e_{i(m)}$ and $c_{i(m)}$ the previous equation can be integrated to give:

$$N_i = -\frac{c_{i(m)} D^e_{i(m)}}{x_m} \frac{(x_{i(m)P} - x_{i(m)F})}{l} \tag{16}$$

Now it is required to relate the outside and inside membrane molar fractions and the chemical potential balance provides this relation.

Chemical Potential Balance

Feed:

$$\mu_{iF} = \mu_{i(m)F} \tag{17}$$

$$\mu_{iF}^{\ 0} + RT\ln(\gamma_{iF}x_{iF}) + \overline{V}_i(p_F - p_{isat}) = \mu_{i(m)F}^{\ 0} + RT\ln(\gamma_{i(m)F}x_{i(m)F}) + \overline{V}_i(p_{(m)F} - p_{isat}) \tag{18}$$

Once that:

$$p_{(m)F} = p_F \tag{19}$$

We obtain:

$$\ln(\gamma_{iF}x_{iF}) = \ln(\gamma_{i(m)F}x_{i(m)F}) \quad \text{or} \quad x_{i(m)F} = K_i^{molar}x_{iF} \tag{20}$$

With the molar partition coefficient given by:

$$K_i^{molar} = \frac{\gamma_{iF}}{\gamma_{i(m)F}} \tag{21}$$

Permeate:

$$\mu_{iP} = \mu_{i(m)P} \tag{22}$$

$$\mu_{iP}^{\ 0} + RT\ln(\gamma_{iP}x_{iP}) + v_i(p_p - p_{isat}) = \mu_{i(m)P}^{\ 0} + RT\ln(\gamma_{i(m)P}x_{i(m)P}) + \overline{V}_i(p_{(m)P} - p_{isat}) \tag{23}$$

Once that:

$$p_{(m)P} = p_{(m)F} = p_F = p_0 \text{ and } p_p = p_l \tag{24}$$

We obtain:

$$x_{i(m)P} = \frac{\gamma_{iP}}{\gamma_{i(m)P}}x_{iP}\exp(-\frac{\overline{V}_i(p_0 - p_l)}{RT}) \tag{25}$$

Assuming:

$$\frac{\gamma_{iP}}{\gamma_{i(m)P}} = \frac{\gamma_{iF}}{\gamma_{i(m)F}} = K_i^{molar} \tag{26}$$

We get:

$$x_{i(m)P} = K_i^{molar}x_{iP}\exp(-\frac{\overline{V}_i(p_0 - p_l)}{RT}) \tag{27}$$

Recently it was suggested (Peeva et al, 2004) that the following relation works better for highly rejected concentrate solutions:

$$x_{i(m)P} = K_i^{molar} \frac{\gamma_{iP}}{\gamma_{iF}} x_{iP} \exp(-\frac{\overline{V}_i(p_0 - p_l)}{RT}) \tag{28}$$

Therefore, this relation was adopted in this thesis. Substituting Eqs. (20) and (28) in Eq (16) the solution-diffusion equation is derived:

$$N_i = \frac{c_{i(m)} D_{iM}^e K_i^{molar}}{l} \left(x_{iF} - x_{iP} \frac{\gamma_{iP}}{\gamma_{iF}} \exp\left(-\frac{\overline{V}_i(p_0 - p_l)}{RT} \right) \right) \tag{27}$$

grouping parameters the one parameter (permeability) version of the solution-diffusion model is obtained:

$$N_i = P_i \left(x_{iF} - x_{iP} \frac{\gamma_{iP}}{\gamma_{iF}} \exp\left(-\frac{\overline{V}_i(p_0 - p_l)}{RT} \right) \right) \tag{28}$$

In Eq. (27) it is assumed that the species activity coefficients inside the membrane stays constant through all membrane thickness instead of the usual solution-diffusion assumption Eq. (25), that considers constant the solution activity coefficient-membrane activity coefficient ratio in the feed and permeate sides.

Bowen's Pore-Flow Model

To deduct the pore-flow model used in solute transport studies the best starting point is the extended Nernst-Plank equation for a solute i (Bowen and Welfoot, 2002):

$$N_i = -\frac{c_{i(m)} D_{i(m)}}{RT} \frac{d\mu_i}{dz} + K_{ic} c_{i(m)} V_s \tag{29}$$

Where V_s is the solvent velocity given by the Hagen-Poiseuille relation (Bowen and Welfoot, 2002):

$$V_s = \frac{r_p^2}{8\eta\Delta z}(\Delta p - \Delta\Pi) \tag{30}$$

$D_{i(m)}$ is the solute diffusivity inside the pore and is given by the product of the liquid phase diffusion coefficient by an hindrance factor:

$$D_{i(m)} = D_i^e K_{id} \tag{31}$$

The values of both hidrance factors for convection and diffusion K_{ic} and K_{id} respectively were determined by Deen (1987):

$$K_{ic} = (2 - \Phi_i)(1 + 0.0054\lambda_i - 0.988\lambda_i^2 + 0.441\lambda_i^3) \quad (32)$$

$$K_{id} = -2.30\lambda_i + 1.154\lambda_i^2 + 0.224\lambda_i^3 \quad (33)$$

Where Φ_i is the solute partition coefficient into the pore. For cylindrical pores is given by:

$$\Phi_i = (1 - \lambda_i)^2 \quad (34)$$

And λ_i is the ratio between the solute radius and the membrane pore radius.
Going back to Eq. (29) and knowing that:

$$\mu_i = RT \ln a_i + \overline{V}_i p + cons\tan t \quad (35)$$

The following equation is derived:

$$N_i = K_{ic} V_s - D_{ip} \frac{dc_i}{dz} - \frac{c_i D_{ip}}{RT} \overline{V}_i \frac{dp}{dz} \quad (36)$$

Knowing that the solute flux can also be written as:

$$N_i = C_{ip} V_s \quad (37)$$

And considering that the pressure gradient is constant and given by a Hagen-Poiseuille relashionhip, the following is verified:

$$\frac{dp}{dz} = \frac{(\Delta p - \Delta\Pi)}{\Delta z} = \frac{8\eta V_s}{r_p^2} \quad (38)$$

After the relations derived above Eq (36) can be written as:

$$\frac{dc_i}{dz} = \frac{V_s}{D_{i(m)}} \left[\left(K_{ic} - \frac{D_{i(m)}}{RT} \overline{V}_i \frac{8\eta}{r_p^2} \right) c_i - C_{ip} \right] \quad (39)$$

Integrating for the boundary conditions:

$$c_{i,z=0} = \Phi_i C_{iF(m)} \text{ and } c_{i,z=\Delta z} = \Phi_i C_{ip} \tag{40}$$

We obtain the following expression for the real rejection (Eq. (29) chapter 2):

$$RR = 1 - \frac{C_{iF(m)}}{C_{ip}} = 1 - \frac{\left\{K_{ic} - \frac{D_{ip}\overline{V}_i 8\eta}{RTr_p^2}\right\}\Phi}{1 - \left[1 - \left\{K_{ic} - \frac{D_{ip}\overline{V}_i 8\eta}{RTr_p^2}\right\}\Phi\right]\exp\left[Pe'\right]} \tag{41}$$

Where the modified Peclet number Pe' is given by:

$$Pe' = \frac{\left(K_{ic} - \frac{D_{ip}\overline{V}_i 8\eta}{RTr_p^2}\right) r_p^2 N_v}{8\eta D_{ip} P_{jm}} \tag{42}$$

Being P_{jm} the solvent permeability.